

ABSTRACT

BURNS, KATHIE LEE. A Rotating Disk Study of the Mechanisms of Calcite Dissolution in the Presence of Environmentally Benign Polyaspartic Acid. (Under the direction of Christine S. Grant.)

A rotating disk technique was used to investigate the mechanisms of calcite (CaCO_3) dissolution using environmentally benign polyaspartic acid (PASP) under controlled hydrodynamic conditions. Additional techniques including scanning electron microscopy and dynamic light scattering explored the specific role of PASP in the dissolution process. Using this approach, rates of dissolution were evaluated as a function of pH, rotating speed, polymer concentration and molecular weight. In this research, it was determined that PASP is an effective dissolving agent for calcite mineral over a range of pHs (3.5-10.0), rotating speeds (150-1500 rpm), PASP concentrations (0.001-0.1M) and PASP molecular weights (3,000 and 10,000 Mw). An enhancement factor, η_{enh} , was developed to quantify the effect of PASP on dissolution behavior. It is defined as the rate of dissolution in PASP over the rate in water. Maximum enhancement was observed at pHs in the range of 4-5 for high concentrations and low molecular weights of PASP. Results demonstrate that dissolution is governed primarily by interfacial phenomena, including adsorption and surface reaction, at high pHs (>7), while limited chiefly by mass transport at low pHs (<7). Dissolution at high pHs proceeds via a surface complexation mechanism involving the chelation of calcium by PASP. At the high pHs, dissolution is inhibited by small amounts of PASP (0.001-0.01M) and enhanced by large quantities (0.1M) of PASP. In contrast, at low pHs, dissolution occurs predominantly by acid attack, or the reaction of hydrogen ion with calcite. At low pHs, PASP enhances dissolution over the entire concentration range (0.001-0.1M). For the

two molecular weights studied, the lower molecular weight (3,000) is the most efficient dissolving agent at low pH, while both molecular weights dissolve calcite at comparable rates at high pH. Finally, a model was developed based on fundamental calcite and sequestration chemistry to predict the dissolution kinetics of calcite in the presence of PASP at pHs above 7. The model agrees closely with experimental dissolution rates at pH 10 and shows that the water reaction with calcite dominates dissolution at low PASP concentrations while the PASP ligand reaction with calcite is the primary interfacial reaction at high PASP concentrations.

**A ROTATING DISK STUDY OF THE MECHANISMS OF CALCITE DISSOLUTION IN
THE PRESENCE OF ENVIRONMENTALLY BENIGN POLYASPARTIC ACID**

By

KATHIE LEE BURNS

A thesis submitted to the Graduate Faculty of
North Carolina State University
In partial fulfillment of the requirements for the
Degree of Master of Science

DEPARTMENT OF CHEMICAL ENGINEERING

Raleigh, North Carolina
2002

APPROVED BY:

Dr. Christine S. Grant
(Chair of Advisory Committee)

Dr. John van Zanten
(Member of Advisory Committee)

Dr. Saad Khan
(Member of Advisory Committee)

DEDICATION

This work is sincerely dedicated to my mother, who has supported me through all points of life, my fellow graduate students who have made my experience at North Carolina State so enjoyable, and Dr. Christine Grant, for being not only my advisor but also a friend.

BIOGRAPHY

Kathie Burns began her undergraduate studies at the University of Virginia in 1996, and was awarded a degree of BS in Chemical Engineering with honors in May 2000. During the summers between undergraduate semesters and after graduation, she worked as an intern at the Carbon Plant at Westvaco Chemical Division in Covington, Virginia. She has been in attendance at NCSU graduate school since August 2000 and plans to begin working with the federal government in September 2002.

ACKNOWLEDGEMENTS

I would like to express my deepest thanks to several individuals for their help in this work:

Dr. Christine Grant, my Research Advisor and Committee Chair, for her guidance, support and devotion to the project; Dr. van Zanten, Committee Member, who provided assistance with light scattering analysis; Dr. Khan, Committee Member; Dr. You-Ting Wu, Postdoctoral researcher, who spent many hours training me in the lab, sharing his knowledge of the project, and editing papers; Dr. Lee Yu, Staff Member at the National Institute of Standards and Technology (NIST), for his guidance with chromatography studies and insight to polymer separation techniques; Undergraduate students - Lucas Revellon, Leah Taylor, Elisa Enders, and Merrick Miles, who each contributed to various aspects of laboratory work; Donlar employees - Dr. Bob Pietrangelo, Dr. Grace Fan and Kimberley Henley, for their communication and assistance with providing polyaspartate samples; Kristen Bunker and Roberto Garcia for assistance and training on the scanning electron microscope; Graduate students Shaun Tanner, Chris Kloxin and Jim Semler, who provided insight on dynamic light scattering and polymer behavior; Ruchi Singhal and Aysa Akad for their loyal support and laughter; and finally, the entire Grant research group for their support.

TABLE OF CONTENTS

| | Page |
|--|------|
| LIST OF TABLES | viii |
| LIST OF FIGURES | ix |
| LIST OF SYMBOLS | xiii |
| OVERVIEW..... | 1 |
| CHAPTER 1: INTRODUCTION | 2 |
| 1.1 Scaling and fouling in industry..... | 2 |
| 1.2 Cleaning and importance of environmentally benign processes..... | 2 |
| 1.3 Polyaspartic acid as a cleaning agent..... | 3 |
| 1.4 Research objective..... | 5 |
| CHAPTER 2: THEORY | 7 |
| 2.1 Introduction - Mechanisms of mineral dissolution | 7 |
| 2.2 Calcite dissolution..... | 8 |
| 2.3 Mass transfer to rotating disk surface | 11 |
| 2.4 Interfacial phenomena and chemistry..... | 12 |
| 2.4.1 Chelation..... | 12 |
| 2.4.2 Calcium-PASP surface interactions..... | 16 |
| 2.5 Polymer configuration and potential adsorption mechanisms..... | 23 |
| 2.5.1 Stokes-Einstein model for polymer diffusion..... | 23 |
| 2.5.2 Adsorption studies..... | 25 |
| CHAPTER 3: EXPERIMENTAL | 27 |
| 3.1 Overall experimental approach..... | 27 |
| 3.2 Analytical theory..... | 28 |

| | |
|---|-----|
| 3.3 Experimental design and data acquisition. | 35 |
| 3.3.1 Rotating disk. | 35 |
| 3.3.2 SEM imaging. | 39 |
| 3.3.3 HPLC | 40 |
| 3.3.4 DLS. | 40 |
| 3.4 Data analysis. | 41 |
| CHAPTER 4: RESULTS AND DISCUSSION | 44 |
| 4.1 Dissolution of Calcite Using Environmentally Benign Polyaspartic Acid: A Rotating Disk Approach. | 44 |
| 4.2 Additional rotating disk results | 81 |
| 4.3 Polymer transport and conformation | 84 |
| CHAPTER 5: CONCLUSIONS AND IMPACT. | 88 |
| 5.1 Conclusions. | 88 |
| 5.2 Impact. | 90 |
| CHAPTER 6: RECOMMENDATIONS FOR FUTURE WORK. | 92 |
| REFERENCE MATERIALS. | 95 |
| APPENDICES. | 99 |
| Appendix A: Additional studies | 100 |
| A.1. High performance liquid chromatography | 101 |
| A.2. Scanning electron microscopy. | 109 |
| Appendix B: Details of experimental method | 114 |
| B.1. Material preparation. | 115 |
| B.2. Instrument calibration | 118 |

| | |
|--|-----|
| B.3. Instrument operation | 120 |
| Appendix C: Data analysis. | 122 |
| C.1. Rotating disk raw data and dissolution rate calculations. | 123 |
| C.2. Reproducibility of dissolution experiments. | 126 |
| C.3. Alternative method of dissolution analysis | 130 |
| C.4. Summary of dissolution experiments. | 134 |
| C.5. Dynamic light scattering analysis. | 140 |

LIST OF TABLES

| | | |
|------------|--|-----|
| Table 2.1 | Summary of interfacial reactions during calcite dissolution in PASP. | 18 |
| Table 2.2 | Theoretical PASP dissociation and calcium binding constants | 19 |
| Table 4.1. | Polyaspartic acid dissociation and calcium complexation reactions. | 51 |
| Table 4.2. | Model parameters for calcite dissolution in PASP solutions (pH=10) | 62 |
| Table 4.3. | Summary of dynamic light scattering results. | 85 |
| Table C.1. | Intercepts of dissolution rate vs. square root rotating speed from linear regression | 132 |
| Table C.2. | Summary of dissolution experiments. | 134 |

LIST OF FIGURES

| | | |
|-------------|---|----|
| Figure 2.1 | Schematic of overall calcite dissolution process | 9 |
| Figure 2.2 | Structure of EDTA | 13 |
| Figure 2.3 | Structure of PASP | 14 |
| Figure 2.4 | Hypothetical PASP chelating unit surrounding calcium metal ions to create a water-soluble complex. | 15 |
| Figure 2.5. | Theoretical PASP species distribution plot. | 16 |
| Figure 2.6 | Schematic of polymer adsorption onto a substrate. | 25 |
| Figure 3.1 | Schematic of overall experimental approach. | 28 |
| Figure 3.2 | Atomic absorption experimental apparatus | 29 |
| Figure 3.3 | Schematic of SEM apparatus with illustration of electron detection | 31 |
| Figure 3.4 | Dynamic light scattering experimental design. | 33 |
| Figure 3.5 | Rotating disk experimental apparatus. | 36 |
| Figure 3.6 | Experimental dissolution data with free and total calcium concentration as a function of time | 42 |
| Figure 4.1 | Structure of polyaspartate | 49 |
| Figure 4.2 | Theoretical PASP species distribution plot. | 50 |
| Figure 4.3 | Rate of calcite dissolution versus square root rotational speed with and without PASP at pH=10. | 59 |
| Figure 4.4 | Theoretical versus experimental dissolution rate at pH=10. | 63 |
| Figure 4.5 | Theoretical contributions of PASP ligand (r_L) and water (r_w) reactions to dissolution at pH 10. | 64 |
| Figure 4.6 | Rate of calcite dissolution versus square root rotational speed with and without PASP at pH=5 | 66 |

| | | |
|--------------|--|----|
| Figure 4.7 | Rate of calcite dissolution versus square root rotational speed with and without PASP at pH=3.5 | 67 |
| Figure 4.8 | Rate versus PASP concentration at pH 3.5. | 68 |
| Figure 4.9 | Rate versus PASP concentration at pH 10 | 69 |
| Figure 4.10 | Rate of dissolution over pH range in absence and presence of PASP | 70 |
| Figure 4.11 | Mechanisms of calcite dissolution in the presence of PASP | 71 |
| Figure 4.12 | Total (Ca_T) and free (Ca^{++}) calcium concentration versus time for dissolution at 1200 rpm in 0.1M PASP 10,000 Mw at a) pH=10 and b) pH=3.5. | 72 |
| Figure 4.13 | PASP enhancement of calcite dissolution. | 73 |
| Figure 4.14 | PASP enhancement of brushite (DCPD) dissolution for 600 ppm PASP and 1.2 m/s flow rate. | 74 |
| Figure 4.15 | Calcite surface prior to dissolution (2000X) | 75 |
| Figure 4.16 | Calcite surface after dissolution in 0 M PASP at pH=3.5, 1 hr (1000 X) | 76 |
| Figure 4.17 | Calcite surface after dissolution in 0.1M PASP at pH=3.5, 1 hr (1000X) | 76 |
| Figure 4.18. | Calcite surface after dissolution in 0 M PASP at pH=10, 3.5 hr (2000X). | 76 |
| Figure 4.19. | Calcite surface after dissolution in 0.1 M PASP at pH=10, 3.5 hr (2000X). | 76 |
| Figure 4.20. | Calcium concentration profiles for dissolution in PASP at pH 3.5. | 82 |
| Figure 4.21. | Calcium concentration profiles for dissolution in PASP at pH 4 | 82 |
| Figure 4.22. | Calcium concentration profiles for dissolution in PASP at pH 5 | 83 |
| Figure 4.23. | Calcium concentration profiles for dissolution in PASP at pH 6 | 83 |

| | |
|--|----|
| Figure 4.24. Calcium concentration profiles for dissolution in PASP at pH 10 | 84 |
|--|----|

Appendix A.1.

| | |
|--|-----|
| Figure A.1.1. General molecular structure of PASP..... | 101 |
| Figure A.1.2. Block flow diagram of HPLC experimental setup..... | 104 |

Appendix A.2.

| | |
|--|-----|
| Figure A.2.1. Polished calcite surface before dissolution (x2000) | 109 |
| Figure A.2.2. 0 M PASP pH 10, 1200 rpm, 1 hr (x2000)..... | 109 |
| Figure A.2.3. 0.1M 10,000 Mw PASP pH 10, 150 rpm, 0.5 hr (x1000)..... | 109 |
| Figure A.2.4. 0.1M 10,000 Mw PASP pH 10, 150 rpm, 0.5 hr (x1000) | 109 |
| Figure A.2.5. 0.1 M 10,000 Mw PASP pH 10, 1500 rpm, 3.5 hr (x1000)..... | 110 |
| Figure A.2.6. 0.1 M 10,000 Mw PASP pH 10, 1500 rpm, 3.5 hr (x4000) | 110 |
| Figure A.2.7. 0.1 M EDTA, pH 10, 1200 rpm, 1 hr (x2000) | 110 |
| Figure A.2.8. 0.01M 10,000 Mw PASP pH 5, 1200 rpm, 1 hr (x2000) | 111 |
| Figure A.2.9. 0.1 M 10,000 Mw PASP pH 5, 1200 rpm,0.5 hr (x2000) | 111 |
| Figure A.2.10. 0.1M 10,000 Mw PASP pH 5, 1200 rpm, 0.5 hr (x500) | 111 |
| Figure A.2.11. 0.1M 3,000 Mw PASP pH 5, 1200 rpm, 1 hr (x1000) | 111 |
| Figure A.2.12. 0.1M 3,000 Mw PASP pH 5, 1200 rpm, 1 hr (x500) | 111 |
| Figure A.2.13. 0 M PASP pH 3.5, 1200 rpm, 0.5 hr (x1000) | 112 |
| Figure A.2.14. 0 M PASP pH 3.5, 1200 rpm, 1 hr (x2000) | 112 |
| Figure A.2.15. 0.01M 10,000 Mw PASP pH 3.5, 300 rpm, 0.5 hr (x1000) | 112 |
| Figure A.2.16. 0.01 M 10,000 Mw PASP pH 3.5, 600 rpm, 0.5 hr (x2000) | 112 |

| | |
|--|-----|
| Figure A.2.17. 0.01M 10,000 Mw PASP pH 3.5, 1200 rpm, 0.5 hr (x1000) | 112 |
| Figure A.2.18. 0.01M 10,000 Mw PASP pH 3.5, 1200 rpm, 0.5 hr (x2000) | 112 |
| Figure A.2.19. 0.1 M 3,000 Mw PASP pH 3.5, 1500 rpm, 1 hr (x350) | 113 |
| Figure A.2.20. 0.1 M 3,000 Mw PASP pH 3.5, 1500 rpm, 1 hr (x1000) | 113 |

Appendix C.

| | |
|---|-----|
| Figure C.1. Calcium concentration versus time for dissolution in 0.01M 3,000 Mw PASP, 300 rpm, at pH=3.5 | 124 |
| Figure C.2. Calcium concentration versus time for dissolution in 0.01M 3,000 Mw PASP, 300 rpm, at pH=5 | 124 |
| Figure C.3. Calcium concentration versus time for dissolution in 0.01M 3,000 Mw PASP, 300 rpm, at pH=10. | 125 |
| Figure C.4. Reproducibility of dissolution experiment at pH=5, in 0.1M 3,000 Mw PASP at 1200 rpm | 126 |
| Figure C.5. Reproducibility of dissolution experiment at pH=10, in 0.1M 10,000 Mw PASP at 1200 rpm. | 127 |
| Figure C.6. Reproducibility of dissolution experiment at pH=5, in 0.01M 3,000 Mw PASP over full range of rotating speeds. | 127 |
| Figure C.7. Effect of energy shift of AA lamp energy on calcium concentration measurement. | 129 |
| Figure C.8. Comparison of data analysis for dissolution at pH 3.5, for 0.1 M PASP (3,000 Mw) | 130 |
| Figure C.9. Scattering data for 0.001M PASP (3,000 Mw) in 0.2M KCl aqueous solution at pH 10 (log-log plot). | 140 |
| Figure C.10. Exponential fit of decay portion of correlation function. | 141 |

LIST OF SYMBOLS

- $J, J_{M.T.}$ = molar flux ($\text{mol/m}^2\text{-s}$)
 $j_{\text{Ca}^{++}}$ = mass flux of calcium ion
 k_m = mass transfer coefficient (cm/s)
 ω = rotating speed (s^{-1})
 \mathcal{D} = diffusion coefficient (cm^2/s)
 ν = kinematic viscosity (cm^2/s)
 Sc = Schmidt number (D/ν)
 C_b = bulk concentration (mol/L)
 C_i = interfacial concentration (mol/L)
- L = PASP ligand
 $H_m L^{4-m}$ = partially protonated PASP ligand
 $K_{A,m}$ = PASP dissociation constants
 $K_{B,m}$ = Ca-PASP binding constants
 k_L = surface reaction rate constant of PASP ligand with calcite (mol/min)
 k_w = surface reaction rate constant of water with calcite (mol/min)
 K_j ($j = \text{CaL}, \text{Ca}, \text{H}, \text{L}, \text{CO}_3, \text{OH}$) = adsorption equilibrium constant
 K_{sp} = solubility product
 K_{eq} = reaction equilibrium constant
 θ_c = fraction of cationic adsorption sites
 θ_a = fraction of anionic adsorption sites
- k_B = Boltzmann's constant (J/K)
 T = temperature (K)
 η = solution viscosity (cp)
 R_H = hydrodynamic radius (nm)
 M_w = weight average molecular weight (g/mol)
 ϕ = solvent quality
- q = scattering vector
 n = refractive index
 λ = wavelength (nm)
 $g^{(1)}$ = correlation function
 τ = correlation time
 θ = scattering angle
- D = diameter of reaction vessel
 V = volume of reaction vessel
- η_{enh} = enhancement factor

OVERVIEW

The chapters presented in this work are structured in the following manner. Chapters 1 and 2 include background and theory relevant to the project. Chapter 3 describes the experimental design and analytical techniques used in the research. Chapter 4 is the main chapter, which includes a manuscript as submitted for journal publication, with references for the paper listed at the end of section 4.1. Additional results are also presented in section 4.2 of chapter 4. Chapter 5 discusses the final conclusions and recommendations for future work. References that were cited in chapters 1-3 and chapter 5 are listed in the Reference Materials following chapter 5. Appendices A, B and C include additional results, detailed experimental procedures, and methods of data analysis.

CHAPTER 1. INTRODUCTION

1.1 Scaling and fouling in industry

Calcium mineral scaling and fouling of metal and other surfaces is a ubiquitous problem encountered in a variety of industries, including dairy processing, oil production, acid neutralization in lakes, and carbonate sedimentation in aqueous systems [1-7]. Due to the inverse solubility of calcium with increasing temperature, calcium salts precipitate at elevated temperatures to form deposits on surfaces of industrial equipment such as heat exchangers and cooling towers, thereby reducing their heat transfer efficiency. During oil production, as salt water from the sea mixes with water present in oil formations, mineral scales form on inner pipe linings and greatly reduce the rate of oil recovery by blocking fluid flow [8,9]. Thus, the costs and downtime associated with alleviating problems due to fouling in many industrial applications are considerable. In the oil industry alone, the global market potential for corrosion and scale inhibitors is estimated to be hundreds of millions of dollars [10].

1.2 Cleaning and importance of environmentally benign processes

In industry, traditional cleaning agents such as hydrochloric and sulfuric acids have been used to eliminate undesirable mineral deposits. However, these materials are highly toxic and reactive. Other inorganic additives have also been employed as corrosion and scale inhibitors, but have slowly been replaced by less toxic organic species such as organic phosphates and phosphonates [4,8]. More recently, polyacrylates and polyamines have been used for scale inhibition and removal applications [3,4].

However, these materials are highly persistent and will not degrade easily in the environment.

Over time, environmental awareness has shifted attention to more benign materials for cleaning practices. Consequently, certain chelating agents (e.g. EDTA (ethylenediaminetetraacetic acid), CDTA (1,2-cyclohexanediaminetetraacetic acid), DTPA (diethylenediaminepentaacetic acid), and NTA (nitrilotriacetic acid)) have replaced conventional hazardous materials in a variety of calcium scale removal applications [5,11]. Chelating agents, which are less toxic to the environment than strong acids, dissolve mineral scale by forming stable ring-like structures around metal ions to form water-soluble molecules. EDTA, the most commonly employed calcium chelant, has been used extensively in calcium dissolution procedures, including: (1) metal ore extraction, (2) mineral agitation in clay assemblages, (3) removal of boiler scales, (4) cleaning of radioactive deposits in nuclear power plants, and (5) calcium extraction from atherosclerotic aortas [1,12]. However, because EDTA is such a strong chelating species, there are major concerns about mobilization of heavy metals in groundwater. Other chelating agents such as citric and acetic acids have also been used in calcium removal applications, though they are much less effective than EDTA [5]. As a result, the search remains to find an efficient yet environmentally responsible material for calcium dissolution.

1.3 PASP as a cleaning agent

In recent years, the ready biodegradable, non-toxic chelating agent polyaspartic acid (PASP) has emerged as a potential ‘green’ alternative to conventional agents for calcium salt dissolution. It offers environmental benefits, can be manufactured in an

economically competitive manner that does not require any harsh solvents or catalysts [10,13]. Furthermore, there is a substantial economic opportunity for PASP in a variety of applications such as mineral scale and corrosion control, agricultural products, superabsorbent diapers, and detergents [14]. The present global sales potential for environmentally friendly products in oilfield markets alone is estimated to be greater than \$600 million [9]. In addition, anionic polymers such as PASP are used extensively as water treatment additives, dispersing agents, detergent constituents, redeposition inhibitors, mineral scale inhibitors, processing aids, emulsifiers and thickeners [15,16].

The potential for PASP as a calcium removal agent was first recognized when it was found in oyster shells as a naturally residing inhibitor of calcium mineral growth [17]. It has been demonstrated to prevent corrosion of steel surfaces and effectively inhibit calcium phosphate and carbonate mineral growth [3,18,19]. Recently, PASP has been incorporated as a dispersing agent for particulates in detergent formulations, paints and coatings, toothpastes, and polymeric emulsions [20].

Within the last 10 years, Donlar Corporation has developed thermal polyaspartate (TPA)-based products for application in agriculture (to increase fertilizer efficiency), oil recovery platforms, diapers, and laundry and dishwashing detergents. As a result, in 1996, Donlar was awarded the first Presidential Green Chemistry Challenge Award from the EPA for its development of environmentally safe products and manufacturing processes [4]. In May 2001, Donlar demonstrated the success of its TPA products in improving down-hole squeeze operations for oil recovery in the Norwegian Heidrun oilfields of the North Sea [9]. The polyaspartate products were highly successful in preventing scale formation and sustaining oil formation pressure, which are key

components of oil production [9]. In September, 2001, Donlar also received a patent for its technology of manufacturing ‘green’ TPA based products for the prevention of metal corrosion in industrial water treatment and agricultural (chiefly fertilizer storage) applications. According to Donlar, these polyaspartates inhibit calcium scale formation at levels comparable to or better than commercial polyacrylates. However, to date there have been limited studies to test the application of polyaspartate for industrial scale removal.

1.4. Research objective

The current study aims to investigate the fundamentals of mineral dissolution using PASP, and to determine the optimal conditions for cleaning with PASP. The particular focus is on the mechanisms of dissolution of calcium carbonate (as calcite) using PASP.

Previous research in our group has demonstrated the ability of polyaspartic acid to remove calcium phosphate deposits from stainless steel tubes under turbulent flow, as well as the efficacy of PASP to dissolve calcium carbonate powder in batch aqueous suspensions [21-25]. However, these studies did not investigate the interplay of reaction chemistry and mass transport during dissolution. To evaluate dissolution in the presence of well-defined hydrodynamics, a rotating disk technique is employed in the present study. The theory for this system is explained in section 2.3. By combining results from the rotating disk experiments with those from earlier batch studies, it is possible to determine the relative contributions of interfacial and transport phenomena during calcite dissolution in PASP. With this in mind, the overall objective is to study the mechanisms

of dissolution and the influence of PASP with the goal of predicting dissolution kinetics in the presence of PASP.

CHAPTER II. THEORY

2.1 Introduction - Mechanisms of dissolution

Dissolution of calcium minerals in aqueous solution is generally governed by one of the three following fundamental mechanisms: 1) mass transport, 2) interfacial reaction kinetics, or 3) shear removal [26]. In a mass transfer controlled system, dissolution is limited by the rate of transport of reactant species from the bulk fluid to the solid-liquid interface or the transport of product species from the interface to the bulk. For the reaction controlled regime, dissolution is determined by the rate of reaction at the mineral surface. Under shear control, a mineral deposit is removed from a surface by exceeding a critical shear stress at high flow rates.

The prevailing dissolution mechanism depends on numerous conditions, including solution pH and temperature, flow characteristics and system geometry. For example, calcite dissolution is usually reported to be mass transfer limited at low pH, while governed by reaction kinetics at alkaline pH [27-30]. Under turbulent flow conditions, shear forces typically dominate the dissolution process, while for laminar flow, mass transfer and interfacial reaction are the primary means of dissolution. In addition, dissolution characteristics depend on the system design (i.e., flow through a cylindrical pipe versus batch or rotating disk geometries).

Several experimental approaches are available for measuring experimental dissolution rates, including: bulk measurement, surface evaluation, in situ, ex-situ, real-time and discontinuous. The rotating disk setup combines aspects from each of these approaches to ideally represent industrial processes. The major advantage of the rotating

disk arrangement is that the rate of mass transfer may be easily manipulated by adjusting the rotational speed of the disk. Furthermore, the flow characteristics of this system are well defined and the surface area available for reaction may be calculated since the dimensions of the mineral disk are known.

2.2 *Calcite dissolution*

Dissolution of calcite consists of three primary steps: 1) mass transfer of the reactant from the bulk fluid to the solid-liquid interface, 2) heterogeneous reaction with CaCO_3 solid at the interface, and 3) mass transfer of products from the surface back out into the bulk [1,2,11,31]. The rates of steps 1 and 3 depend on the values for k_{m1} and k_{m3} , the mass transfer coefficients of the reactant and product, respectively, as well as species concentration gradients between the bulk fluid and the mineral-liquid interface. The rate of the reversible reaction in step 2 depends on the equilibrium reaction rate constant, K_2 , which is the ratio of the forward and reverse rate constants, k_2/k_{-2} .

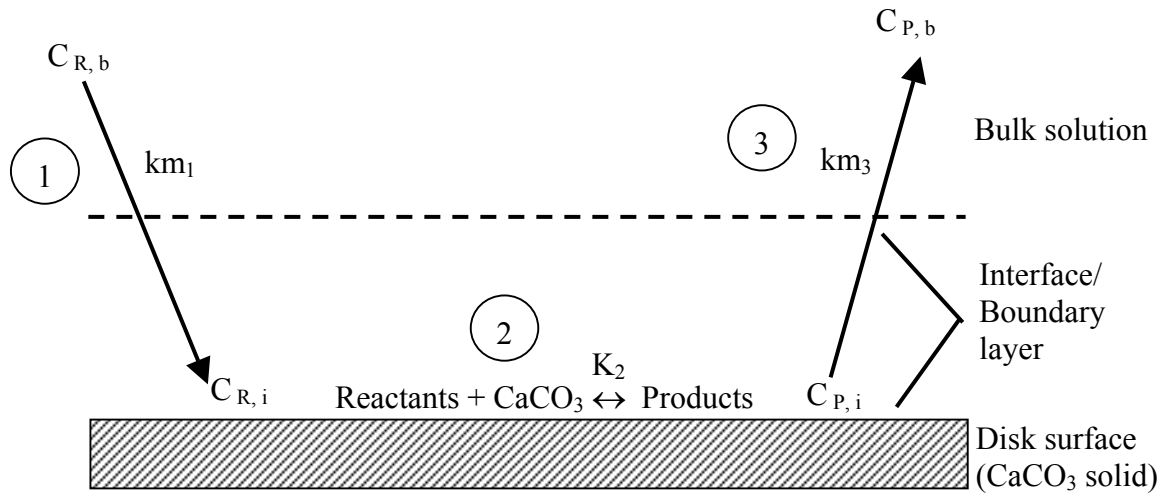


Figure 2.1. Schematic of overall calcite dissolution process.

During dissolution, one of these three processes may be significantly slower than the other two, and is considered to be the rate-limiting mechanism. As such, the overall dissolution rate is equal to the rate of the slowest step. Thus, the dominant mechanism for dissolution may be mass transport (1 or 3), surface reaction (2), or a combination of the two depending on pH, reactant concentration, and disk rotating speed.

The rotating disk technique has been used in a number of calcite dissolution studies for various solutions containing water, salt, acids and chelating agents. Plummer et al. [29] determined that calcite dissolution in water is a result of various reactions depending on the pH. Hydrogen, carbonic acid and water are the main species that react with calcite as in Equations 2.1-2.3.



In the pH range 2.0-5.5, dissolution was found to depend on reactions 2.1 and 2.2 (H^+ being the dominant reactant), while at $pH > 5.5$, reaction 2.3 and the rates of reversible surface reaction additionally influenced the net dissolution rate. Compton and Daly [28,32] found that the flux, $j_{Ca^{++}}$, of Ca^{2+} during calcite dissolution in water over the pH range 3.0-6.2 follows the form:

$$j_{Ca^{++}} = k_1 [H^+] + k_2 \quad (2.4)$$

where the term $k_1 [H^+]$ represents the mass transport of hydrogen and k_2 describes the role of surface reaction between water and calcite. Sjoberg and Prickard [27] ascertained that calcite dissolution in water containing 0.1M KCl is controlled by: (i) mass transfer at pH 2.0-4.5, (ii) mixed kinetics involving a surface reaction of water with calcite at $pH > 5.5$, and (iii) a combination of these in the transitional pH regime from pH 4.5-5.5.

Lund and Fogler [2] reported the dissolution of calcite in strongly acidic (0.1-9.0 M HCl) solutions to be limited by the diffusion of protons to the calcite surface, since the proton reaction with the surface is essentially irreversible in this case. In the presence of 0.5M acetic acid (a weak acid), dissolution was found to be influenced by a mixture of mass transport and reaction, but predominantly controlled by interfacial reaction kinetics above pH around 3.7 [1]. Fredd determined that reaction products remaining on the surface thermodynamically limit the reversible surface reaction, as well as the rate of product mass transport.

Fredd and Fogler also investigated mechanisms of calcite dissolution using chelating agents such as EDTA, DTPA and CDTA [11]. Over the pH range 3.3-12, dissolution in 0.25 M EDTA was observed to be limited chiefly by the rate of calcium complexation reaction, with small limitations due to transport of product species away

from the interface. However, at lower concentrations of 0.001M EDTA, dissolution is limited by the rate of reactant mass transport. The reaction of water with calcite was also found to influence dissolution, and the relative contributions of water and chelate reactions to the interfacial reaction rate depend on pH. Similar results were reported for DTPA and CDTA.

A previous study by our research group investigated the effect of PASP on the removal of calcium phosphate minerals (hydroxyapatite and brushite) from stainless steel in turbulent flow. In these experiments, PASP was found to promote interfacial dissolution of calcium via complexation reactions over a broad range of pH (4-10) [22-25]. These findings led to subsequent work involving the batch dissolution of calcium carbonate powder in order to investigate the role of PASP chelation chemistry during dissolution [21]. From these studies, it was determined that for sufficiently high PASP concentrations, PASP enhances dissolution over a range of pH (3.5-10) due to chelant attack at the calcite surface. Results indicated that at high pH values (>7), PASP replaces water as the primary reactant species, and at low pH (<5), both hydrogen and PASP react with calcite. Furthermore, the dissolution rate at high pH was described by a surface adsorption-complexation mechanism similar to the interfacial kinetics of calcite dissolution in EDTA proposed by Fredd and Fogler.

2.3 Mass transfer to rotating disk surface

In 1962, Levich [33] solved the Navier-Stokes and Continuity equations for velocity profiles in cylindrical coordinates to approximate the convective transport of species from a bulk solution to the surface of a rotating disk under laminar flow ($Re < \sim 3 \times 10^5$). Levich assumed an infinitely large reaction vessel, a sufficiently large disk

radius so as to ignore edge effects, and a constant diffusion boundary layer thickness over the entire disk surface. Assuming a large Schmidt number ($Sc \gg 1$), various terms were neglected to estimate the maximum diffusive flux, $J_{M.T.}$, as:

$$J_{M.T.} = 0.62048 Sc^{-2/3} (\omega\nu)^{1/2} C_b \quad (2.5)$$

Where $Sc = \nu / \mathcal{D}$, and ν and \mathcal{D} are the kinematic viscosity and diffusion coefficient of the reacting species. ω is the rotating speed of the disk and C_b is the bulk concentration of the reactant. Although this correlation is accurate to within 3% for Schmidt numbers greater than 1000, Newman [34] obtained an analytical solution for the above flux that is accurate to within 0.1% for $Sc > 100$. This expression is shown below.

$$J_{M.T.} = \frac{0.62048 Sc^{-2/3} (\omega\nu)^{1/2}}{1 + 0.2980 Sc^{-1/3} + 0.1451 Sc^{-2/3}} (C_b - C_i) \quad (2.6)$$

In this expression, the flux is proportional to a concentration gradient ($C_b - C_i$) and a group of terms that collectively represent the mass transfer coefficient, k_m (this k_m is equivalent to k_{m1} from Figure 2.1). It is important to note the dependence of the flux on the square root of ω , the rotating speed, which indicates that under mass transfer limitation, a linear relationship will exist between dissolution rate and $\omega^{1/2}$.

2.4 *Interfacial Phenomena and Chemistry*

2.4.1 *Chelation*

The chelation chemistry of PASP with calcium plays an important role in the interfacial dissolution process. Chelation, or sequestration, is the process by which a chelating molecule combines with a metal ion to form a metal-ligand complex. The chelant species contains functional groups (usually COOH^- , which have the strongest

binding ability) that surround a metal ion (e.g. Ca^{2+} , Fe^{2+} , Mg^{2+} , etc.) and form a stable ring-like structure via multiple coordination bonds [5,6,11]. In the case of EDTA (ethylene diamine tetra acetic acid), there are six functional groups per molecule; four carboxyl and two nitrogen groups, shown in Figure 2.2, such that each EDTA molecule may form six bonds with a metal ion.

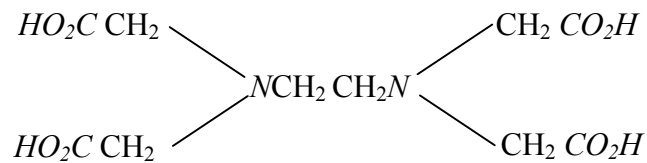


Figure 2.2. Structure of EDTA.

This gives rise to the high leaching or chelating ability of EDTA. EDTA is one of the strongest known chelants for calcium ions, illustrated by the high stability constants for Ca-EDTA complexes ($\log K_{\text{Ca-EDTA}} \sim 10.5$) [6,11].

Citric and acetic acids are other known calcium chelants. However, these acids are weaker chelants than EDTA because they have fewer reactive sites for metal coordination. Citric acid contains two carboxyl groups and one hydroxyl group for a total of three coordination sites, while acetic acid has only one carboxyl group. Polyaspartic acid, a polymeric chelating agent, which is a weaker chelant than EDTA but comparable to citrate [23-25], contains multiple carboxyl and amine groups repeated along the polymer chain (Figure 2.3).

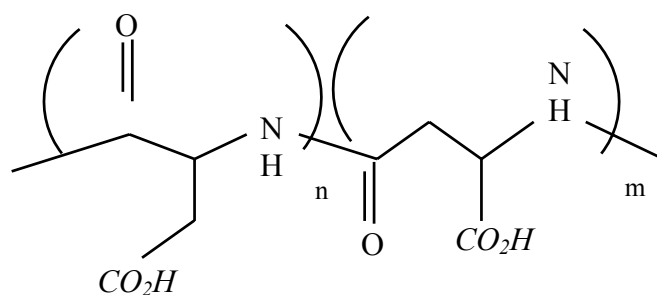


Figure 2.3. Structure of PASP.

Figure 2.3 represents two adjacent segments, n and m, located along the polymer backbone. Segments n and m correspond to the beta and alpha conformations, respectively, which signify the position of the carboxyl group in a particular unit. In a given PASP chain, the distribution of these segments is random, and the number of repeated units will depend on the molecular weight of the polymer.

Polyaspartate contains four carboxyl groups in each ligand, or “effective” chelating molecule. Each of these units are capable of forming a water-soluble metal-ligand complex with calcium ions as illustrated in Figure 2.4.

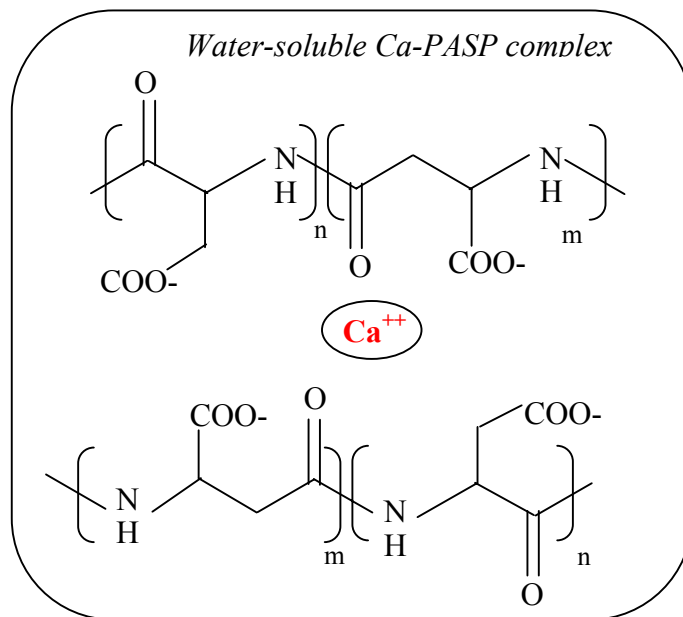


Figure 2.4. Hypothetical PASP chelating unit surrounding calcium metal ions to create a water-soluble complex.

The reason for modeling a hypothetical effective chelating unit of PASP as consisting of four repeat segments is related to the titration chemistry of PASP. During the titration of a PASP solution, there are no distinct observable equivalence points. Rather, deprotonation occurs gradually via many consecutive dissociation steps. However, Silverman et. al [18] discovered that it is possible to accurately model the deprotonation of PASP as a series of four subsequent dissociation steps, by assuming four pK values. Using this model, the species distribution plot in Figure 2.5 was constructed by Wu and Grant [21] from experimental titration data.

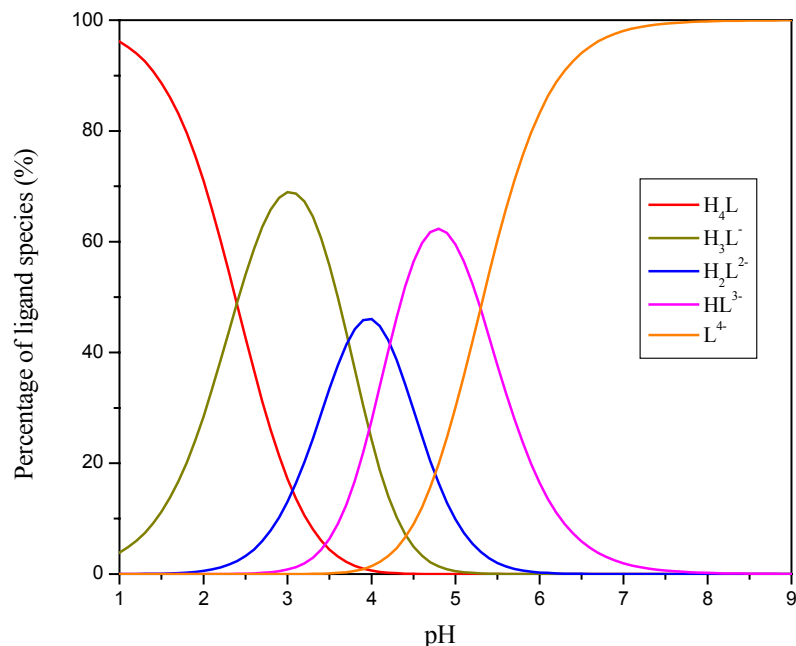


Figure 2.5. Theoretical PASP species distribution plot [21].

The percentage of each PASP species (H_4L , H_3L^- , H_2L^{2-} , HL^{3-} and L^{4-}) is a function of pH. At the lowest pH, all PASP molecules in solution are present in the form H_4L , the fully protonated species. As pH increases, PASP begins to dissociate, forming H^+ and H_3L^- , until around pH 2.4 H_3L^- becomes the dominant species in solution. Further dissociation of this molecule to form H_2L^{2-} followed by HL^{3-} and L^{4-} continues until above pH ~ 5.3 the primary PASP species in solution is L^{4-} . Since each of these polymer species exhibits a different calcium leeching power, the chelating ability of PASP will depend on the pH of the polymer solution.

2.4.2. Calcium-PASP surface interactions

The efficacy of PASP for dissolving calcium deposits is strongly related to the chemistry that occurs at the solid-liquid interface during dissolution. In aqueous

solutions, the dissolution of calcite involves numerous chemical reactions, including the key reactions presented in Table 2.1.

Table 2.1. Summary of interfacial reactions during calcite dissolution in PASP.

| <u>Reactions</u> | | |
|---|--|--------|
| Calcite Solubility: | | |
| $\text{CaCO}_3(\text{s}) \leftrightarrow \text{Ca}^{+2}(\text{i}) + \text{CO}_3^{-2}(\text{i})$ | | (2.7) |
| Water Dissociation: | | |
| $\text{H}_2\text{O} \leftrightarrow \text{H}^+ + \text{OH}^-$ | | (2.8) |
| Carbonic Acid Equilibrium: | | |
| $\text{H}_2\text{O} + \text{CO}_2 \leftrightarrow \text{H}^+ + \text{HCO}_3^- \leftrightarrow \text{H}_2\text{CO}_3$ | | (2.9) |
| PASP Dissociation: (K_{Am}) | | |
| $\text{H}_4\text{L} \leftrightarrow \text{H}^+ + \text{H}_3\text{L}^{-1}$ | | (2.10) |
| $\text{H}_3\text{L}^{-1} \leftrightarrow \text{H}^+ + \text{H}_2\text{L}^{-2}$ | | (2.11) |
| $\text{H}_2\text{L}^{-2} \leftrightarrow \text{H}^+ + \text{HL}^{-3}$ | | (2.12) |
| $\text{HL}^{-3} \leftrightarrow \text{H}^+ + \text{L}^{-4}$ | | (2.13) |
| Calcium-Polymer Complexation: (K_{Bm}) | | |
| $\text{Ca}^{+2} + \text{L}^{-4} \leftrightarrow \text{CaL}^{-2}$ | | (2.14) |
| $\text{Ca}^{+2} + \text{HL}^{-3} \leftrightarrow \text{CaHL}^{-1}$ | | (2.15) |
| $\text{Ca}^{+2} + \text{H}_2\text{L}^{-2} \leftrightarrow \text{CaH}_2\text{L}$ | | (2.16) |
| Adsorption: | | |
| $\text{L}^{-4}(\text{b}) \leftrightarrow \text{L}^{-4}(\text{i})$ | | (2.17) |
| $\text{HL}^{-3}(\text{b}) \leftrightarrow \text{HL}^{-3}(\text{i})$ | | (2.18) |
| $\text{H}_2\text{L}^{-2}(\text{b}) \leftrightarrow \text{H}_2\text{L}^{-2}(\text{i})$ | | (2.19) |
| $\text{H}_3\text{L}^{-1}(\text{b}) \leftrightarrow \text{H}_3\text{L}^{-1}(\text{i})$ | | (2.20) |
| $\text{H}_4\text{L}(\text{b}) \leftrightarrow \text{H}_4\text{L}(\text{i})$ | | (2.21) |
| Reactions with Mineral Surface: | | |
| Water attack: | | |
| $\text{H}_2\text{O}(\text{i}) + \text{CaCO}_3(\text{s}) \leftrightarrow \text{H}_3\text{L}^-(\text{i}) + \text{Ca}^{+2}(\text{i}) + \text{HCO}_3^{-1}(\text{i})$ | | (2.22) |
| Proton attack: | | |
| $\text{H}^+(\text{i}) + \text{CaCO}_3(\text{s}) \leftrightarrow \text{Ca}^{+2}(\text{i}) + \text{HCO}_3^{-1}(\text{i})$ | | (2.23) |
| $\text{H}_4\text{L}(\text{i}) + \text{CaCO}_3(\text{s}) \leftrightarrow \text{H}_3\text{L}^-(\text{i}) + \text{Ca}^{+2}(\text{i}) + \text{HCO}_3^{-1}(\text{i})$ | | (2.24) |
| $\text{H}_3\text{L}^-(\text{i}) + \text{CaCO}_3(\text{s}) \leftrightarrow \text{H}_2\text{L}^{-2}(\text{i}) + \text{Ca}^{+2}(\text{i}) + \text{HCO}_3^{-1}(\text{i})$ | | (2.25) |
| $\text{H}_2\text{L}^{-2}(\text{i}) + \text{CaCO}_3(\text{s}) \leftrightarrow \text{HL}^{-3}(\text{i}) + \text{Ca}^{+2}(\text{i}) + \text{HCO}_3^{-1}(\text{i})$ | | (2.26) |
| $\text{HL}^{-3}(\text{i}) + \text{CaCO}_3(\text{s}) \leftrightarrow \text{L}^{-4}(\text{i}) + \text{Ca}^{+2}(\text{i}) + \text{HCO}_3^{-1}(\text{i})$ | | (2.27) |
| Ligand attack: | | |
| $\text{L}^{-4} + \text{CaCO}_3 \leftrightarrow \text{CaL}^{-2} + \text{CO}_3^{-2}$ | | (2.28) |
| $\text{HL}^{-3} + \text{CaCO}_3 \leftrightarrow \text{CaHL}^{-1} + \text{CO}_3^{-2}$ | | (2.29) |
| $\text{H}_2\text{L}^{-2} + \text{CaCO}_3 \leftrightarrow \text{CaH}_2\text{L} + \text{CO}_3^{-2}$ | | (2.30) |
| Desorption: | | |
| $\text{CaL}(\text{i}) \leftrightarrow \text{CaL}(\text{b})$ | | (2.31) |
| $\text{CaHL}(\text{i}) \leftrightarrow \text{CaHL}(\text{b})$ | | (2.32) |
| $\text{CaH}_2\text{L}(\text{i}) \leftrightarrow \text{CaH}_2\text{L}(\text{b})$ | | (2.33) |

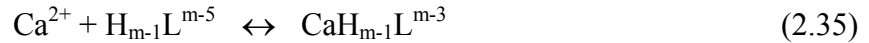
*b=bulk, i=interface

Values for theoretical and experimental dissociation (K_A) and binding (K_B) constants calculated from titration data [18,21] for reactions (2.10-2.16), respectively, are listed in Table 2.2 below. K_A values represent proton dissociation constants, given by



e.g., $K_{A,1(m=1)} = [HL^{-3}]/[H^+][L^{-4}]$

and K_B values represent calcium-polymer complexation as



e.g., $K_{B,1(m=1)} = [CaL^{-2}] / [Ca^{+2}][L^{-4}]$

Table 2.2. Theoretical PASP dissociation and binding constants.

| | Log $K_{A,1}$ | Log $K_{A,2}$ | Log $K_{A,3}$ | Log $K_{A,4}$ | Log $K_{B,1}$ | Log $K_{B,2}$ | Log $K_{B,3}$ |
|-------------|-------------------|------------------|------------------|------------------|---------------|---------------|---------------|
| | 10,000 M_w PASP | | | | | | |
| [21] | 5.17 | 4.09 | 3.60 | 2.27 | 3.02 | 2.55 | 2.16 |
| | 5.3* | 4.22* | 3.72* | 2.4* | 3.52* | 3.05* | 2.66* |
| [18] | 5.4 ⁺ | 4.3 ⁺ | 3.6 ⁺ | 2.2 ⁺ | -- | -- | -- |
| | 3,000 M_w PASP | | | | | | |
| [This work] | 5.22 | 4.07 | 3.60 | 2.49 | 2.88 | 2.47 | 2.14 |

*True equilibrium constants, assuming activity coefficients of different deprotonated PASP species have the same values as corresponding calcium-polyaspartate complexes

⁺Molecular weight= 9,200 Mw.

The affinity of the individual PASP species for calcium varies, with L^4 demonstrating the highest stability and H_4L the lowest stability for complexation with calcium. This is shown by the increase in K_B with polymer ionization ($K_{B,1} > K_{B,2} > K_{B,3}$). However, the binding constants are nearly equal for the two molecular weights investigated in this study.

With all of the reactions in Table 1 occurring simultaneously, interfacial dissolution becomes quite complex in the presence of PASP. Therefore, it is crucial to

identify the reactions that are dominant under various experimental conditions. Perhaps the most significant factor is pH, since this determines the form and amount of each species in solution.

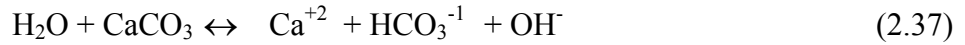
Influence of pH on Dissolution

In general, one or a combination of the following reactions dominates calcite dissolution in aqueous PASP solution, depending on pH.

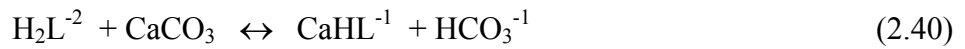
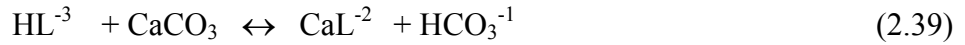
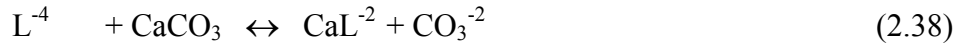
Proton attack:



Water attack:



Ligand attack:



Reaction (2.36) is significant at low pH (below about pH 4), while the water (2.37) and ligand (2.38-2.41) reactions dominate at higher pH values. The contribution of each ligand reaction depends on the polymer species distribution (Figure 2), which is also closely related to pH.

pH 10

Above pH ~6, the primary free PASP species in solution is L^{-4} . Thus, at pH 10, reactions (2.37) and (2.38) dominate the interfacial dissolution process. The individual contributions of the two reactions to the overall dissolution rate will depend on the

concentration of PASP ligand, with the water reaction dominating at low PASP concentration and the ligand reaction dominating at high PASP concentration.

Since calcite dissolution is generally controlled by interfacial reaction kinetics at high pH conditions [1,11,27-31], reactions (2.37) and (2.38) are considered the rate-determining steps. With this in mind, we have developed a model to predict the dissolution of calcite in PASP at pH 10, where the overall rate of reaction (r_T) is the sum of the rates of the water (r_w) and ligand (r_L) reactions:

$$r_T = r_w + r_L \quad (2.42)$$

where r_w and r_L are given by:

$$r_w = k_w \theta_c \theta_a (1 - [\text{Ca}^{2+}]_{(i)} [\text{CO}_3^{2-}]_{(i)} / K_{sp}) \quad (2.43)$$

$$r_L = k_L K_L \theta_c \theta_a ([\text{L}^{4-}]_{(i)} - [\text{CaL}^{2-}]_{(i)} [\text{CO}_3^{2-}]_{(i)} / K_{eq}) \quad (2.44)$$

Equations 2.43 and 2.44 are derived from Langmuir-Hinshelwood adsorption kinetics, following the work of Fredd and Fogler [11] and Wu [21]. In these equations, k_w and k_L are the surface reaction rate constants for water and ligand with calcite, and K_L is the adsorption equilibrium constant for PASP ligand. K_{sp} is the solubility product for calcium carbonate, and K_{eq} is the product of K_{sp} and the Ca-L binding constant, $K_{B,1}$. θ_c and θ_a are the fraction of cationic and anionic adsorption sites, respectively, given by:

$$\theta_c = 1 / (1 + K_{CaL} [\text{CaL}^{2-}]_{(i)} + K_{Ca} [\text{Ca}^{2+}]_{(i)} + K_H [\text{H}^+]_{(i)}) \quad (2.45)$$

$$\theta_a = 1 / (1 + K_L [\text{L}^{4-}]_{(i)} + K_{CO_3} [\text{CO}_3^{2-}]_{(i)} + K_{OH} [\text{OH}^-]_{(i)}) \quad (2.46)$$

where K_j ($j = \text{Ca}^{2+}, \text{CaL}^{2-}, \text{H}^+, \text{L}^{4-}, \text{CO}_3^{2-}$ or OH^-) are the Langmuirian adsorption equilibrium constants. The HCO_3^- species does not enter into the expression of θ_a , since between the two carbonate species only CO_3^{2-} is found to be in significant concentration on the calcite surface in alkaline solutions [35].

At steady state, the overall rate of reaction is equal to the rate of transport of calcium product species from the interface to the bulk fluid. This is expressed as:

$$r_T = k_m ([Ca]_{T,i} - [Ca]_{T,b}) \quad (2.47)$$

where k_m is the effective mass transfer coefficient for calcium and $[Ca]_{T,i}$ and $[Ca]_{T,b}$ are the interfacial and bulk concentrations of total calcium concentration, respectively.

Solving equations 2.42, 2.43, 2.44 and 2.47 simultaneously using equilibrium values from Table 4.1 in Section 4.2 and from literature [1], model parameters for reaction rate constants and ligand adsorption equilibria may be calculated to yield a theoretical dissolution rate. In this model, k_m values are calculated according to equation 2.5 in Section 2.3. The model will later be used to predict calcite dissolution rates in PASP.

pH 5

At pH 5, the principal polymer species in solution are HL^{-3} (60% of total PASP) and L^{-4} (30%), with H_2L^{2-} constituting the remainder (10%). Thus, in the presence of these species, reactions (2.39) and (2.40) begin to influence the dissolution rate, in addition to reactions (2.37) and (2.38). Furthermore, at this lower pH, the reaction between hydrogen and calcite (2.36) becomes important, and dissolution is partly limited by the mass transport of H^+ . Consequently, it is not trivial to predict dissolution behavior at pH 5, where various interfacial reactions as well as mass transfer play a role in calcite dissolution.

pH 3.5

The dominant forms of PASP ligand at pH 3.5 are H_3L^{-1} (56% of total ligand species) and H_2L^{2-} (33%). In this regime, dissolution is again complicated by the presence of several polymer species which each react with calcium. Dissolution is

strongly dependent on the rate of H⁺ transport as well as the mass transport of chelating species to the interface. As with pH 5, the numerous equilibria creates difficulty in calculating the large number of parameters necessary to complete a model for dissolution at pH 3.5.

2.5 Polymer configuration and potential adsorption mechanism

In the presence of a polymer, the interfacial dissolution process also involves the adsorption of polymer molecules onto the mineral surface. Under certain conditions, this may be a rather slow process, providing significant limitations to the overall rate of dissolution. The adsorption of polymer species from an aqueous solution onto a surface is strongly dependent on pH. The pH determines the effective size and conformation of polymer molecules in solution, which directly influence the rate of adsorption.

2.5.1 Stokes-Einstein model for polymer diffusion

The Stokes-Einstein model is used to describe the Brownian motion of polymer molecules through a liquid medium, taking into account the interactions between the polymer and solvent molecules [36]. In this model, the polymer chain is represented as a string of connected beads, which, in a dilute solution, are spread out such that there is little polymer-polymer interaction but significant polymer-solvent interaction [26]. In the dilute regime, as in the case of this study, if a solvent is considered a “good” solvent, high polymer-solvent interaction causes the polymer chain to swell, whereas in a “poor” solvent, the chain contracts into a small blob. Between these extremes, in an “ideal” or “theta” solvent, the polymer is neither fully expanded nor contracted, which is referred to

as the random coil configuration. Under theta conditions, the diffusion coefficient, \mathcal{D} , of a polymer molecule is given by the Stokes-Einstein equation as [36]:

$$\mathcal{D} = \frac{k_B T}{6\pi\eta R_H} \quad (2.48)$$

where k_B is Boltzmann's constant, T is solution temperature, η is solution viscosity and R_H is the hydrodynamic radius of a polymer molecule. In equation 2.48, the quantity $6\pi\eta R_H$ represents the viscous drag force that the polymer chain experiences as it travels through the medium. Because solvent effects are included in the above expression, the hydrodynamic radius describes the effective size of the polymer molecules in solution. It is important to note that equation 2.48 applies to theta conditions, and deviates significantly for non-ideal solutions. The ideality of the solution, and consequently the size and extent of swelling of the polymer, will depend strongly on pH. Therefore, the rate of polymer adsorption onto a solid surface (e.g. calcite) will be heavily influenced by pH, which governs the extended or contracted nature of the polymer configuration.

Using dynamic light scattering techniques, the effective diffusion coefficient (\mathcal{D}) and size (R_H) of a polymer in solution can be directly measured under various conditions of pH, polymer concentration and molecular weight. From these experiments, values for \mathcal{D} and R_H can be used to predict the transport properties of PASP during dissolution. Furthermore, estimates for R_H may help explain the qualitative behavior of polymer molecules at the interface during adsorption.

The diffusion coefficient of the polymer is also related to molecular weight as:

$$\mathcal{D} \propto M_w^{-\phi} \quad (2.49)$$

where $\phi = 1/2$ for a theta solvent and $\phi = 3/5$ for a good solvent [36]. Thus, polymer chains of lower molecular weight should diffuse through a solvent faster than those of higher molecular weight.

2.5.2. Adsorption studies

The size and shape of a polymer in solution strongly affect the degree of adsorption onto a surface. Some segments of the polymer may attach to the substrate surface in a flat, “train”-like configuration, and other segments may protrude from the surface in a “loop” or “tail” configuration, as illustrated in Figure 2.6. The portion of polymer residues that adopts the train configuration versus the loop or tail arrangement is heavily dependent on the interactions of the polymer functional groups with the surface.

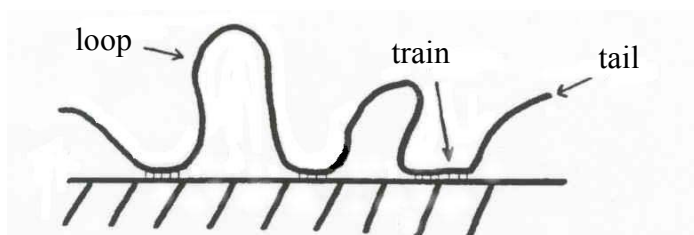


Figure 2.6. Schematic of polymer adsorption onto a substrate [37].

Although it is known that PASP has a high affinity for calcium mineral surfaces, the conformation of PASP onto calcium salt crystals remains ambiguous. In one study, researchers interpreted from isotherm data that PASP adsorbs onto hydroxyapatite in a relatively flat configuration, with train and loop segments [37]. In a separate study [38], adsorption of PASP onto calcite was investigated by growing calcite crystals in the presence of PASP. Using AFM techniques, it was found that PASP adsorbs

preferentially to specific faces of calcite crystals, and with large binding energies. This strong adsorption was attributed to the interaction of the polymer carboxyl functional groups with the calcium ions in the crystal lattice. The high binding energies suggest that PASP lies in a flat conformation along the calcite surface. It has also been reported that polyelectrolytes adapt a flat configuration on highly charged surfaces of minerals such as calcite [39].

Studies have also found that the amount of PASP and other poly-electrolytes adsorbed onto calcium minerals exhibits a maximum at low pH [37]. Schaad and coworkers determined that adsorption of anionic polymers onto hydroxyapatite is strongest at low pH due to the lower chain flexibility that results from internal hydrogen bonding [40]. Chang and fellow researchers observed that adsorption of anionic chelating agents onto hematite increases at low pH, because at pH's above the isoelectric point, polymer molecules adopt a change in conformation which requires more energy for adsorption [41]. Maximum adsorption of PASP onto barium titanate also increases with lowering pH [20]. Zeta potential measurements of the barium-PASP system indicate that adsorption occurs via electrostatic interactions and/or hydrogen bonding at low pH (5), while adsorption occurs via a different mechanism at high pH (10), such as adsorption of neutral functional groups. During calcite dissolution, it is possible that PASP adsorbs via electrostatic interactions at low pHs and by interactions of neutral amine groups with the calcite surface at high pH.

CHAPTER III – EXPERIMENTAL DESIGN AND DATA ANALYSIS

3.1 Overall experimental approach

Several analytical techniques were used cooperatively to measure the rate of dissolution of calcite in aqueous solutions of polyaspartic acid (Figure 3.1). Using a rotating disk apparatus, dissolution experiments were carried out under controlled mass transfer conditions with four variable parameters: pH, disk rotating speed, polymer concentration and polymer molecular weight. During each dissolution experiment, a calcium ion selective electrode was immersed in solution to continuously monitor the concentration of free calcium (Ca^{2+}) in the bulk fluid. Bulk samples were also acquired periodically throughout the experiment to be analyzed using an atomic absorption (AA) spectrometer to measure levels of total calcium (Ca_T) in solution. Total calcium includes both free (Ca^{2+}) and bound, or complexed, calcium (Ca-PASP), and enables calculation of the ratio of the two concentrations.

After dissolution, surface images of dissolved and undissolved calcite disks were obtained using scanning electron microscopy (SEM) so as to examine changes in calcite surface morphology during dissolution. Dynamic light scattering experiments were also performed to measure the effective size and motion of PASP molecules in solution under various conditions.

In addition, a limited study using high performance liquid chromatography (HPLC) was carried out to investigate the possible separation of different polymer-calcium complex species. The work was done by an undergraduate student at NCSU, Lucas Revellon, as part of a project at the National Institute of Standards and Technology, and is summarized in Appendix A.1. The immediate goal of the study was

to determine the feasibility of polymer species separation and to begin developing an online method for the detection of separate Ca-PASP species.

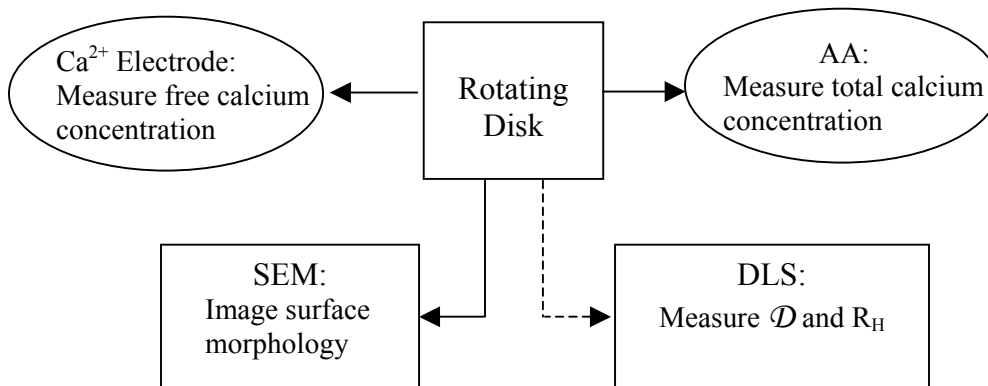


Figure 3.1. Schematic of overall experimental approach.

3.2 Analytical theory

Atomic Absorption

Atomic Absorption (AA) is used to determine the concentration of an elemental species in solution. A liquid sample containing the analyte is fed through a sample tube to the burner system. In the burner, a mixed acetylene-air flame at 2300°C burns the sample solution to an aerosol, which is then converted to an atomic vapor. Using a hollow cathode lamp as a light source, light is shone through the vapor and is absorbed by the atoms. As the atoms absorb this energy, they are “excited” from their ground state to a higher energy state. Then, as the atoms decay, they release energy in the form of light, which can be detected by the AA apparatus (Figure 3.2). The wavelength of the emitted light is unique to the elemental species. Thus, selecting the wavelength of light

to be detected, a particular element can be accurately determined. For example, calcium is best detected at 422.7 nm.

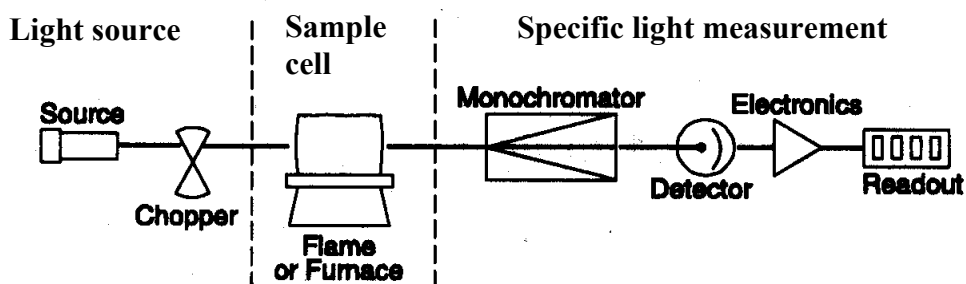


Figure 3.2. Atomic absorption experimental apparatus [42].

The intensity of light emitted from the element of interest is directly related to the amount of the element in solution. According to Beer's law, the concentration of a species is directly proportional to absorbance ($\text{conc} = k \cdot \text{abs}$). Although the relationship deviates from Beer's law at high concentrations, this can easily be corrected using a calibration curve for absorbance versus concentration. For calibration, standard solutions must be prepared covering the range of calcium concentrations to be analyzed. The standards should also include matrix or background species (all species in solution other than the analyte), to account for interferences in absorbance readings from other elements. For example, in the current study, moderate to high concentrations of PASP and salt in the samples interfere with calcium measurement, resulting in absorbance readings lower than the true values. To alleviate this problem in our experimental setup, appropriate concentrations of PASP and KCl were also added to AA standards to obtain accurate calibration curves for each run.

Scanning Electron Microscopy

Scanning electron microscopy (SEM) utilizes an electron gun combined with a set of electrostatic and electromagnetic lenses to form and focus an electron probe onto a specimen surface. As the electrons bombard the sample material, they collide with atoms in the solid, thereby undergoing both elastic and inelastic scattering. Elastic scattering is defined as a change in trajectory without a loss of kinetic energy. Inelastic scattering occurs when a beam electron continues along its path but decelerates upon interaction with atoms or other electrons.

The two main types of SEM signals used for imaging include back-scattered electrons (BSE) and secondary electrons (SE). Backscattered electrons are electrons with high energy (kV) from the incident electron beam that travel through the sample and re-emit from the surface. Secondary electrons are electrons of low energy (<50 eV) that are generated from atoms in the material. For example, when a high-energy electron from the primary beam bombards an atom, it can eject a loosely bound outer shell electron or cause inner-shell ionization, which may lead to fluorescence or the ejection of an Auger electron. Both BSE and SE are emitted from the sample, and may be collected using a detector placed strategically within the sample chamber, at an angle above the sample surface. One of the most common detectors used today is an Everhart-Thornley detector, which consists of a biased shield for electron collection, a scintillator to convert electrons to photons, and a photomultiplier tube (PMT) to carry the photons to the cathode ray tube, or other type of display. The detector may be set to a positive bias (+300V) for pure BSE mode (no secondary electrons will be detected because of their low energy), or a negative bias (-100V) for detection of both SE and BSE.

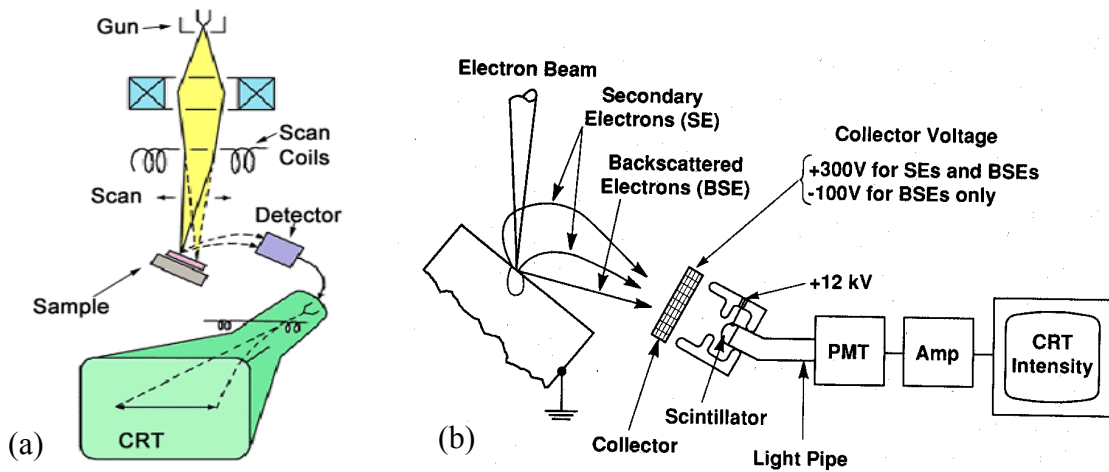


Figure 3.3. Schematic of (a) SEM apparatus with (b) illustration of electron detection [43].

Backscattered and secondary electron images yield different types of information.

Because materials of higher atomic number have higher BSE yields (more particles scatter when colliding with a heavy atom), images in pure BSE mode indicate compositional contrast. In this mode, brighter spots correspond to heavier atoms. However, in SE mode, images yield topographic information. Since SE are generated from a very small region near the surface of the specimen, SE images are used to observe the smoothness or roughness of a surface. Most of the imaging in this work was performed using SE mode, and a few images were obtained using BSE detection.

One major problem that may be encountered when imaging with SEM is a phenomenon called charging. This occurs in insulating materials, such as calcium carbonate, where electrons entering the specimen cannot be sufficiently conducted out of the sample material. This causes areas of the surface to build up a negative charge, so that drifting white spots appear on the image. The specimen may also be damaged from

charging effects. In order to avoid this problem, it is necessary to operate the SEM at low electron beam voltage, usually below ~ 5 kV. For the studies performed in this project, charging was frequently an issue. Hence, using a Hitachi 3400 Environmental SEM, the beam voltage was maintained at about 2-15 kV for imaging.

High Performance Liquid Chromatography

High Performance Liquid Chromatography (HPLC) is a technique commonly used to separate components in a liquid sample. An HPLC system typically includes a column to perform the separation in conjunction with a detector to detect species leaving the column. While there are various types of columns and detectors, this project utilized a Size Exclusion Chromatography (SEC) column coupled with an UltraViolet (UV) detector.

In the design used here, a liquid is pumped through a column packed with silica particles, and molecules in the flowing solution are separated based on their size. Larger molecules elude from the column faster than smaller molecules, which are retained by the pores in the packing material. Upon leaving the column, the solution is continuously pumped through the UV detector, which measures absorbance of light at a particular wavelength. The detector is set to the wavelength at which the analyte (PASP in this case) exhibits maximum absorbance. From the peaks from the UV detector, one can measure the elution time (or time it takes to exit the column) for each molecular species.

The level of separation achieved is highly dependent on a number of factors, including column efficiency, flow rate, and pressure. For example, if the column has low sensitivity, it may not be able to separate two species of similar size. Non-ideal

separation will also result from excess flow rates or pressures. Therefore, it is necessary to set the conditions for HPLC to obtain optimal separation.

Dynamic Light Scattering

Dynamic light scattering (DLS) is a method used to determine the dynamic properties (e.g. diffusion coefficient) of polymer molecules subject to random, or Brownian motion. In an experiment (Figure 3.4), light from a laser is directed through a solution, and particles in the solution scatter the light in different directions.

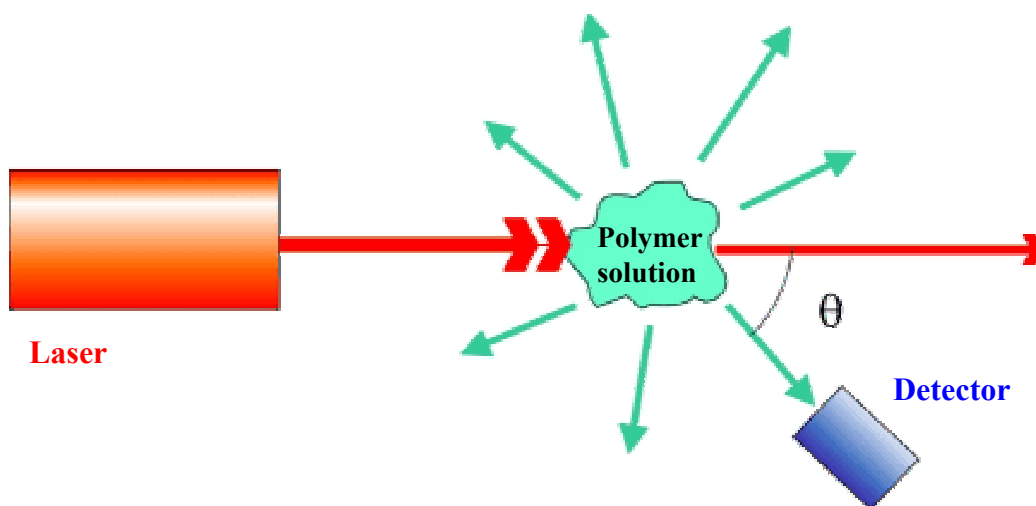


Figure 3.4. Dynamic light scattering experimental design [44].

The light is scattered with an intensity, I , which fluctuates with time due to the motion of particles. The intensity of the scattered light is then collected by a detector, which is placed at an angle θ with respect to the incident light beam. Once collected, the intensity data are analyzed by a correlator, which evaluates the autocorrelation function, $g^{(1)}(t)$.

From the decay rate of $g^{(1)}(t)$, the diffusion coefficient of the molecules in solution may be determined using equation 3.1 [45]:

$$G(t) = A[1 + B\exp(-2Dq^2t)] \quad (3.1)$$

where A and B are the baseline and intercept, respectively, of the correlation function. D is the translational diffusion coefficient, q is the scattering vector, and t is the time delay. The scattering vector is calculated as:

$$q = 4\pi n/\lambda \cdot \sin(\theta/2) \quad (3.2)$$

In equation 3.2, n represents the refractive index of the solution, and λ is the wavelength of the light emitted from laser. Thus, dynamic light scattering directly measures the diffusion coefficient D of the polymer molecules in solution. From this value, estimates of the hydrodynamic radius may be calculated using Equation 2.47.

In the case of polyelectrolytes (such as PASP) in aqueous solution, there are numerous problems that may be encountered in dynamic light scattering experiments. The scattering results are highly sensitive to experimental conditions such as salt concentration, refractive index, viscosity, and anomalies due to skewed scattering from dust or other large particles. Salt concentration is perhaps the most significant parameter for polyelectrolyte solutions, as it has a considerable effect on the conformation of polymer molecules in solution [46]. In the absence of added salt, the electrostatic repulsion between charged segments of polymer chains causes polymer molecules to extend in a rigid conformation. However, in the presence of added salt, coulombic interactions are effectively screened, causing the chains to collapse in a coil configuration. In the current study, DLS experiments were carried out at relatively high

ionic strength (0.2 M) to simulate dissolution experimental conditions described below. Hence, results from DLS will be strongly affected by the presence of salt.

3.3 Experimental design and data acquisition

This section discusses the various experimental techniques, equipment and conditions used for dissolution studies, including rotating disk, scanning electron microscopy and dynamic light scattering.

3.3.1. Rotating disk

Materials and equipment

Dissolution experiments were performed using a Pine Instruments Rotating Disk apparatus (Figure 3.5), equipped with a plastic rotor shaft, connection piece for disk attachment and variable speed motor. The rotating speed was controlled using a Pine Instrument MSRX Speed Control device. Calcite disks were prepared from marble core acquired from the Durham Marble Company and were determined to be 96% pure by dissolving a known amount of marble in HCl and measuring calcium content using AA analysis.

Polymer solutions containing sodium polyaspartate (40 wt% solids, pH = 8-9.5, CAS No. 34345-47-6) of weight average molecular weights 10,000 and 3,000 provided by Donlar Corporation were prepared in 1L glass beakers and immersed in the water bath during experiments. A Fisher Scientific Isotemp Model 730 Immersion Circulator thermostat was used to maintain constant temperature in the water bath. The polymer solutions also contained analytical grade KCl purchased from Fisher Scientific and deionized water.

Free calcium (Ca^{2+}) and pH measurements were obtained using a Denver Instrument Model 225 pH/ISE meter, with Orion pH probe and Calcium Ion Selective Electrode Model 97-20 *ionplus* electrode. Winwedge software was used for continuous collection of Ca^{2+} concentration and pH readings. Total calcium concentrations were determined using a Perkin Elmer 100 Atomic Absorption Spectrometer with lumina lamp set to 422.7 nm wavelength. The spectrometer was operated using AAWinLab 100 AAnalyst software. Calcium stock solution (0.1M) used to prepare standards for AA and electrode calibration was supplied by Fisher Scientific.

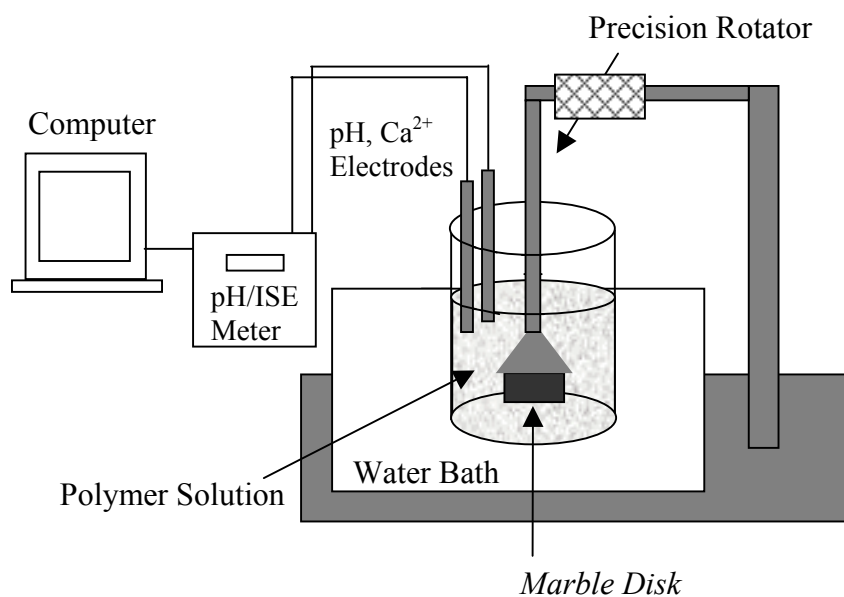


Figure 3.5. Rotating disk experimental apparatus.

Dissolution experimental procedure

The following steps represent the experimental procedure for calcite dissolution experiments. The details for material preparation, instrument calibration and instrument operation are included in Appendix B as noted in the text. A comprehensive summary of the experimental conditions for each run are listed in Table C.2 in appendix C.4.

1. Calibrate pH and Calcium Ion Selective Electrodes (Appendix B.2), using standards prepared as described in Appendix B.1.
2. Prepare calcite marble disk (Appendix B.1). Disks are cut from a marble core to a diameter of 3.2 cm, polished to a smoothness of 3,000 mesh using diamond polishing disks, and then coated with polystyrene on the bottom and sides to isolate the top surface for dissolution.
3. Heat water bath to 25°C.
4. Prepare 800 mL polymer (PASP) solution in 1 L beaker with appropriate concentration of polymer and salt (Appendix B.1) and adjust to desired pH using NaOH or HCl.
5. Place solution beaker in water bath in a secured stand.
6. Attach polished calcite disk to end of rotor shaft and insert disk into the polymer solution. The disk is placed in the radial center of the vessel, to a height where the exposed disk surface sits ~ 4 cm above the bottom of the vessel. This is done to model infinite vessel volume consistent with rotating disk theory.
7. Insert pH and Ca²⁺ ISE electrodes into solution, near the air-liquid interface. Only the tips of the electrodes should be immersed in liquid to avoid damage to the probes.

8. Start Winwedge software to obtain electrode readings (Appendix B.3).
9. Set the desired rotational speed on the motor control.
10. Flip the motor switch on to begin the experiment, and immediately start stopwatch to begin timing.
11. Obtain a bulk solution sample with a 2 mL syringe at the start of the experiment, and every 2 minutes for the remainder of the experiment. Store each sample in a 3 mL plastic vial. These are to be analyzed with atomic absorption at the end of the experiment. *Note: samples cannot sit overnight before analysis due to evaporation.
12. Throughout the experiment, maintain a constant solution pH by addition of either HCl or NaOH.
13. Approximately 20 minutes before the end of the experiment, turn on Atomic Absorption machine to allow the flame to become stable before analyzing samples (Appendix B.3).
14. At the end of the experiment (30 minutes; approximately 10-20% of total dissolution), switch off the motor to stop rotation and remove the disk from the solution. Disconnect the calcite disk from the rotor shaft and set aside for repolishing. (The disks are reused for later experiments). Rinse the beaker containing the polymer solution for future experiments. Close the Winwedge software and save the data file.

AA analysis of total calcium

15. Once the AA flame is stabilized, calibrate the AA spectrometer using the standards prepared earlier (Appendix B.2)

16. Analyze the bulk samples for total calcium content. Insert the tubing into each sample to aspirate the liquid in the AA flame. The result will be an average of 3 calcium concentration readings.
17. Record total calcium concentration readings manually.
18. After all samples have been analyzed, shut down the AA equipment.
19. Rinse all plastic sample vials in DI water thoroughly and soak in a beaker of DI water overnight. The following day, remove the vials from the beaker, rinse off once more, and let dry for 24 hours. The excessive rinsing is necessary to eliminate calcium residues from the vials for future experiments.
20. Rinse the pH and Ca⁺⁺ electrodes and store overnight (Appendix B.3)

3.3.2. SEM imaging

After dissolution experiments, some disks were reserved for SEM imaging to determine changes in calcite surface morphology during dissolution. A Hitachi S-3200 Environmental Scanning Electron Microscope (E-SEM) was used for specimen imaging. The variable pressure E-SEM allows imaging of insulating materials such as calcium carbonate at low beam voltages without gold coating. Signals were collected using an Everhart-Thornley secondary electron detector and Robinson backscattered electron detector.

The majority of images presented in this thesis were obtained while operating in backscattered detection mode. This mode was originally chosen because it does not require extremely low voltages, where resolution is often compromised. However, when it was later realized that topographic information is better acquired using secondary

electron detection, disks samples were thereafter imaged using SE mode. Results are presented for each mode.

Images were taken at magnifications of 500X-4000X. Samples were sometimes tilted for increased scattering (and better signal detection), and working distances of around 10-15 mm were used to optimize resolution and depth of field.

Leah Taylor, an undergraduate student from the University of Missouri, was instrumental in performing SEM analysis of calcite disks. Leah was a participant in the summer Research Experience for Undergraduate (REU) program at NCSU during the Summer of 2001. Some additional SEM images taken by Leah and the author are included in Appendix A.2.

3.3.3. HPLC

Separation studies using HPLC were performed by Lucas Revellon, an undergraduate student at NCSU. The research was conducted at the National Institute of Standards and Technology in Gaithersburg, MD, under the direction of Dr. Lee Yu. Dr. Yu is a staff member of the Chemical Science and Technology Laboratory, where the experiments were performed. The HPLC results are included in Appendix A.1.

3.3.4. DLS

Samples for dynamic light scattering were prepared in the same manner as the solutions for rotating disk experiments so as to mimic the conditions of dissolution. The samples contained PASP and added KCl for a total ionic strength of 0.2M, and pH was adjusted using NaOH or HCl. Although solutions did not contain calcium carbonate, the experiments reasonably represent conditions from dissolution studies since dissolved

calcium concentrations were on the order of 0.01-10 ppm. Sample solutions were placed in glass vials so that light could be transmitted through the solution.

For each light scattering experiment, the sample (in the glass vial) was placed appropriately in the path of the laser light so as to attain high signal count rates from the detector. A 200 megawatt Argon laser provided the light source and a Brookhaven Instruments BI-PMT 9836 photomultiplier tube was used as a detector. The detector was positioned at an angle of 90 degrees from the incident beam for all runs. Brookhaven Instruments BI-9000 AT autocorrelator and software (9kdls version 2.15) were used to generate correlation functions from the scattering data. The output data from the software was then fit to an exponential curve using Microcal Origin 6.0 software to calculate parameters for the scattering vector, q , and translational diffusion coefficient, \mathcal{D} .

DLS experiments were conducted at the extreme pH values of 3.5 and 10 to observe the effect of pH on the polymer conformation and mobility in solution. Initially, polymer concentrations of 0.1M (the highest in our dissolution studies) were tested, but the data were spurious and could not be fit to exponential curves. This may have been due to polymer entanglement at high concentration, which is problematic during scattering measurements. Thus, a lower concentration of 0.001M PASP was tested for both molecular weights (3,000 and 10,000). Four samples were tested, one for each molecular weight at the two different pHs. Data were collected for 10 minutes during each run, and three runs were performed for each sample. Average values for \mathcal{D} and R_H were calculated from the three experiments.

3.4 Data analysis

For each rotating disk dissolution experiment, total and free calcium concentrations ($[Ca]_T$ and $[Ca^{2+}]$) were plotted versus time as shown in Figure 3.6. The data below represent calcite dissolution in 0.01M Pasp (10,000 Mw) at 1200 rpm and pH 5.

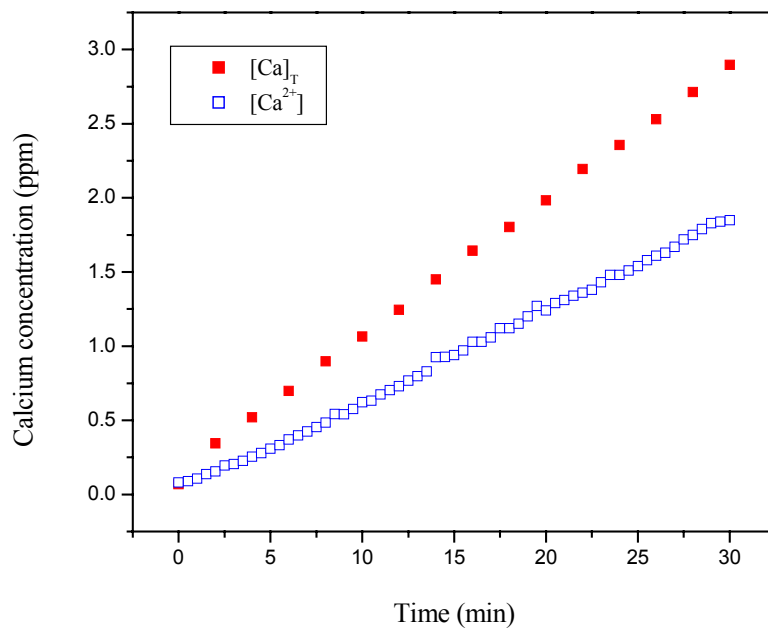


Figure 3.6. Experimental dissolution rate with free and total calcium concentration as a function of time.

The experimental dissolution flux, J_{exp} , was then calculated directly from the initial slope of total calcium concentration over time.

$$J_{exp} \text{ (mol/m}^2\text{-s)} = \frac{V}{\pi D^2/4} \left(\frac{d[Ca]_T}{dt} \right)_{t=0} \quad (3.3)$$

where V = volume of reaction vessel, D = average diameter of marble disk as measured using a caliper, $[Ca]_T$ = total calcium concentration in bulk solution.

Dissolution rates were calculated using only the linear portions of the total calcium data. Below $pH \sim 8$, concentration profiles were linear over the extent of experiment (30-60 minutes), whereas at high pH , $[Ca]_T$ values began to level off after 15-20 minutes. This leveling off may have been due to changes in calcite surface morphology or the accumulation of an adsorbed layer of PASP on the calcite surface during interfacial dissolution. To eliminate these effects, dissolution rates at high pH (10) were calculated using linear slopes over the first 10-15 minutes of dissolution (see Appendix C.1).

As explained in the theory, the relationship between dissolution rate and the square root of rotating speed yields information about the governing mechanisms for calcite dissolution. Therefore, experimental dissolution rates are presented as a function of $\omega^{1/2}$ over a range of rotating speed (150-1500 rpm) and covering three orders of magnitude of PASP concentration (0.001 - 0.1M). The same graphs are also presented for water containing 0.2M KCl. Experiments are highly reproducible (see Appendix C.2) since disks were finely polished and initial rates were used to avoid discrepancies due to possible changes in surface morphology. Small sources of error in the experimental data include non-uniform disk polishing, limited sensitivity of the AA spectrometer and instability of the AA flame.

CHAPTER IV – RESULTS AND DISCUSSION

Section 4.1 includes the manuscript entitled “Dissolution of Calcite Using Environmentally Benign Polyaspartic Acid: A Rotating Disk Approach” as submitted to *Langmuir* for publication. A comprehensive discussion of the calcite dissolution studies is presented in the paper. The development of a theoretical model to predict calcite dissolution kinetics in aqueous PASP solution is also described in the paper. Section 4.2 includes additional results from rotating disk studies that demonstrate the role of PASP as a calcium complexing agent. Results from DLS, measuring the polymer size and diffusion coefficient at different conditions, are shown in section 4.3. HPLC results and additional SEM images are included in Appendix A.1 and A.2, respectively.

4.1 Dissolution of Calcite Using Environmentally Benign Polyaspartic Acid: A Rotating Disk Approach

INTRODUCTION

Motivation

The accumulation of calcium mineral deposits on metal surfaces causes significant problems with equipment inefficiency and costs associated with repair and maintenance. Because of the inverse solubility of calcium at elevated temperatures, calcium salts precipitate from aqueous streams during many processes, particularly in the dairy industry, and in other systems such as petroleum oil wells and sedimentation basins [1,2]. These deposits reduce the efficiency of heat exchangers and cooling towers, and often obstruct the fluid flow of oil in pipes during oil recovery procedures. As the global costs for alleviating these fouling problems are enormous, the demand remains for effective cleaning formulations.

Traditionally, strongly acids such as hydrochloric and sulfuric acids have been used in calcium scale removal applications. In previous years, inorganic additives were employed as corrosion and scale inhibitors in numerous fields, but were gradually replaced by organic materials such as organic phosphates and phosphonates [3, 4]. Due to environmental concerns, less toxic materials were investigated for scale inhibition and removal, including polyacrylic acid and polyamines [3]. However, polyacrylic acid and its derivatives are not biodegradable, and are unsuitable for the environment due to their persistence. Deposit removal formulations have also employed chelating agents, which readily dissolve metals by forming water-soluble metal complexes via multiple coordinative bonds. Some common chelants that have been studied for calcium mineral dissolution include EDTA (ethylenediaminetetraacetic acid), acetic acid and citric acid. However, acetic and citric acids do not form highly stable complexes with calcium, and while EDTA has proven to be an extremely successful calcium chelant, there are environmental concerns about heavy metal mobilization in ground water sources and non-biodegradability.

In recent years, a non-toxic, environmentally benign polymer, polyaspartic acid, has been identified as a possible “green” alternative to traditional calcium cleaning agents [3,5,6, 7,8]. Donlar Corporation was awarded the 1996 Presidential Green Chemistry Challenge Award for developing environmentally safe thermal polyaspartate for use as a scale inhibitor for calcium carbonate, calcium sulfate and barium sulfate [3]. In a variety of tests, commercial polyaspartates of 3,000-30,000 molecular weight met criteria for ready biodegradability, the most stringent measure of biodegradability [9]. PASP is currently used in various applications, including as a dispersing agent in detergent and

paint formulations, and as an antiscalant in oil recovery platforms and agricultural fertilizers [6,10]. In this study, we will look specifically at the role of PASP in the dissolution of calcite and will investigate the mechanisms of this process.

Mechanisms of Dissolution

Calcite dissolution in various aqueous media has been shown to be limited by one or both of the following mechanisms: 1) reactions occurring at the interface between the liquid and solid deposit, and 2) mass transfer of reacting and/or product species between the bulk solution and the solid mineral surface [1,11,12,13,14]. It is reported that both in the absence and presence of cleaning agents, calcite dissolution in aqueous solutions is generally controlled by mass transport under acidic conditions, by interfacial reactions under basic conditions, and by a combination of the two at intermediate pHs [1,2,14,15,16,17]. However, calcite dissolution proceeds via different mechanisms in the presence of water, acidic species and complexing agents.

Rotating disk studies, which allow mass transfer control under well-defined hydrodynamics, have demonstrated that in the pH range 3-6.2, the dissolution of calcite in water is controlled by both the flux of hydrogen to the calcite surface and the reaction of water with calcite at the solid-liquid interface [15]. In solutions of KCl, dissolution was found to be diffusion-limited below pH ~4-5.5 and influenced by interfacial kinetics above this pH [14,18]. Rotating disk experiments have also determined that calcite dissolution in HCl, a strong acid, is governed by the rate of H⁺ transport [11]. In the presence of acetic acid, a weak acid, the calcite dissolution rate is dependent on the transport of reactants to the interface, the kinetics of the surface reaction, and the transport of products away from the interface [1]. The thermodynamics of the reversible

surface reaction were found to significantly influence the overall rate of dissolution due to the surface dissociation of the weak acid. Additional rotating disk studies have shown that dissolution of calcite using chelating agents such as EDTA and citrate are diffusion-controlled at low pH and reaction limited at high pH [1,2]. The rate of dissolution in chelating agents depends on the stability of the metal-chelate complexes formed during dissolution.

The goal of the present research is to evaluate the role of environmentally benign polyaspartic acid (PASP) in enhancing the dissolution of calcite and to determine the influence of mass transport on dissolution. PASP is an effective calcium chelant, and has been shown to both inhibit crystallization of calcium salts and to promote dissolution of calcium minerals under various conditions [19,20,21,22]. A study done by our group investigated the effect of PASP on the dissolution of calcium phosphate minerals DCPD and HAP/DCPD under turbulent flow conditions. Dissolution was enhanced at alkaline pHs over a wide range of PASP concentrations and at low pHs from moderate to high PASP concentrations [8]. It was concluded that PASP accelerates the rate of calcium phosphate removal via calcium sequestration during the interfacial dissolution step.

In a separate study by our group, batch dissolution experiments involving calcium carbonate powder further demonstrated the ability of PASP as an effective sequestrant for CaCO_3 [20]. PASP was found to increase the rate of CaCO_3 dissolution as compared to the rate in water over a range of pH and PASP concentration. However, as hydrodynamics in a batch system are not well-characterized, it is difficult to resolve the mechanism of dissolution for this case. Combining results from previous batch experiments and current rotating disk studies will enable a complete analysis of the

contributions of surface reaction and mass transfer to the overall rate of calcite dissolution. This approach will also allow the calculation of an enhancement factor to quantify the effect of PASP on dissolution rate. However, it is first necessary to understand the fundamentals of transport, PASP chelation chemistry and polymer configuration in order to develop a comprehensive picture of the dissolution process.

THEORY

Mass Transport

The following expression describes the diffusive flux ($J_{M.T.}$) of a reacting species to the surface of a rotating disk under laminar flow ($Re < \sim 3 \times 10^5$ [23]) through the solution of the Navier-Stokes and Continuity equations [2,24,25]:

$$J_{M.T.} = \left[\frac{0.62048 Sc^{-2/3} (\omega \nu)^{1/2}}{1 + 0.2980 Sc^{-1/3} + 0.1451 Sc^{-2/3}} \right] (C_b - C_i) = k_m (C_b - C_i) \quad (4.1)$$

where Schmidt number, $Sc = \nu/D$, ν and D are the kinematic viscosity and effective diffusion coefficient of the reacting species (e.g. H^+ or H_mL), and ω is the rotating speed of the disk. This solution is valid for high Schmidt numbers, large reaction vessel volume, and negligible disk edge effects. These criteria are maintained in the current work.

In this expression, the flux is proportional to a concentration gradient ($C_b - C_i$) and an overall mass transfer coefficient, k_m . It is important to note the dependence of the flux on the square root of ω , the rotating speed. For systems where the rate of mass transport

is the rate-limiting step, the overall rate of dissolution is equal to the mass flux, and is therefore linearly dependent on $\omega^{1/2}$. However, for regimes where dissolution is dominated by reaction kinetics, the dissolution rate is independent of ω .

Chelation Chemistry

Polyaspartic acid serves as a calcium chelating agent by forming stable, water-soluble complexes through coordination bonds with calcium ions. Functional groups located along the polymer chain surround calcium ions and extract them from the salt crystal lattice in a secure metal-ligand complex. The chelating ability of PASP arises from the presence of the carboxyl groups in each polymer segment, as illustrated in the structure of PASP (Figure 4.1).

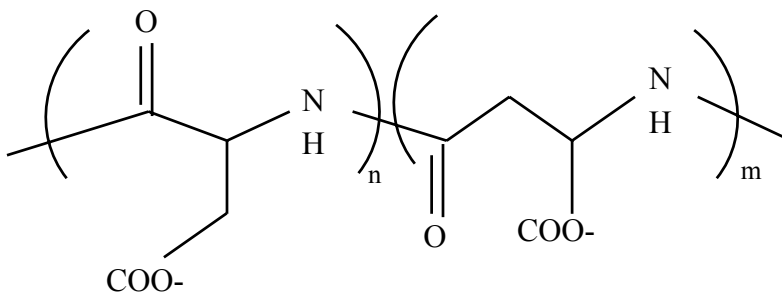


Figure 4.1. Structure of Polyaspartate.

Figure 4.1 represents two repeating segments, n and m, of polyaspartate, which are randomly distributed along the backbone of the polymer. The total number of units will depend on the molecular weight. For instance, there are approximately 72 segments in a 10,000 (weight average) molecular weight sodium-polyaspartate (Na-PASP) chain,

and 22 segments in a 3,000 M_w Na-PASP chain for an equivalent molecular weight of 137 for each segment. Thus, the overall chelating ability of the species will be a function of molecular weight. It has been reported that the most effective range of PASP molecular weight for calcium scale inhibition is 1,000-4,000 M_w [9]. Therefore, this study will compare the dissolution efficiencies for 3,000 and 10,000 M_w PASP products.

A hypothetical “effective chelating unit” of PASP is modeled as four residues, consisting of four carboxyl groups. This is related to the titration chemistry of PASP, where deprotonation occurs gradually through many consecutive dissociation steps. Silverman et. al [26] discovered that it is possible to accurately model the deprotonation of PASP as a series of four subsequent dissociation steps, by assuming four pK values. Thus, using this model of four pK values, the species distribution plot in Figure 4.2 was constructed from data of titration experiments done in our group [20].

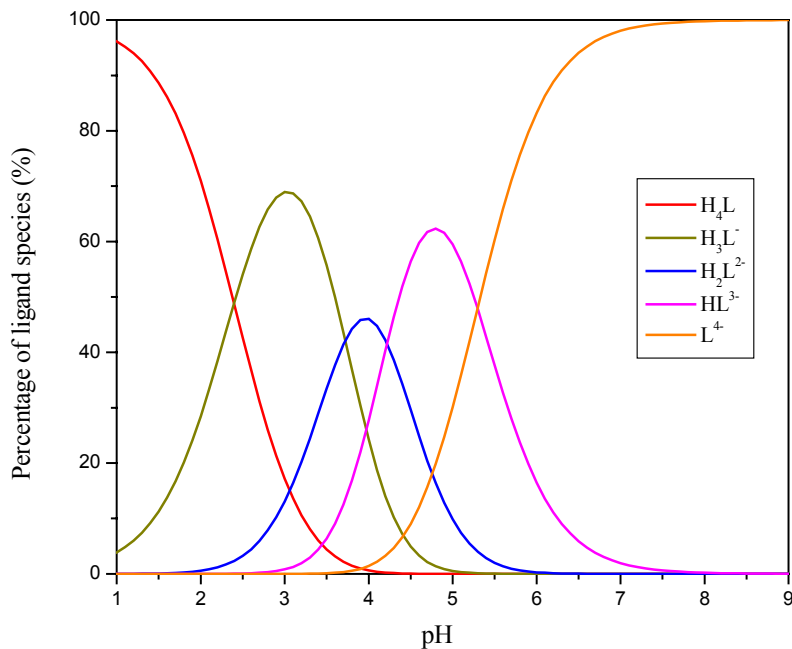


Figure 4.2. Theoretical PASP species distribution plot [20].

Figure 4.2 illustrates that at a specific pH, there are multiple polymer species present in solution. The behavior of these individual species and their cooperative influence on the rate of dissolution is crucial to understanding the dissolution process. Therefore, calcium-polyaspartate chelation chemistry is important in investigating the mechanisms of dissolution. Table 4.1 summarizes the PASP dissociation and complexation reactions that occur during calcite dissolution.

Table 4.1. Polyaspartic acid dissociation and calcium complexation reactions.

| PASP Dissociation: ($K_{A,m}$) | - log K_{eq} (25°C) |
|---|---|
| $H_4L \leftrightarrow H^+ + H_3L^{-1}$ | 2.27 [*] , 2.2 ⁺ |
| $H_3L^{-1} \leftrightarrow H^+ + H_2L^{-2}$ | 3.60 [*] , 3.6 ⁺ |
| $H_2L^{-2} \leftrightarrow H^+ + HL^{-3}$ | 4.09 [*] , 4.3 ⁺ |
| $HL^{-3} \leftrightarrow H^+ + L^{-4}$ | 5.17 [*] , 5.4 ⁺ |
| Calcium-Polymer Complexation: ($K_{B,m}$) | |
| $Ca^{+2} + L^{-4} \leftrightarrow CaL^{-2}$ | 3.02 [*] , 2.88 ^{**} |
| $Ca^{+2} + HL^{-3} \leftrightarrow CaHL^{-1}$ | 2.55 [*] , 2.47 ^{**} |
| $Ca^{+2} + H_2L^{-2} \leftrightarrow CaH_2L$ | 2.16 [*] , 2.14 ^{**} |

^{*} Values for 10,000 Mw PASP determined by Wu and Grant [20].

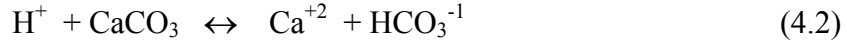
^{**} Values for 3,000 Mw PASP determined by titration experiments in this work.

⁺ Values for 9,200 Mw PASP determined by Silverman et. al. [26].

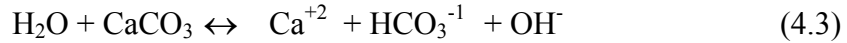
In Table 4.1, $K_{A,m}$ are theoretical pK values of PASP and $K_{B,m}$ represent binding constants for calcium-polymer complexation. These values are important for calculating interfacial reaction rates during calcite dissolution at various pH's. Combining this information with mass transport rates calculated from rotating disk results will enable a theoretical prediction of overall calcite dissolution in PASP. To investigate the effect of pH on interfacial dissolution, we evaluate the dominant PASP species and significant reactions that occur for three representative pH conditions.

In general, one or a combination of the following reactions dominates calcite dissolution in aqueous PASP solution, depending on pH.

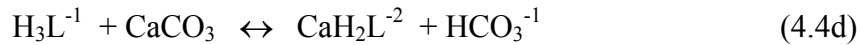
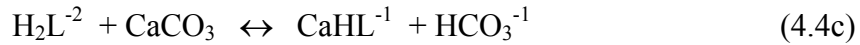
Proton attack:



Water attack:



Ligand attack:



Reaction (4.2) is significant at low pH (below \approx pH 4-5), while the water (4.3) and ligand (4.4) reactions dominate at higher pH values [2,14,15,16,17]. The contribution of each ligand reaction (4.4a-d) depends on the polymer species distribution (Figure 4.2), which is also closely related to pH.

pH 10

Above pH \sim 6, according to the species distribution plot, the primary free PASP species in solution is L^{-4} . Thus, at pH 10, reactions (4.3) and (4.4a) dominate the interfacial dissolution process. The individual contributions of the two reactions to the overall dissolution rate will depend on the concentration of PASP ligand, with the water reaction dominating at low PASP concentration and the ligand reaction dominating at high PASP concentration.

Since calcite dissolution in aqueous media is generally controlled by interfacial reaction kinetics at high pH, reactions (4.3) and (4.4a) are considered the rate-determining steps. With this in mind, a model has been developed to predict the dissolution of calcite in PASP at pH 10, where the overall rate of reaction (r_T) is the sum of the rates of the water (r_w) and ligand (r_L) reactions:

$$r_T = r_w + r_L \quad (4.5)$$

where r_w and r_L are given by:

$$r_w = k_w \theta_c \theta_a (1 - [\text{Ca}^{2+}]_{(i)} [\text{CO}_3^{2-}]_{(i)} / K_{sp}) \quad (4.6)$$

$$r_L = k_L K_L \theta_c \theta_a ([\text{L}^4]_{(i)} - [\text{CaL}^{2-}]_{(i)} [\text{CO}_3^{2-}]_{(i)} / K_{eq}) \quad (4.7)$$

In equations 4.6 and 4.7, k_w and k_L are the surface reaction rate constants for water and ligand with calcite, and K_L is the adsorption equilibrium constant for PASP ligand. θ_c and θ_a are the fraction of cationic and anionic adsorption sites, respectively. K_{sp} is the solubility product for calcium carbonate, and K_{eq} is the product of K_{sp} and the Ca-L binding constant, $K_{B,1}$. Equations 4.6-4.7 are derived from Langmuir-Hinshelwood adsorption kinetics, following the work of Fredd and Fogler [2] and Wu and Grant [20].

At steady state, the net rate of reaction is equal to the rate of calcium transport from the interface to the bulk. This is expressed as:

$$r_T = k_m ([\text{Ca}]_{T,i} - [\text{Ca}]_{T,b}) \quad (4.8)$$

where $[\text{Ca}]_{T,i}$ and $[\text{Ca}]_{T,b}$ are the interfacial and bulk concentrations of total calcium concentration, respectively. Solving equations 4.5-4.8 simultaneously using equilibrium values from Table 4.1 and literature [1], model parameters for reaction rate constants and ligand adsorption equilibria may be calculated to yield a theoretical dissolution rate. A comparison of the model to experimental rate data are included in the results section.

pH 5

At pH 5, the principal polymer species in solution (see Figure 4.2) are HL^{-3} (60% of total PASP) and L^{-4} (30%), with H_2L^{2-} constituting the remainder (10%). Thus, in the presence of these species, reactions (4.4b) and (4.4c) begin to influence the dissolution rate, in addition to reactions (4.3) and (4.4a). Furthermore, at this lower pH, the reaction between hydrogen and calcite (4.2) becomes important, and dissolution is partly limited by the mass transport of H^+ . Consequently, it is not trivial to predict dissolution behavior at pH 5, where various interfacial reactions as well as mass transfer play a role in calcite dissolution.

pH 3.5

The dominant forms of PASP ligand at pH 3.5 are H_3L^{-1} (56% of total ligand species) and H_2L^{2-} (33%). In this regime, dissolution is again complicated by the presence of several polymer species which each react with calcium. Dissolution is strongly dependent on the rate of H^+ transport as well as the mass transport of chelating species to the interface. As with pH 5, the numerous equilibria creates difficulty in calculating the large number of parameters necessary to complete a model for dissolution at pH 3.5.

Polymer Conformation and Adsorption

The rate of mineral dissolution in the presence of PASP is also dependent on the conformation of polymer molecules in solution and at the solid-liquid interface. Solution pH has a strong influence on the solvent conditions, which determine whether the

polymer chains are extended or coiled. Consequently, pH affects the size and configuration of polymer molecules as well as the transport properties of the polymer.

Polymer chain length also affects the transport properties of the molecules. As a general rule, the translational diffusion coefficient, \mathcal{D} , of the polymer is related to molecular weight, Mw as [27]:

$$\mathcal{D} \propto Mw^{-\varphi} \quad (4.9)$$

where φ is a measure of solvent quality and ranges from about 0.5-0.6 for theta to good solvent conditions [27]. Thus, polymer chains of lower molecular weight should diffuse through a solvent faster than those of higher molecular weight.

The extent of polymer adsorption onto a solid surface (e.g. calcite) is also heavily influenced by pH, which governs the swollen or contracted nature of the polymer chains at the interface. Some segments of the polymer may attach to the substrate in a flat configuration, and other segments may protrude from the surface. Studies have shown that adsorption of polyelectrolytes such as PASP onto calcium minerals is generally favorable at low pH [28,29,30,10], and the polyelectrolytes likely adopt a flat conformation on the mineral surfaces. One study demonstrated that PASP adsorbs onto hydroxyapatite (a form of calcium phosphate) in a relatively flat configuration, with train and loop segments [28]. Results from a separate study suggested that PASP adsorbs strongly onto calcite in a flat conformation [31].

Using dynamic light scattering (DLS) techniques, the translational diffusion coefficient, \mathcal{D} , of a polymer in solution can be directly measured under various conditions of pH, polymer concentration and molecular weight. From these experiments, values for \mathcal{D} can be used to estimate the hydrodynamic radius, R_H , the effective size of

polymer chains in solution. R_H indicates how coiled the polymer molecules are in solution including solvent effects. Thus, DLS studies are useful for a qualitative understanding of the dynamic behavior of PASP in solution and at the interface during dissolution.

EXPERIMENTAL METHODS

Materials

Sodium polyaspartate samples (40 wt% solids, >95% purity, pH = 8-9.5) of weight average molecular weights (Mw) 10,000 and 3,000 were provided by Donlar Corporation. Calcium standard solution (0.1M) was obtained from Fisher Scientific for calcium ion electrode calibration. Calcite marble of 96% purity (determined analytically in this study) was supplied by the Durham Marble Company. All other reagents and solutions were analytical grade and all water was deionized.

Equipment

Rotating disk studies were performed using a Pine Instruments Rotating Disk apparatus (see Figure 3.5 in chapter 3), equipped with Pine Instrument MSRX Speed Control. The temperature of the waterbath surrounding the polymer solution was controlled using a Fisher Scientific Isotemp Model 730 Immersion Circulator thermostat. Calcium ion (Ca^{2+}) and pH data were measured with a Denver Instrument Model 225 pH/ISE meter (Orion pH probe and calcium Ion Selective Electrode Model 97-20 *ionplus*). Continuous (Ca^{2+}) and pH readings were recorded on a computer using Winwedge software. Total calcium concentrations were determined using a Perkin Elmer AAnalyst 100 Atomic Absorption Spectrometer, operated with AAWinLab software.

Scanning electron images were obtained using a Hitachi 3400 Environmental Scanning Electron Microscope, operated at beam voltages of 4-15 kV. Dynamic light scattering experiments were performed using a 200 megawatt Argon laser light source, Brookhaven Instruments PMT 9836 photomultiplier detector positioned at a scattering angle of 90°, and Brookhaven Instruments 9000 AT correlator and software (9kdls version 2.15) for data acquisition.

Method

Calcite disks were prepared based on techniques described in earlier research [1,2,12,15]. In summary, disks were cut to 3.2 cm diameter and 1.5 cm thickness from a marble core and polished to 3,000 mesh surface smoothness using 150, 300, 600, 1,000 and 3,000 mesh (8 μ m) polishing disks successively. To isolate the top surface of the disks for solution exposure, the sides of the disks were coated with a polystyrene-CCl₄ solution. The disks were attached to the rotor shaft by gluing a magnetic insertion piece to the bottom of the disks using an epoxy resin. All disks were rinsed with DI water prior to experimentation.

Polyaspartic acid solutions (0.001 M, 0.01 M and 0.1 M) were prepared by diluting sodium polyaspartate (40 wt % stock solution) to 800 mL total volume using DI water. KCl was added to maintain a constant solution ionic strength (I) of 0.2 M. Solutions without polymer also contained KCl for constant I. Upon stirring and allowing the mixture to reach ambient temperature, solution pH was adjusted manually via dropwise addition of HCl or NaOH.

A beaker containing the polymer solution was placed in a water bath maintained at 25 \pm 0.5°C, and the calcite disk was then immersed into the solution to a height of

approximately 4 cm from the bottom of the reaction vessel to avoid edge effects. The pH and Ca^{2+} ISE electrodes were then placed in the solution for bulk measurements. The disk was rotated at the desired speed between 150 and 1500 rpm (equivalent to $3.8 \times 10^4 < \text{Re} < 3.8 \times 10^5$) for 30-60 minutes. Bulk fluid samples were obtained every 2 minutes using a 2 mL syringe and were subsequently analyzed for total calcium concentration using the Atomic Absorption Spectrometer.

Profiles for total calcium concentration and free calcium concentration were plotted as a function of time. Dissolution rates were calculated directly from the initial linear slopes of the total calcium concentration plots.

RESULTS AND DISCUSSION

Governing Mechanisms of Calcite Dissolution at Different pHs

Dissolution results are divided into three pH regimes (pH 10, 5 and 3.5) corresponding to a study of the different dominating polymer ligand species in solution. According to equation 4.1, plotting dissolution rate versus $\omega^{0.5}$ yields information about the governing mechanisms for calcite dissolution. These graphs are shown in Figures 4.3, 4.6 and 4.7 for dissolution at pH 10, 5, and 3.5, respectively, over the range of rotating speeds (150-1500 rpm) and spanning three orders of magnitude of polymer concentration (0.001-0.1M). Results are also shown for water containing 0.2 M KCl. Experiments are highly reproducible since disks were finely polished and initial rates were used to avoid discrepancies due to possible changes in surface morphology.

pH 10

Dissolution rates at pH 10 (Figure 4.3) are presented for water, three concentrations of 10,000 Mw PASP, and an intermediate concentration of 3,000 Mw PASP at low, intermediate, and high ω values. A non-linear relationship between rate and $\omega^{0.5}$ is observed for each concentration of PASP, indicating that dissolution is governed primarily by the reactions at the solid-liquid interface. These reactions involve a series of adsorption and surface complexation reactions between calcium and PASP ligand as described by equations 4.4a-4.4d.

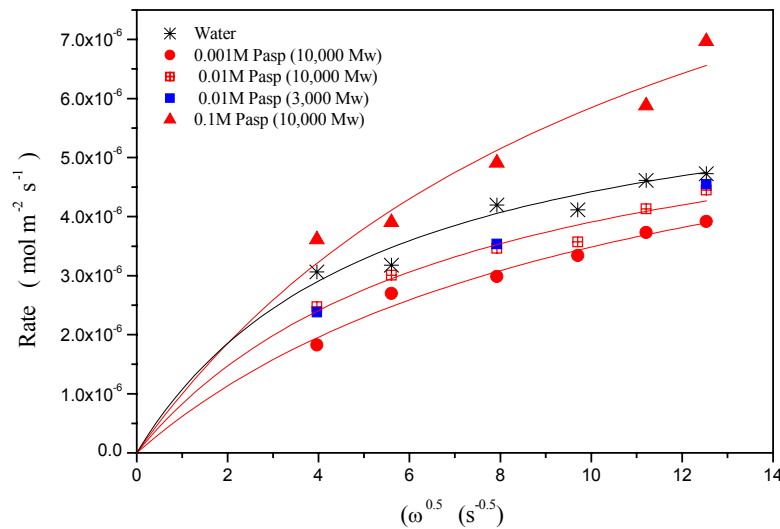


Figure 4.3. Rate of calcite dissolution versus square root rotational speed with and without PASP at pH=10.

At high pH, dissolution is inhibited by the presence of small amounts of PASP, as rates are lower in 0.001 and 0.01 M PASP than in water. However, as PASP concentration increases, the rate exceeds the rate in water, and dissolution is enhanced at 0.1M PASP. This agrees with similar studies of calcite dissolution in dicarboxylic acid

solutions, where dissolution was inhibited at concentrations below $\sim 0.01\text{M}$ [32]. Inhibition was attributed to the blocking of dissolution sites by the adsorbed dicarboxylic acid species. In the presence of acetic acid, which is a weak acidic species like PASP, calcite dissolution was found to be limited by the transport of product species away from the surface [1].

For the case of PASP, dissolution at high pH is limited by each step of the interfacial dissolution process, including adsorption, complexation and desorption. Since calcium minerals typically adopt a negative surface charge due to OH^- adsorption at pHs $> 9.0\text{-}9.5$ [33], adsorption of anionic PASP molecules is relatively slow, resulting in a low interfacial ligand concentration, $[\text{L}]_i$. Consequently, the ligand reaction with calcite (equation 4.7) is inhibited, generating a small amount of Ca-PASP product, $[\text{Ca}]_{\text{T},i}$. The low interfacial concentration of calcium product is not sufficient to drive the transport of species to the bulk (equation 4.8). Thus, dissolution is inhibited until a high enough surface concentration of PASP is attained.

Interfacial limitations to dissolution are further supported by dynamic light scattering (DLS) results obtained in this study. From DLS experiments, the diffusion coefficients of 3,000 and 10,000 Mw PASP were measured as $6.4 \times 10^{-6} \text{ cm}^2/\text{s}$ and $5.0 \times 10^{-6} \text{ cm}^2/\text{s}$, respectively, corresponding to hydrodynamic radii of 0.34 nm and 0.53 nm, respectively. While the values for \mathcal{D} seem rather high and those for R_{H} seem rather low for polymer molecules, they are reasonable due to the presence of added salt in solution, which screens coulombic interactions between charged polymeric species [27,36]. The ionic strength of 0.2 M used in the dissolution and DLS experiments could account for the collapse of polymer chains, leading to large diffusion coefficients. These

high \mathcal{D} values suggest that molecules are transported rapidly to the calcite interface, such that mass transfer is not a rate limiting step. Also, the extremely low values of R_H imply that the PASP chains are tightly coiled in solution, which may lead to loop and tail configurations at the interface. These conformations are not favorable for strong adsorption. On the other hand, it is also possible that R_H is much smaller than the radius of gyration, R_g , which is a measure of the polymer size based on the center of mass. If this is the case, a large R_g would suggest that water flows freely through the polymer coils, meaning that water is a good solvent for PASP and the chains are actually extended. In a good solvent, it is favorable for the molecules to remain in solution, so that adsorption requires a large amount of energy. In either case, the DLS results indicate that dissolution at pH 10 is controlled by interfacial interactions, including the adsorption process.

In addition, rates are comparable for 3,000 and 10,000 Mw at pH 10. This is because dissolution is not largely dependent on diffusion, but rather depends on the surface reaction kinetics. Comparing values for the calcium binding constants of 3,000 and 10,000 Mw PASP from Table 4.1, it is apparent that the extent of complexation is similar for the two molecular weights. Therefore, under surface reaction control, the polymer molecular weight has a negligible effect on the overall rate of dissolution.

Comparisons of theoretical and experimental rates at pH 10 are shown in Figure 4.4. The solid diagonal line represents a perfect correlation between calculated and experimental dissolution rates. Theoretical data were calculated from the model previously described, and agree closely with experimental data. The model adequately predicts dissolution rates at high pH over the range of ω , PASP concentration and

molecular weight studied. The model is consistent with surface reaction rate constants of $9.6 \times 10^{-6} \text{ mol min}^{-1}$ and $9.33 \times 10^{-5} \text{ mol min}^{-1}$ for k_w and k_L , respectively, and adsorption equilibrium constants of $2.8 \times 10^2 \text{ dm}^3 \text{ mol}^{-1}$ and $2.9 \times 10^5 \text{ dm}^3 \text{ mol}^{-1}$ for K_L and K_{CaL} , respectively (see Table 4.2). The parameter K_{CaL} appears in the calculation of θ_c in Equations 4.6 and 4.7 [20]. Adsorption equilibrium constants for other species included in θ_c and θ_a were estimated from literature as $K_{Ca} = 1000 \text{ dm}^3 \text{ mol}^{-1}$, $K_{CO_3} = 3 \times 10^4 \text{ dm}^3 \text{ mol}^{-1}$, and $K_{OH} = 700 \text{ dm}^3 \text{ mol}^{-1}$ [34].

Table 4.2. Model parameters for calcite dissolution in PASP solutions (pH=10).

| $k_w \text{ (mol min}^{-1}\text{)}$ | $k_L \text{ (mol min}^{-1}\text{)}$ | $K_L \text{ (dm}^3 \text{ mol}^{-1}\text{)}$ | $K_{CaL} \text{ (dm}^3 \text{ mol}^{-1}\text{)}$ |
|-------------------------------------|-------------------------------------|--|--|
| 9.6×10^{-6} | 9.33×10^{-5} | 2.8×10^2 | 2.9×10^5 |

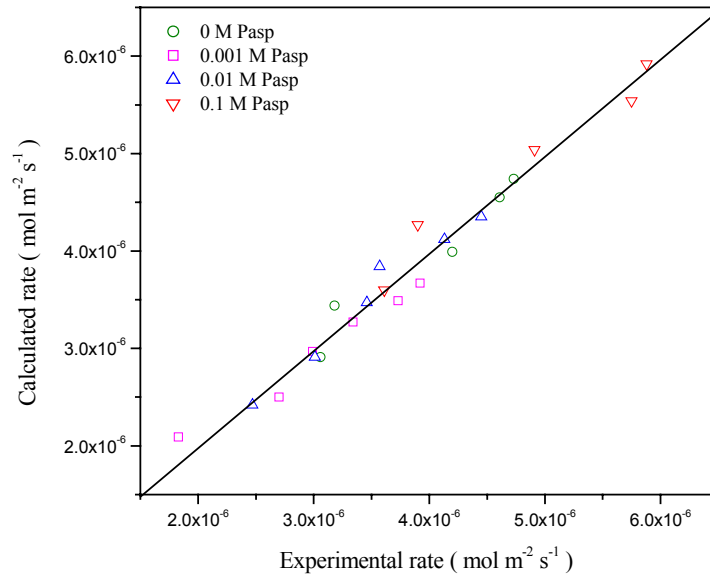


Figure 4.4. Theoretical versus experimental dissolution rate at pH=10.

Using the same model, contributions of the competing water and ligand reactions with calcite at pH 10 were determined and are presented in Figure 4.5. As shown in the graph, at high PASP concentration, the ligand reaction dominates dissolution, whereas at low PASP concentration, the water reaction with the surface is dominant.

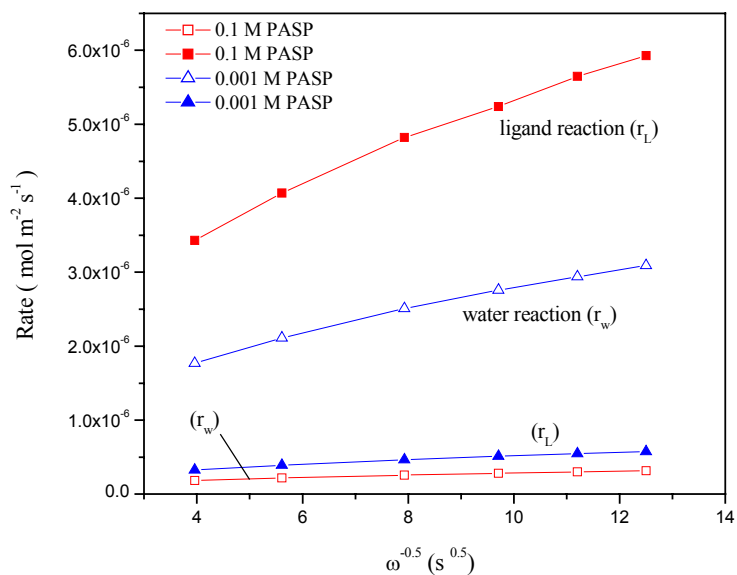


Figure 4.5. Theoretical contributions of PASP ligand (r_L) and water (r_w) reactions to dissolution at pH 10 calculated from Equations 4.6 and 4.7.

pH 5

Rotating disk results for pH 5 (Figure 4.6) are shown for both molecular weights at all concentrations except the lowest (0.001M), where the two molecular weights exhibit nearly identical dissolution curves. Dissolution is enhanced in the presence of PASP for both 0.01 and 0.1M concentrations, and is comparable to the rate in water for 0.001M PASP.

The linear dependence of the rate on $\omega^{0.5}$ at concentrations of 0, 0.001 and 0.01M PASP demonstrates mass transfer control under these conditions. This implies that dissolution is governed by the rate of H^+ and PASP diffusion to the solid-liquid interface, which agrees with literature reports that calcite dissolution is generally diffusion limited at low pH. At high PASP concentration (0.1M), the non-linear correlation between rate and $\omega^{0.5}$ suggests additional limitations due to interfacial reaction.

This transition to a more surface reaction limited regime is likely related to adsorption. At low pH (<6), calcium minerals adopt a positive surface charge [33]. Thus, it is likely that adsorption of PASP onto calcite is rapid due to electrostatic interactions between the carboxyl groups of PASP and the positively charged calcite surface. At low and moderate concentrations of PASP, the polymer molecules adopt a flat configuration on the calcite surface. However, as the ligand concentration increases, polymer segments begin to adsorb along the surface in more loop and tail arrangements, slowing the rate of adsorption and forming a thicker diffuse layer through which calcium product species must be transported.

Dissolution proceeds more rapidly in solutions of 3,000 molecular weight PASP than 10,000 Mw. Since dissolution is limited primarily by mass transport at this pH, dissolution is enhanced as the diffusion coefficient of the reactant increases (larger \mathcal{D} increases k_m). Referring back to Equation 4.9, the diffusion coefficient of a polymer species is inversely proportional to the molecular weight ($\mathcal{D} \sim Mw^{-\phi}$). Thus, smaller molecules (i.e. lower Mw or tightly coiled chains) travel faster to the calcite interface than larger molecules, thereby increasing the rate of dissolution. In addition, interfacial dissolution is faster for lower Mw species, because adsorption is energetically favored for smaller chains. Using atomic force microscopy, Sikes and Wierzbicki [35] determined that the energy required for PASP molecules to bind to calcite was approximately twice as large for chains with 45 residues than those with only 15 monomer units. Therefore, adsorption of 3,000 Mw PASP is stronger than adsorption of 10,000 Mw species.

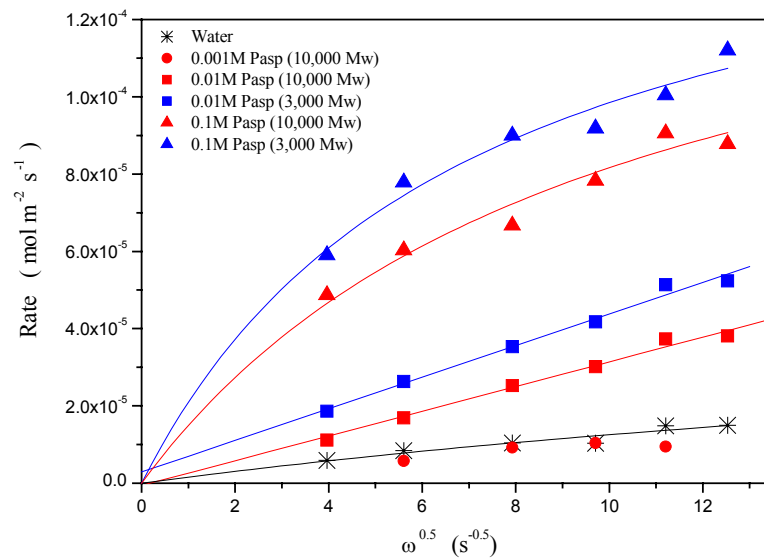


Figure 4.6. Rate of calcite dissolution versus square root rotational speed with and without PASP at pH=5.

pH 3.5

Dissolution rates at pH 3.5 (Figure 4.7) are shown for water, three concentrations of 3,000 Mw PASP, and the intermediate concentration (0.01M) of 10,000 Mw PASP. Since trends for the two molecular weights at 0.01M are similar, data for 0.001M and 0.1M 10,000 Mw PASP are also expected to follow curves similar to 3,000 Mw PASP, as they do at pH 5 (Figure 4.6). This is verified by the data at 300 and 900 rpm for 0.1M 10,000 Mw PASP, which lie directly below the same data for 3,000 Mw PASP, indicating comparable dissolution behavior at the high concentration.

At this pH, dissolution proceeds on a much faster time scale than at pH 5 and 10, and dissolution rates are 1-2 orders of magnitude higher than for pH 10. PASP increases the rate of calcite dissolution compared to the rate in water for all concentrations, even at 0.001M. At zero and 0.001M PASP, dissolution is mass transfer limited. At the middle

concentration (0.01M), the slight curvature of the rate vs. $\omega^{0.5}$ plot indicates that while mass transport is still a limiting mechanism, interfacial phenomena also begin to influence dissolution. As PASP concentration increases to 0.1M, the non-linear nature of the data illustrates the increasing role of surface interaction.

Finally, 3,000 Mw PASP results in higher rates of dissolution than 10,000 Mw, owing to the faster diffusion of lower molecular weight species. This is consistent with our DLS results, where the diffusion coefficients for 3,000 Mw and 10,000 Mw PASP were measured as $2.8 \times 10^{-6} \text{ cm}^2/\text{s}$ and $7.7 \times 10^{-7} \text{ cm}^2/\text{s}$, respectively, at pH 3.5. From these values, R_H was calculated as 0.79 nm and 3.20 nm for 3,000 Mw and 10,000 Mw PASP, respectively.

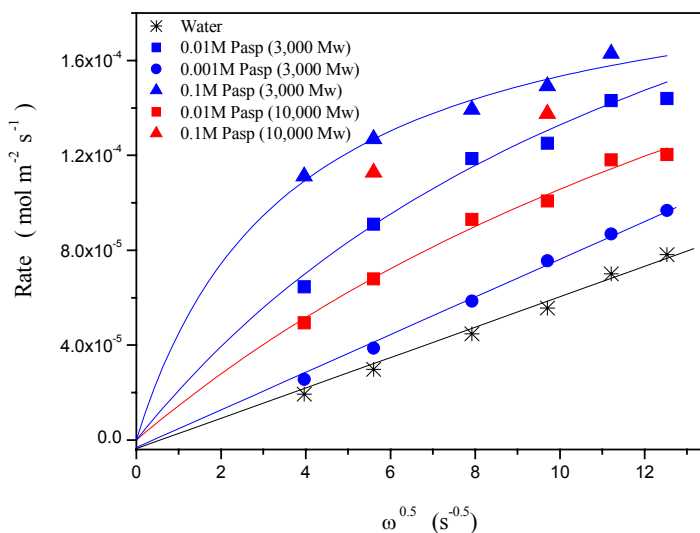


Figure 4.7. Rate of calcite dissolution versus square root rotational speed with and without PASP at pH=3.5.

The influence of polymer concentration on dissolution rate is illustrated in Figures 4.8 and 4.9 for dissolution at 1200 and 300 rpm. At pH 3.5 (Figure 4.8), as PASP concentration increases, the rate of dissolution increases and begins to level off at the highest concentration. Thus, PASP promotes dissolution over the range of concentrations studied here. The rate levels off at 0.1M PASP because the reaction process begins to influence dissolution, and the polymer chains begin to adsorb in more loops and tails at high concentration. In contrast, at pH 10 (Figure 4.9), a minimum in the dissolution rate is observed at 0.001M PASP and above this concentration the rate increases until dissolution is enhanced at 0.1M PASP. In this pH regime, PASP inhibits dissolution at low concentrations and promotes dissolution at high concentrations. This is similar to the behavior of citrate in calcium phosphate dissolution studies [8,22,37].

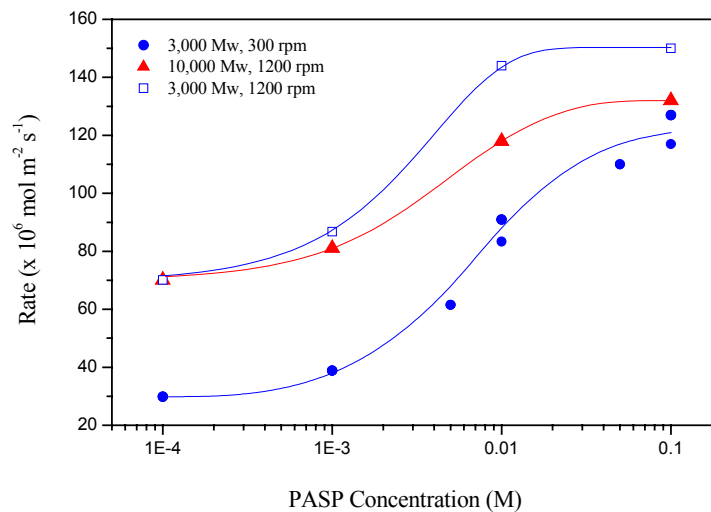


Figure 4.8. Rate versus PASP concentration at pH 3.5.

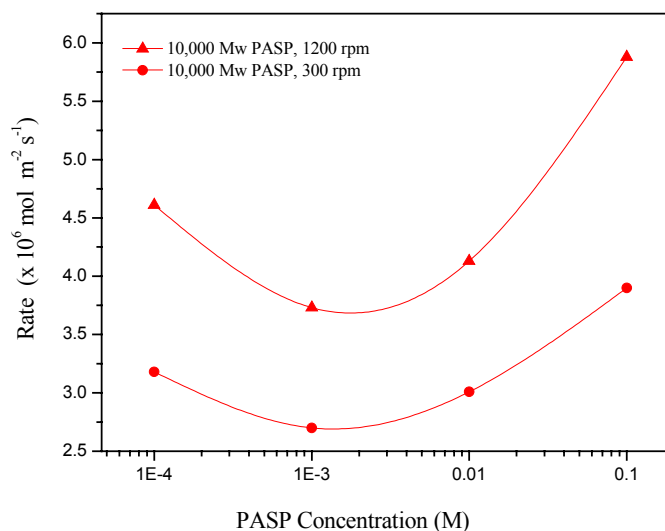


Figure 4.9. Rate versus PASP concentration at pH 10.

Proton-promoted versus Ligand-promoted Dissolution

The overall effect of pH on dissolution in PASP is demonstrated in Figure 4.10 for various molecular weights and concentrations of polymer, with smoothed fit lines of the data to show trends. The dominant polymer species at each pH region are represented below the graph to illustrate the effect of chelation chemistry on dissolution. The rate of dissolution is greatest at pH 3.5 and decreases with higher pH, both in the presence and absence of PASP. Interestingly, a local maximum in the rate is observed at pH 5 for both Mw at the highest concentration of polymer. This maximum rate occurs in the pH region where HL^{3-} and L^{4-} are the principal PASP species. Since dissolution at pH 5 in high PASP concentration is limited by both mass transfer and surface reaction kinetics (Figure 4.6), the mixture of HL^{3-} and L^{4-} yields an optimal combination for H^+ transport, acid attack and ligand attack.

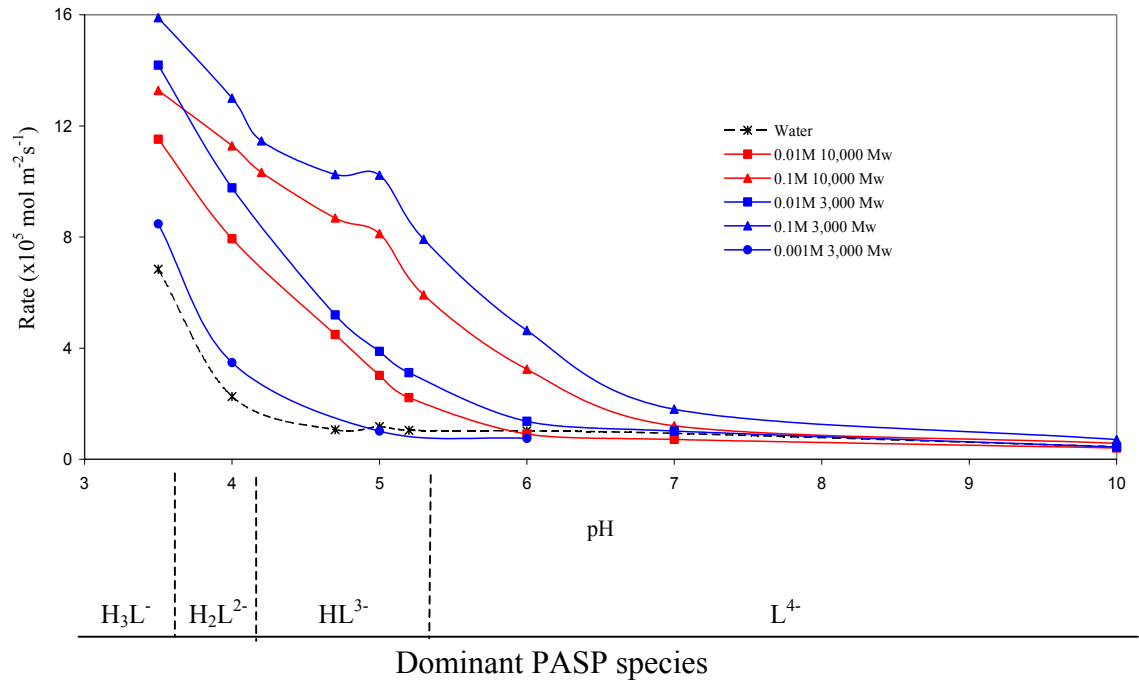


Figure 4.10. Rate of dissolution over pH range in absence and presence of PASP.

Calcite dissolution in the presence of polyaspartic acid occurs via different mechanisms at high and low pH conditions. In the proposed overall mechanism (Figure 4.11), the polymer species H_mL^{m-4} ($m=3$ in this example, but will depend on pH) travels from the bulk fluid to the interface and subsequently dissociates at the calcite surface, generating H^+ and deprotonated ligand ($H_{m-1}L^{m-5}$). As a result, free calcium, bicarbonate and calcium-polymer complexes are formed during interfacial reaction. If the Ca-PASP complex is unstable, it collapses in the bulk fluid to release Ca^{2+} and free polymer ligand species. In this case, the principal role of PASP is proton transport and dissociation. However, if the complex is stable, it remains in solution and the primary function of PASP is chelation.

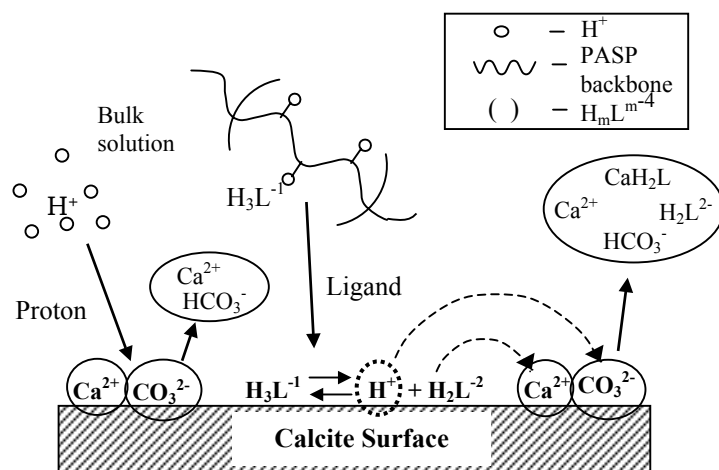


Figure 4.11. Mechanisms of calcite dissolution in the presence of PASP.

In Figure 4.12a, plots of calcium concentration versus time from dissolution studies at pH 10 show that while total calcium increases, bulk Ca^{2+} remains at nearly zero, indicating that all calcium in solution is bound to PASP. At this pH, the dominant polymer species in solution is L^{4-} . Since the Ca-PASP binding constant is largest for L^{4-} , this is the most stable metal-ligand complex. Thus, the dissolution of calcium at high pH (>7) is chiefly promoted by complexation.

Comparing this to Figure 4.12b for dissolution at pH 3.5, we observe that the free calcium concentration is equal to the total calcium concentration, indicating that all calcium is unbound as Ca^{2+} . At this pH, PASP is predominantly in the form of H_3L^- and H_2L^{2-} , which have lower binding constants with calcium than L^{4-} . Upon reaction with calcium at the interface, these less stable complexes (CaH_3L and CaH_2L) break up to release Ca^{2+} and free polymer. In addition to the chelation reaction, PASP also provides additional H^+ for reaction (4.1) as it undergoes rapid dissociation at the interface. Thus,

at low pH, calcium dissolution in the presence of PASP occurs via a combination of chelation and acid attack of the calcite surface.

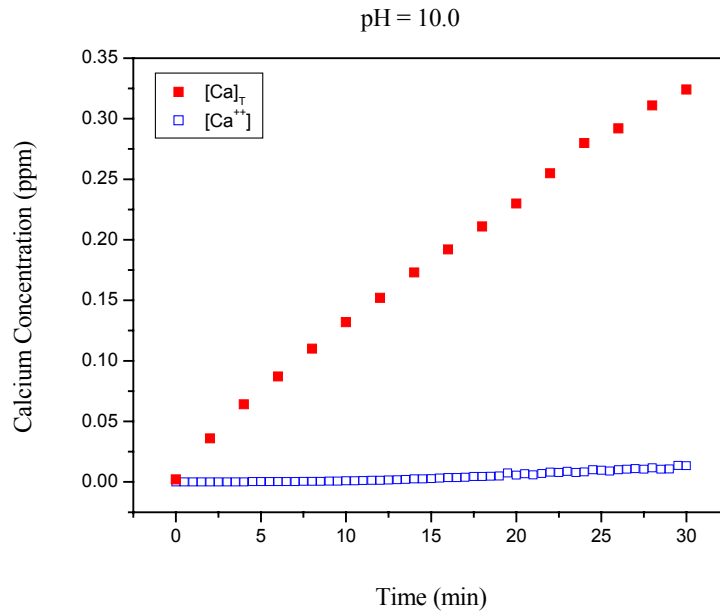


Figure 4.12 (a)

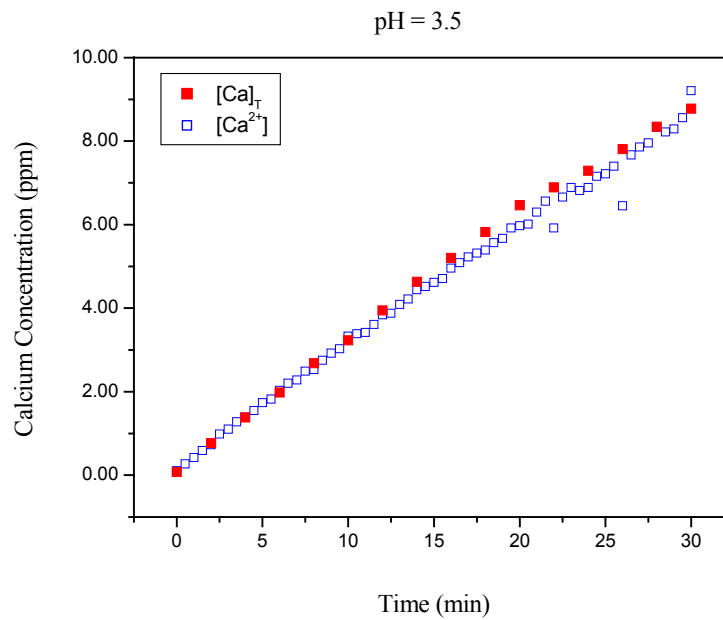


Figure 4.12 (b)

Figure 4.12. Total (Ca_T) and free (Ca^{++}) calcium concentration versus time for dissolution at 1200 rpm in 0.01M PASP 10,000 Mw at a) pH=10 and b) pH=3.5.

To quantify the performance of PASP over a range of pHs, we have defined an enhancement factor, η_{enh} , as the ratio of the rate of dissolution in PASP over the rate of dissolution in water. Figure 4.13 demonstrates that for various conditions of ω , polymer concentration and molecular weight, η_{enh} has a maximum at pH $\sim 4.0 - 4.7$. Similar results are shown for our earlier research on the dissolution of calcium phosphate in PASP (manufactured by Rohm and Haas) under turbulent flow, with a maximum enhancement at pH ~ 5 (Figure 4.14) [22].

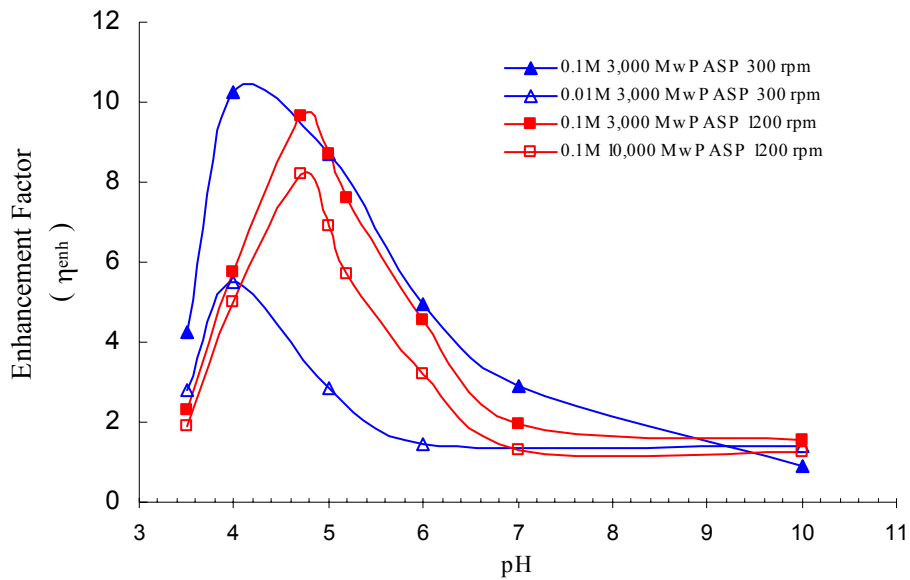


Figure 4.13. PASP enhancement of calcite dissolution.

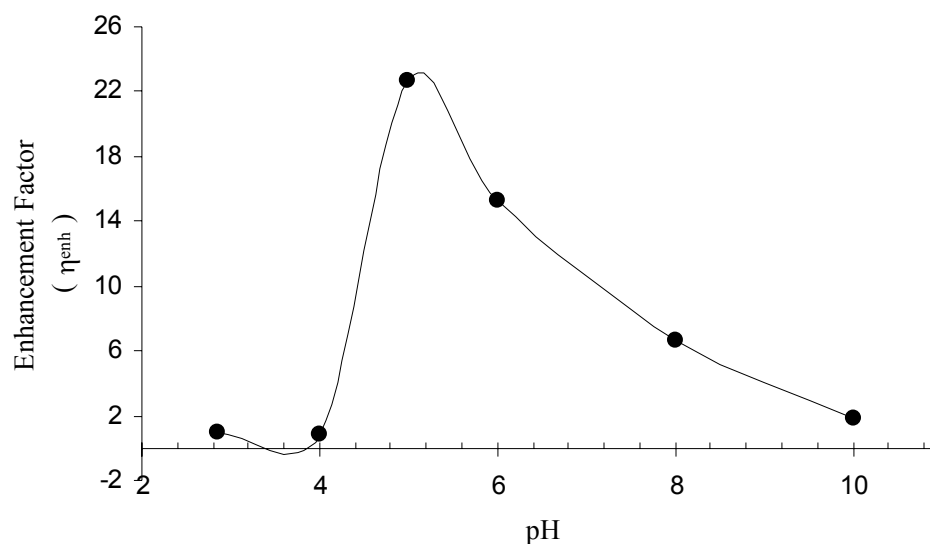


Figure 4.14. PASP enhancement of brushite (DCPD) dissolution for 600 ppm PASP and 1.2 m/s flow rate [22].

Surface Morphology

While the rotating disk is a convenient method for investigating the microscopic features of dissolution, it is also useful to examine the macroscopic characteristics of this process. Scanning electron microscopy is a valuable technique for monitoring the evolution of calcite surface morphology during dissolution, which may reveal information on the interactions of various species (e.g. H^+ and PASP) with the calcite surface during dissolution.

Figures 4.15-4.19 represent scanning electron images of calcite disks taken before and after dissolution both in the presence and absence of PASP. In Figure 4.15, the calcite surface is polished prior to dissolution. In Figures 4.16 and 4.17, at pH 3.5, the calcite surface is relatively smooth and uniform for dissolution without polymer, while the surface resulting from dissolution in PASP exhibits a series of pitted holes. In Figures 4.18 and 4.19, the surfaces are considerably different for dissolution in the

absence and presence of polymer at pH 10. The calcite surface dissolved in PASP solution contains many grooves and deep carvings, where the polymer is assumed to attack dislocation sites.

These images clearly demonstrate that calcite dissolution in the presence of PASP occurs via different mechanisms than dissolution without PASP. The polymer attacks and dissolves the surface in a very different manner than water molecules or H^+ ions, consistent with a surface adsorption-complexation reaction mechanism [2, 20]. Furthermore, Figure 4.19 gives substantial evidence that the ligand reaction with calcite dominates at pH 10 for high PASP concentration, as the surface is significantly more pitted and non-uniform than the surface dissolved in water (Figure 4.18). It is also apparent that the dissolution process depends strongly on pH, comparing images of the calcite surface upon dissolution at pH 3.5 and 10 in the same PASP concentration (Figures 4.17,4.19). This is due to the additional effect of hydrogen ion attack at low pH, similar to that observed by Fredd and Fogler for calcite dissolution in EDTA [2].

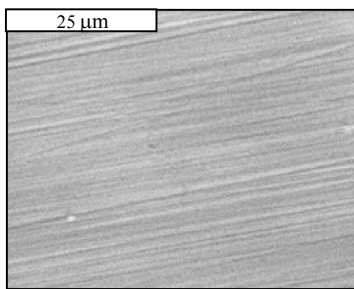


Figure 4.15. Calcite surface prior to dissolution (2000X).

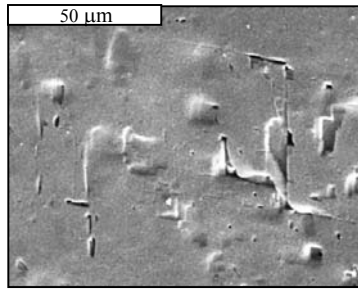


Figure 4.16. Calcite surface after dissolution in 0 M PASP at pH=3.5, 1 hr (1000X).

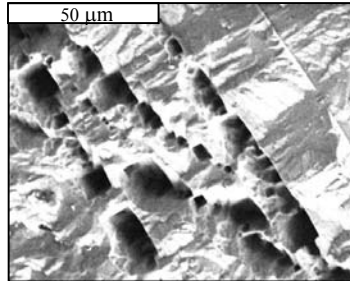


Figure 4.17. Calcite surface after dissolution in 0.1M PASP (3,000 Mw) at pH=3.5, 1 hr (1000X).

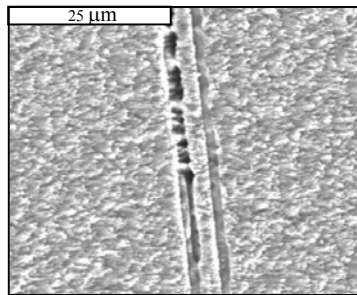


Figure 4.18. Calcite surface after dissolution in 0 M PASP at pH=10, 3.5 hr (2000X).

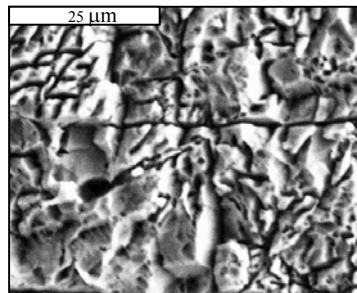


Figure 4.19. Calcite surface after dissolution in 0.1 M PASP at pH=10, 3.5 hr (2000X).

CONCLUSIONS

Calcite dissolution proceeds most rapidly at low pHs both in the absence and presence of polyaspartic acid. At the lowest pH studied here (3.5), dissolution is governed chiefly by the proton reaction with calcite. At the highest pH (10), dissolution occurs via complexation between calcium and the PASP ligand. Between these extremes, a combination of H^+ and ligand reaction with calcite govern dissolution. In addition, dissolution is mainly surface reaction controlled at high pH, and mass transfer limited at low pH, with some interfacial reaction limitations at high PASP concentration. The theoretical model developed in this work further supports the experimental findings at pH 10. The molecular weight of PASP has a more pronounced effect at low pH, where mass transport is the rate-determining step. In this regime, lower molecular weight (3,000) PASP increases the dissolution rate due to its higher diffusion coefficient.

Polyaspartic acid is most effective for calcite dissolution in the range of pHs ~ 4-5, where the enhancement factor, η_{enh} , exhibits a maximum. The parameter η_{enh} is a method to quantify the behavior of the cleaning material in dissolution applications. In the case of PASP, η_{enh} is related to the species distribution and chelation chemistry of PASP as a function of pH. In the pH range for maximum dissolution enhancement, there is an optimal combination of acidic and chelant attack of the calcite surface, as well as enhanced reactant mass transfer. However, over the entire pH range studied, PASP proved an efficient dissolving agent for calcite, and is therefore considered a practical and environmentally friendly alternative to current calcium salt cleaning agents.

ACKNOWLEDGEMENT

We gratefully acknowledge the financial support of National Science Foundation (Grant number CTS-9905152, 9912339) and National Institute of Standards and Technology (NIST), Donlar Biosyntrex Corporation for donating sodium polyaspartate, and Durham Marble Company for supplying calcite marble. We also thank Dr. van Zanten of North Carolina State University, Dr. Lee Yu of NIST, Leah Taylor of University of Missouri, and Drs. Robert Pietrangelo and Grace Fan of Donlar for their technical assistance.

REFERENCES

- ¹Fredd, Christopher and H.S. Fogler. "The Kinetics of Calcite Dissolution in Acetic Acid Solutions." *Chem. Eng. Sci.* **53**, pp. 3863-3874, 1998.
- ²Fredd, Christopher and H.S. Fogler. "The Influence of Chelating Agents on the Kinetics of Calcite Dissolution." *J. Colloid & Interface Sci.* **204**, pp. 187-197, 1998.
- ³Darling, Diana and Rakshpal, Ram. "Green Chemistry Applied to Corrosion and Scale Inhibitors." Corrosion 98 Paper No. 207, 1998.
- ⁴Tomson, M.B. et. al. "Mechanisms of Mineral Scale Inhibition." SPE 74656, Paper presented at Society of Petroleum Engineers Oilfield Scale Symposium in Aberdeen, UK, 30-31 January 2002.
- ⁵Ashley, Steven. "It Isn't Easy Being Green." *Scientific American*, Vol. **286**, Issue 4, p. 32-34, April 2002.
- ⁶Reisch, Marc. "Butting Heads in Polyaspartic Acid." *Chemical & Engineering News Business*, Vol. 80, No. 8, February 25, 2002.
- ⁷Littlejohn, Felicia, Christine Grant and Eduardo Saez. "Mechanisms for the Removal of Calcium Phosphate Deposits in Turbulent Flow." *Ind. Eng. Chem. Res.*, Vol. **39**, No. 4, pp. 933-942, 2000.
- ⁸Littlejohn, F., C.S. Grant, E. Saez and Y. Wong. "The Effect of Poly(Aspartic Acid) on the Removal Rates of Brushite Deposits From Stainless Steel Tubing in Turbulent Flow." *Ind. Eng. Chem. Res.*, Vol. **41**, No. 18, pp. 4576-4584, 2002.
- ⁹Ross, Robert and Kim Low. "Polyaspartate Scale Inhibitors- Biodegradable Alternatives to Polyacrylates." *Chemical Treatment, Materials Performance*, Vol. 36, No. 4, April 1997.

- ¹⁰Wang, Xinyu et al. "Dispersion of Barium Titanate With Polyaspartic Acid in Aqueous Media". *Colloids and Surfaces A: Physicochemical and Engineering Aspects*, Vol. **202**, Issue 1, pp. 71-80, March 26 2002.
- ¹¹Lund, Kasper and H.S. Fogler. "Acidization-II. The Dissolution of Calcite in Hydrochloric Acid." *Chem. Eng. Sci.* **30**, pp. 825-835, 1975.
- ¹²Zaihua, Liu and Wolfgang Dreybrodt. "Dissolution kinetics of calcium carbonate minerals in H₂O-CO₂ solutions in turbulent flow.", *Geochimica et Cosmochimica Acta*, Volume 61, Issue 14, July 1997, Pages 2879-2889
- ¹³Liang, Y. and D.R. Baer. "Anisotropic Dissolution at the CaCO₃ (1014)-Water Interface." *Surface Science*, **373** pp. 275-287, 1997.
- ¹⁴Sjöberg, E.L. and David Rickard. "Calcite Dissolution Kinetics: Surface Speciation and the Origin of the Variable pH Dependence." *Chemical Geology* **42**, pp. 119-136, 1984.
- ¹⁵Compton, Richard and Padraig Daly. "The Dissolution Kinetics of Iceland Spar Single Crystals." *Journal of Colloid and Interface Science*, Vol. **101**, No. 1, pp.159-166, September 1984.
- ¹⁶Plummer, L.N., T.M.Wigley and D.L. Parkhurst. "The Kinetics of Calcite Dissolution in CO₂-Water Systems at 5°C to 60°C and 0-1 Atm CO₂." *American Journal of Science*, Vol. **278**, pp. 179-216, February 1978.
- ¹⁷Compton, Richard, Pritchard, Keith and Patrick Unwin. "The Dissolution of Calcite in Acid Waters: Mass Transport Versus Surface Control." *Freshwater Biology* **22**, pp. 285-288, 1989.
- ¹⁸Compton, Richard and Padraig Daly. "The Dissolution/Precipitation Kinetics of Calcium Carbonate: An Assessment of Various Kinetic Equations Using a Rotating Disk Method." *J. Colloid and Interfacial Science*, Vol. **115**, No. 2, February 1987.
- ¹⁹Sikes, Yeung and Wheeler. "Inhibition of Calcium Carbonate and Phosphate Crystallization by Peptides Enriched in Aspartic Acid and Phosphoserine." *Surface Reactive Peptides and Polymer, Inhibition of Crystallization*, American Chemical Society, 1991.
- ²⁰Wu, You-Ting and Christine Grant. "Effect of Chelation Chemistry of Sodium Polyaspartate on the Dissolution of Calcite", *Langmuir*, Vol. **18**, No. 18, pp. 6813-6820, 2002.

- ²¹Littlejohn, Felicia, Eduardo Saez and Christine Grant. "Use of Sodium Polyaspartate for the Removal of Hydroxyapatite/Brushite Deposits from Stainless Steel Tubing." *Ind. Eng. Chem. Res.* **37**, pp. 2691-2700, 1998.
- ²²Littlejohn, Felicia. "Effect of Poly(Aspartic Acid) on Calcium Phosphate Removal From Stainless Steel Tubing Under Turbulent Flow Conditions." PhD Dissertation. North Carolina State University, Raleigh, NC, 1999.
- ²³Lund, Kasper and H.S. Fogler. "Acidization-I. The Dissolution of Dolomite in Hydrochloric Acid." *Chem. Eng. Sci.* **28**, pp. 691-700, 1973.
- ²⁴Levich. *Physicochemical Hydrodynamics*. Prentice-Hall, NJ, 1962.
- ²⁵Newman, John. "Schmidt Number Corrections for the Rotating Disk." *Journal of Physical Chemistry*, Vol. **70**, No. 4, pp. 1327-1328, April 1966.
- ²⁶Silverman et al. "Effect of pH on Corrosion Inhibition of Steel by Polyaspartic Acid." *Corrosion Science*, Volume 51, No. 11, pp. 818-825, 1995.
- ²⁷Doi, Masao. *Introduction to Polymer Physics*. Oxford University Press, 1997.
- ²⁸Tsortos and Nancollas. "The Adsorption of Polyelectrolytes on Hydroxyapatite Crystals." *J. Colloid & Interface Sci.* **209**, pp. 109-115, 1999.
- ²⁹Chang, Han-Chyen, Thomas Wealy and Egon Matijevic. "Interactions of Metal Hydrous Oxides with Chelating Agents: Adsorption on Spherical Colloidal Hematite Particles." *J. Colloid and Interfacial Science*, Vol **92**, No. 2, pp. 469-478, April 1983.
- ³⁰Schaad et al. "Inhibition of Dissolution of Hydroxyapatite Powder by Adsorbed Anionic Polymers." *Colloids and Surfaces A: Physicochemical and Engineering Aspects*, **83**, p. 285-292, 1994.
- ³¹Wierzbicki, Sikes, Madura and Drake. "Atomic Force Microscopy and Molecular Modeling of Protein and Peptide Binding to Calcite." *Calcified Tissue Int.* **54**, pp. 133-141, 1994.
- ³²Compton, Richard and Christopher Brown. "The Inhibition of Calcite Dissolution/Precipitation: 1,2-Dicarboxylic Acids." *J. of Colloid and Interface Science* **170**, pp. 586-590, 1995.
- ³³Holmgren, Wu and Forsling. "Surface Hydration of Aqueous Calcium Minerals as Studied by Fourier Transform Raman and Infrared Spectroscopy." *Spectrochimica Acta* Vol. **50A**, No. 11, pp. 1857-1869, 1994.
- ³⁴Compton, Richard and C. Brown. *J. Colloid Interface Sci.*, Vol. **165**, pp. 445-449, 1994.

³⁵Sikes and Wierzbicki. “Atomic Force Microscopy and Molecular Modeling of Branched and Unbranched Polyaspartate Bound to Calcite and Mica.” *Corrosion Paper* No. **166**, 1997.

³⁶Grosberg and Khoklov. *Statistical Physics of Macromolecules*. AIP Press, NY, 1994.

³⁷Christoffersen. *Crystal Growth*, Vol. **62**, 1983.

4.2 Additional rotating disk results: Calcium complexation as a function of pH

The following results visually demonstrate the gradual transition from proton-promoted dissolution to the ligand-promoted dissolution region. Figures 4.20 - 4.24 show concentration profiles of both total (Ca_T) and free (Ca^{2+}) calcium for dissolution in 0.01M PASP at 1200 rpm for various pH values. At the lowest pH of 3.5 (Figure 4.20), the total and free calcium concentrations are equal, indicating that all calcium species in solution are in the form Ca^{2+} . As pH increases successively to 4, 5 and 6 (Figures 4.21, 4.22, and 4.23, respectively) the amounts of both total and free calcium decrease with increasing pH. However, the gap between $[Ca_T]$ and $[Ca^{2+}]$ widens until at pH 10 (Figure 4.24) there is essentially zero Ca^{2+} in the bulk solution, although there are still small amounts of $[Ca]_T$. This demonstrates that at low pH, dissolution generates unbound calcium ions via acid attack, and at high pH, a large percentage of calcium in the bulk fluid is bound to PASP in a metal-ligand complex that results from chelation.

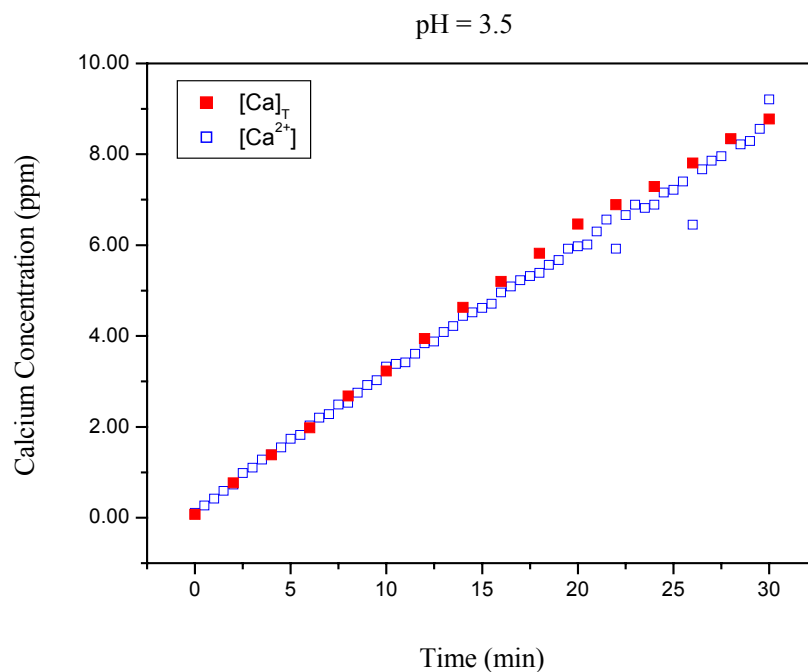


Figure 4.20. Calcium concentration profiles for dissolution in PASP at pH 3.5.

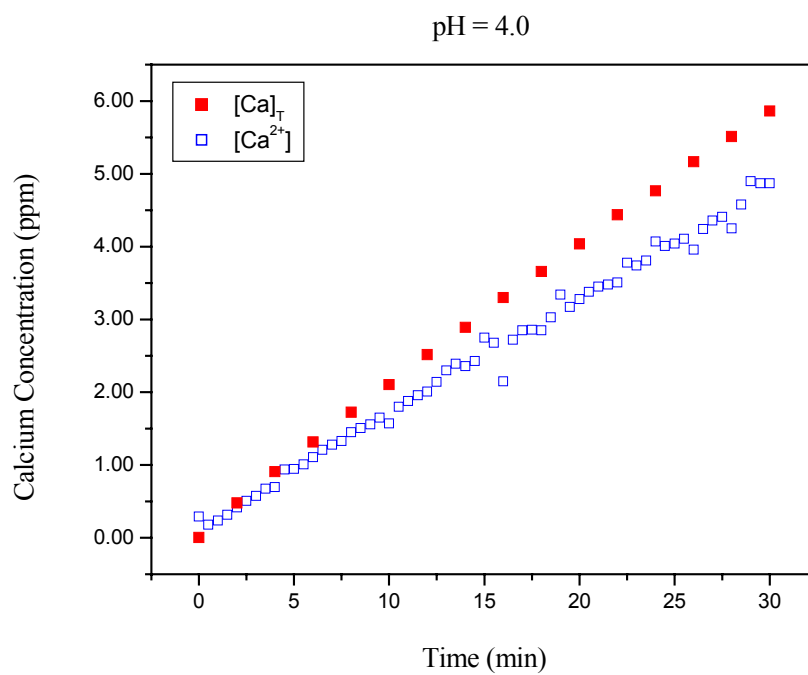


Figure 4.21. Calcium concentration profiles for dissolution in PASP at pH 4.

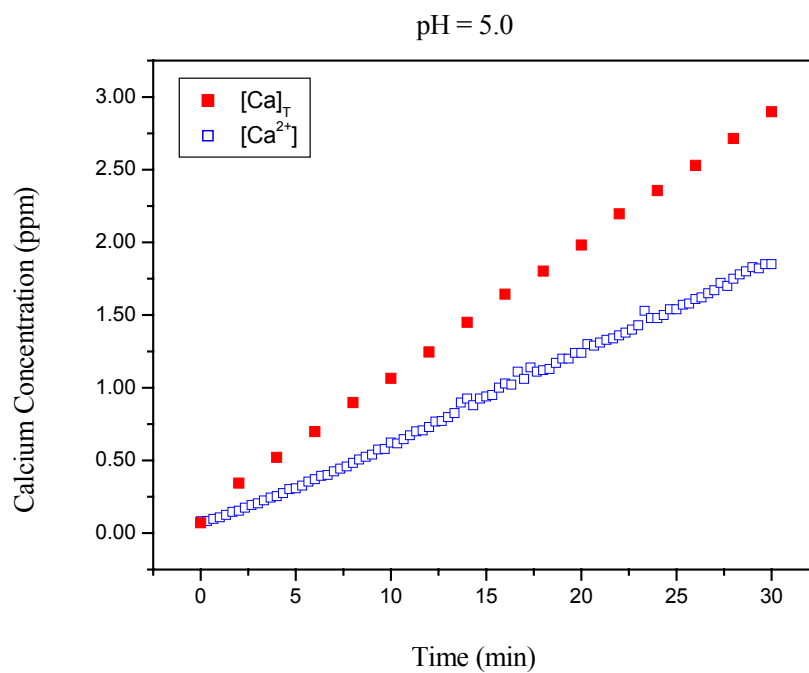


Figure 4.22. Calcium concentration profiles for dissolution in PASP at pH 5.

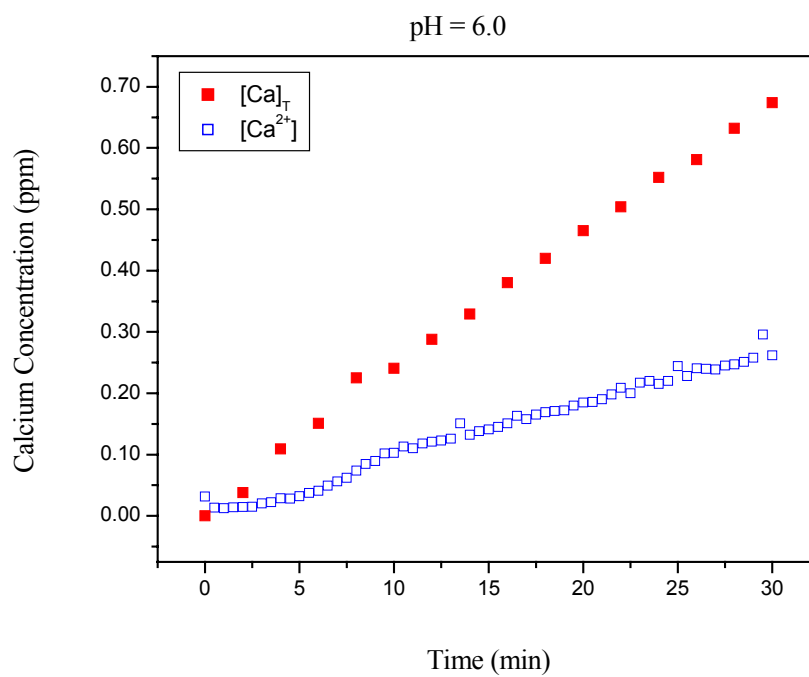


Figure 4.23. Calcium concentration profiles for dissolution in PASP at pH 6.

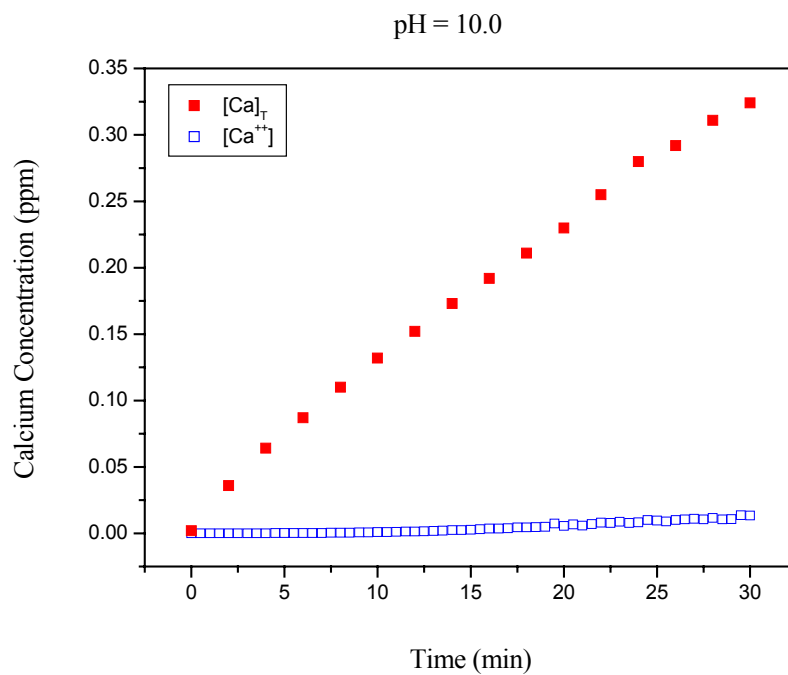


Figure 4.24. Calcium concentration profiles for dissolution in PASP at pH 10.

4.3 *Polymer transport and conformation*

Results from dynamic light scattering are presented in Table 4.3 for 0.001M solutions of 3,000 and 10,000 Mw PASP at pH 3.5 and 10. Diffusion coefficients (\mathcal{D}) were measured directly from DLS experiments, and values for hydrodynamic radii (R_H) were calculated from \mathcal{D} using equation 2.48 in section 2.5.1.

Table 4.3. Summary of dynamic light scattering results.

| | pH 3.5 | | pH 10 | |
|---|---|--|--|--|
| | 3,000 Mw | 10,000 Mw | 3,000 Mw | 10,000 Mw |
| \mathcal{D} (cm ² /s), R_H (nm) (multiple runs) | 2.9x10 ⁻⁶ , 0.75 2.5 x10 ⁻⁶ , 0.86 2.8 x10 ⁻⁶ , 0.77 | 1.1 x10 ⁻⁶ , 1.97 7.4 x10 ⁻⁷ , 2.96 4.7 x10 ⁻⁷ , 4.70 | 6.5 x10 ⁻⁶ , 0.34 6.3 x10 ⁻⁶ , 0.34 | 2.5 x10 ⁻⁶ , 0.86 5.2 x10 ⁻⁶ , 0.42 7.3 x10 ⁻⁶ , 0.30 |
| Average Values: \mathcal{D} (cm ² /s), R_H (nm) | 2.8 x10 ⁻⁶ , 0.79 | 7.7 x10 ⁻⁷ , 3.20 | 6.4 x10 ⁻⁶ , 0.34 | 5.0 x10 ⁻⁶ , 0.53 |

At pH 3.5, the diffusion coefficient is highest for the 3,000 Mw PASP, yielding a smaller hydrodynamic radius for 3,000 Mw than 10,000 Mw PASP. The decrease in \mathcal{D} with increasing molecular weight is consistent with theory (equation 2.49). This also verifies that the rate of mass transport, and thus the overall rate of calcite dissolution, is faster for the lower molecular weight PASP at pH 3.5. At pH 10, the values for \mathcal{D} and R_H are comparable for the two molecular weights. The diffusion coefficients are larger at pH 10 than at pH 3.5, suggesting that mass transport is a relatively rapid process at high pH, where interfacial dissolution is a limiting step. The magnitudes of R_H also indicate the compact nature of the polymer coils in solution at high pH.

The decrease in R_H with higher pH may seem contrary to the predicted behavior. One might expect the polymer chains to swell at high pH due to the electrostatic repulsion between ionized carboxyl groups. At pH 10, 100% of PASP species are in the form L^{4-} , so that the polymer molecules are fully ionized, while at pH 3.5, the dominant form of PASP ligand in solution is H_2L^{2-} . In this case, approximately 50% of the

carboxyl groups are protonated. Hence, the repulsion between negatively charged carboxyl segments is weaker at low pH. However, the PASP molecules are observed to be more coiled at high pH. This is due to the presence of salt, which has a significant influence on polyelectrolyte characteristics in aqueous solution.

In the case of these experiments, the counterions (K^+) from the added salt shield the coulombic interactions between carboxyl units, allowing the molecules to shrink into smaller blobs. Thus, the hydrodynamic radius of PASP at the low concentration studied (0.001M) is very small, even at high pH, where the polyelectrolyte chains would normally extend in the absence of salt. It should also be noted that the polymer dynamics and conformation may be different at higher concentrations (0.1M) due to inter- and intra-polymer interactions.

The small values of R_H at pH 10 may also be attributed to the possibility that the hydrodynamic radius is much smaller than the radius of gyration, R_g , which is a measure of the polymer size based on the center of mass. In such case, R_H gives a somewhat “false” indication of the polymer configuration in solution. If $R_H \ll R_g$, the solvent (water) flows freely through the coils of the polymer chains, resulting in “good” solvent conditions. For this situation, the polymer is actually more extended than the value of R_H suggests.

Although measurements of R_H determined from DLS are related to the configuration of the PASP molecules in solution, the values may be useful for estimating polymer conformation at the calcite interface as well. From literature reports [37-39,41] and results from the current dissolution studies, PASP molecules are believed to adopt a mostly flat configuration on the surface of calcite at low pH's, with more loop and tail

arrangements at high pH's. The flatter, train-like conformation of PASP on calcite at low pH's (<6) may be related to the larger R_H , which allows the chains to stretch out along the calcite surface to facilitate interactions between anionic carboxyl groups of the polymer and cationic sites on the mineral surface. At high pH's (>6), the smaller R_H may lead to a more coiled interfacial configuration, which is preferential due to repulsion between negatively charged carboxyl segments of PASP and the negatively charged calcite surface.

CHAPTER V – CONCLUSIONS AND IMPACT

5.1 Conclusions

In this study, a rotating disk technique was used to determine the mechanisms of calcite dissolution in the presence of environmentally friendly polyaspartic acid (PASP) under controlled mass transfer conditions. Other analytical techniques such as scanning electron microscopy, high performance liquid chromatography and dynamic light scattering were also used to elucidate the role of PASP during mineral dissolution. Dissolution rates were measured at various conditions of pH, rotating speed, and PASP concentration and molecular weight. Finally, a theoretical model was developed to describe dissolution behavior at high pH (=10). Through this research, it was determined that:

- (1) The theoretical model based on a surface adsorption-complexation mechanism for dissolution developed in this work accurately predicts calcite dissolution kinetics in the presence of PASP at alkaline pHs (>7). The model was used to calculate theoretical surface reaction and adsorption equilibrium rate constants for dissolution, and agrees closely with experimental results for dissolution rates at pH 10. Future research and more detailed modeling is required to extend the model to predict dissolution rates at pHs below 7.
- (2) PASP enhances calcite dissolution over the pH range 3.5-10.0 via a combination of calcium chelation and acid attack of the calcite surface.

- (3) An enhancement factor was defined as the rate of dissolution in PASP over the rate of dissolution in water. Using this value to quantify the role of PASP during dissolution, maximum enhancement was observed at pHs around 4.0-5.0.
- (4) Calcite dissolution in the presence of PASP is governed primarily by interfacial phenomena at high pH conditions ($\text{pH} > 7$), and by mass transport at lower pHs ($\text{pH} < 7$). However, for large concentrations of PASP, surface interactions between PASP and calcite additionally influence the dissolution rate at low pHs.
- (5) At the highest pH studied ($\text{pH} = 10$), dissolution is inhibited in the presence of small amounts of PASP (0.001-0.01M), but is enhanced above 0.1M PASP. At the lowest pH studied (3.5), dissolution is enhanced over the entire range of concentrations (0.001-0.1M).
- (5) Molecular weight of PASP has a negligible effect on the dissolution rate at high pH, while dissolution proceeds at a faster rate in 3,000 Mw than 10,000 Mw at low pH.

Polyaspartic acid proved an efficient calcite dissolving agent over the entire range of pHs studied. However, PASP is most effective for calcium dissolution in the range of pHs $\sim 4-5$, where the enhancement factor, η_{enh} , exhibits a maximum. η_{enh} is related to the species distribution and chelation chemistry of PASP as a function of pH. In the pH range for maximum dissolution enhancement, there is an optimal combination of acidic and chelant attack of the calcite surface, as well as enhanced reactant mass transfer. The conformation of the PASP molecules along the calcite surface may also be optimal in this pH range.

Dissolution at high pH (=10) involves a surface adsorption-complexation mechanism, where the water reaction with calcite dominates at low PASP concentrations and the ligand reaction with calcite dominates at high PASP concentrations. The rates of polymer adsorption and complexation are limited at low PASP concentration, and dissolution is inhibited in the presence of small amounts of PASP. High concentrations of PASP promote the surface reaction between calcium and ligand, such that dissolution is enhanced by PASP. The model for dissolution at $\text{pH} > 7$ is consistent with the experimental findings at pH 10.

At low pH (3.5-5), dissolution occurs primarily via acid attack at carbonate sites. Dissolution is enhanced in the presence of PASP at low and high concentrations, due to the increased surface concentration of H^+ as PASP dissociates at the calcite surface. At intermediate pHs, a combination of H^+ and ligand reaction with calcite governs dissolution.

The molecular weight of PASP has a more pronounced effect at low pH, where mass transport is the rate-determining step. In this regime, lower molecular weight (3,000) PASP increases the dissolution rate due to its higher diffusion coefficient. Dissolution rates are comparable for the two molecular weights at high pH, where dissolution depends strongly on the rate of surface reaction. The binding constants of 3,000 and 10,000 Mw with calcium are nearly equal, thus the rate of surface reaction is similar for the two molecular weights.

5.2 Impact

The findings of this research are valuable for application in industrial and domestic cleaning formulations. The results of the thesis demonstrate that polyaspartic

acid is an effective calcite dissolving agent that may be used in a variety of applications, including scale removal and inhibition in industrial cleaning practices and oil recovery procedures, and as an additive in household detergents. The primary advantage of PASP over other cleaning agents is that it is a ready biodegradable, non-toxic material, and can be manufactured in an environmentally benign manner that does not require hazardous solvents or catalysts. In present times, growing environmental concerns and stricter environmental laws shift the demand toward 'green' materials and processes. Thus, PASP has a strong potential to replace conventional agents in many mineral scale dissolution and inhibition applications. While the cost of PASP production may need to become more commercially competitive in order to replace materials such as polyacrylates, EDTA and NTA in current cleaning formulations, the environmental benefits of PASP are major incentives for the use of PASP in industry.

CHAPTER VI – RECOMMENDATIONS FOR FUTURE WORK

Although it has been demonstrated that PASP is an effective calcite dissolving agent over the range of conditions studied here, further research is necessary to investigate the fundamentals of interfacial interactions between calcium and polyaspartate. Within this scope, it would be useful to study details of adsorption, complexation and transport during dissolution. The following actions are recommended to improve the current dissolution experiments and to continue with future studies:

- In order to determine the effectiveness of various ligand species for calcium sequestration, it is recommended that the development of the HPLC separation unit be completed and the unit be incorporated into the design of dissolution experiments. Using a more efficient column or multiple columns in series, it may be possible to separate various calcium-PASP species prior to AA analysis to determine which ligand species most effectively combines with calcium. Although experimental dissolution rates are higher for 3,000 Mw PASP than 10,000 Mw PASP, it is not known whether this is entirely due to mass transport or if interfacial interactions also play a role. As part of this phase, it may be necessary to resolve problems due to complex instability inside the column.
- When the HPLC system is incorporated into the experimental setup, it would be useful to automate each stage of the dissolution experiment and connect all equipment into a continuous process. This includes implementation of: (i) a pH-

stat device to maintain constant pH in polymer solution during dissolution, (ii) an autosampler to retrieve samples from the bulk solution for total calcium concentration measurement, and (iii) continuous AA analysis, including automatic recording of calcium measurements using the AA software.

- Additional microscopic and spectroscopic techniques may also be helpful for investigating the details of PASP adsorption onto calcite at the interface. Atomic force microscopy (AFM) studies may reveal the configuration of PASP chains along the calcite surface during dissolution. Some preliminary AFM work with calcite-PASP is being done at the University of Wyoming in collaboration with our group. These experiments are not being performed at NCSU because AFM required atomically smooth surfaces, i.e. cleaved crystals, for imaging. Fourier Transform Infrared (FTIR) spectroscopy, which has been used to study adsorption of surfactants onto mineral surfaces, may also be useful for interfacial studies. FTIR, coupled with Fourier Transform- Raman (FT-Raman) spectroscopy, may be an effective method for analyzing surface adsorption mechanisms.
- In future studies, it would also be helpful to model dissolution kinetics using Monte Carlo computer simulations. A powerful computer model would facilitate the prediction of dissolution behavior under a wide variety of conditions and could be extended to predict dissolution rates for other minerals, such as barite, using PASP. Along with calcite, barite is one of the most problematic minerals encountered during oil recovery procedures [3,13]. Thus, there is considerable

interest from oil production companies in the application of environmentally friendly additives for barite dissolution.

REFERENCE MATERIALS

- ¹Fredd and Fogler, "The Kinetics of Calcite Dissolution in Acetic Acid Solutions". *Chem. Eng. Sci.* Vol. 53, No. 22, pp. 3863-3874, 1998.
- ²Lund, Kasper, and H.S. Fogler. "Acidization II. The Dissolution of Calcite in Hydrochloric Acid." *Chemical Engineering Science*, **30**, pp. 825-835, 1975.
- ³Ross, Low and Shannon. "Polyaspartate Scale Inhibitors – Biodegradable Alternatives to Polyacrylates." *Chemical Treatment, MP*, April 1997, pp. 53-57.
- ⁴Darling, Diana and Rakshpal, Ram. "Green Chemistry Applied to Corrosion and Scale Inhibitors." Corrosion 98 Paper No. 207, 1998.
- ⁵Chaberek, Stanley. Organic sequestering agents: a discussion of the chemical behavior and applications of metal chelate compounds in aqueous systems. NY, Wiley, 1959.
- ⁶Downey, Thomas. "Organic Chelating Agents" SOAP and CHEMICAL SPECIALTIES Vol. 42, pp.52-55, February 1966.
- ⁷Kallay, Nikola et al. "Calorimetric investigation of kinetics of solid phase dissolution: calcium carbonate dissolution in aqueous EDTA solution." *J. Colloid & Interface Science* **188**, pp. 68-74, 1997.
- ⁸Tomson, M.B. et. al. "Mechanisms of Mineral Scale Inhibition." SPE 74656, Paper presented at Society of Petroleum Engineers Oilfield Scale Symposium in Aberdeen, UK, 30-31 January 2002.
- ⁹"Application of A 'Green Chemistry' Solution for Squeeze Treatment in Preventing Scale Formation In North Sea Oil Production." Paper presented by Donlar Biosyntrex Corporation at the SPE European Formation Damage Conference in The Hague, Netherlands (May 21-22, 2001) (<http://www.donlar.com/pr-Sep1001.cfm>)
- ¹⁰Reisch, Marc. "Butting Heads in Polyaspartic Acid." *Chemical & Engineering News Business*, Vol. 80, No. 8, February 25, 2002.
- ¹¹Fredd and Fogler. "The Influence of Chelating Agents on the Kinetics of Calcite Dissolution." *J. Colloid & Interface Science* **204**, pp.187-197, 1998.
- ¹²Arbel et al. "Dissolution of Hydroxyapatite by Calcium Complexing Agents." *Journal of Crystal Growth*, **110**, pp. 733-738, 1991.
- ¹³Ross, Robert and Paul Ravencroft. "Biodegradable Multifunctional Oil Production Chemicals: Thermal Polyaspartates." Donlar Corporation (company publication), June 1998.

- ¹⁴Donlar Biosyntrex company website: <http://www.donlar.com/cp-profile.cfm> (November 1, 2001).
- ¹⁵Bain, Douglas, Grace Fan and Robert Ross. "The Use of Polyaspartates for Scale and Corrosion Control in Open Recirculating Cooling Systems." Donlar Corporation, Performance Chemicals. Bedford Park, Illinois.
- ¹⁶Garris, John and C.S. Sikes. "Use of Polyamino Acid Analogs of Biomineral Proteins in Dispersion of Inorganic Particulates Important to Water Treatment." *Colloids and Surfaces A*, Vol. **80**, pp. 103-112, 1993.
- ¹⁷Ashley, Steven. "It Isn't Easy Being Green." *Scientific American*, Vol. **286**, Issue 4, p. 32-34, April 2002.
- ¹⁸Silverman et al. "Effect of pH on Corrosion Inhibition of Steel by Polyaspartic Acid." *Corrosion Science*, Vol. **51**, No. 11, pp. 818-825, 1995.
- ¹⁹Benton, William and Larry Koskan. "Inhibition of carbon dioxide corrosion of metals", *Journal for Cleaner Production*, Vol. **5**, Issue 3, p. 243, 1997.
- ²⁰Wang, Xinyu et al. "Dispersion of Barium Titanate With Polyaspartic Acid in Aqueous Media". *Colloids and Surfaces A: Physicochemical and Engineering Aspects*, Vol. **202**, Issue 1, pp. 71-80, March 26 2002.
- ²¹Wu, You-Ting and Christine Grant. "Effect of Chelation Chemistry of Sodium Polyaspartate on the Dissolution of Calcite", *Langmuir*, Vol. **18**, No. 18, pp. 6813-6820, 2002.
- ²²Littlejohn, Felicia, Christine Grant and Eduardo Saez. "Mechanisms for the Removal of Calcium Phosphate Deposits in Turbulent Flow." *Ind. Eng. Chem. Res.*, Vol. **39**, No. 4, pp. 933-942, 2000.
- ²³Littlejohn, F., C.S. Grant, E. Saez and Y. Wong. "The Effect of Poly(Aspartic Acid) on the Removal Rates of Brushite Deposits From Stainless Steel Tubing in Turbulent Flow." *Ind. Eng. Chem. Res.*, Vol. **41**, No. 18, pp. 4576-4584, 2002.
- ²⁴Littlejohn, Felicia, Eduardo Saez and Christine Grant. "Use of Sodium Polyaspartate for the Removal of Hydroxyapatite/Brushite Deposits from Stainless Steel Tubing." *Ind. Eng. Chem. Res.* **37**, pp. 2691-2700, 1998.
- ²⁵Littlejohn, Felicia. "Effect of Poly(Aspartic Acid) on Calcium Phosphate Removal From Stainless Steel Tubing Under Turbulent Flow Conditions." PhD Dissertation. North Carolina State University, Raleigh, NC, 1999.
- ²⁶Cussler, E.L. Diffusion, Mass Transfer in Fluid Systems, Cambridge University Press, Cambridge, 1984.

- ²⁷Sjöberg, E.L. and David Rickard. "Calcite Dissolution Kinetics: Surface Speciation and the Origin of the Variable pH Dependence." *Chemical Geology* **42**, pp. 119-136, 1984.
- ²⁸Compton, Richard and Padraig Daly. "The Dissolution Kinetics of Iceland Spar Single Crystals." *Journal of Colloid and Interface Science*, Vol. **101**, No. 1, pp.159-166, September 1984.
- ²⁹Plummer, L.N., T.M.Wigley and D.L. Parkhurst. "The Kinetics of Calcite Dissolution in CO₂-Water Systems at 5°C to 60°C and 0-1 Atm CO₂." *American Journal of Science*, Vol. **278**, pp. 179-216, February 1978.
- ³⁰Compton, Richard, Pritchard, Keith and Patrick Unwin. "The Dissolution of Calcite in Acid Waters: Mass Transport Versus Surface Control." *Freshwater Biology* **22**, pp. 285-288, 1989.
- ³¹Liang, Y. and D.R. Baer. "Anisotropic Dissolution at the CaCO₃ (1014)-Water Interface." *Surface Science*, **373** pp. 275-287, 1997.
- ³²Compton, Richard and Padraig Daly. "The Dissolution/Precipitation Kinetics of Calcium Carbonate: An Assessment of Various Kinetic Equations Using a Rotating Disk Method." *J. Colloid and Interfacial Science*, Vol. **115**, No. 2, February 1987.
- ³³Levich. Physicochemical Hydrodynamics. Prentice-Hall, NJ, 1962.
- ³⁴Newman, John. "Schmidt Number Corrections for the Rotating Disk." *Journal of Physical Chemistry*, Vol. **70**, No. 4, pp. 1327-1328, April 1966.
- ³⁵Thompson, D.W. and P.G. Pownall. *J. Colloid and Interface Science* **131**, pp. 74-82, 1989.
- ³⁶Doi, Masao. *Introduction to Polymer Physics*. Oxford University Press, 1997.
- ³⁷Tsortos and Nancollas. "The Adsorption of Polyelectrolytes on Hydroxyapatite Crystals." *J. Colloid & Interface Sci.* **209**, pp. 109-115, 1999.
- ³⁸Wierzbicki, Sikes, Madura and Drake. "Atomic Force Microscopy and Molecular Modeling of Protein and Peptide Binding to Calcite." *Calcified Tissue Int.* **54**, pp. 133-141, 1994.
- ³⁹Addadi et. Al. "Structural and Stereochemical Relations Between Acidic Macromolecules of Organic Matrices and Crystals." *Connective Tissue Research*, Vol. **21**, pp. 127-135, 1989.

⁴⁰Schaad et al. "Inhibition of Dissolution of Hydroxyapatite Powder by Adsorbed Anionic Polymers." *Colloids and Surfaces A: Physicochemical and Engineering Aspects*, **83**, p. 285-292, 1994.

⁴¹Chang, Han-Chyen, Thomas Wealy and Egon Matijevic. "Interactions of Metal Hydrous Oxides with Chelating Agents: Adsorption on Spherical Colloidal Hematite Particles." *J. Colloid and Interfacial Science*, Vol **92**, No. 2, pp. 469-478, April 1983.

⁴²Perkin Elmer Atomic Absorption Spectrometer Instrument Manual.

⁴³Goldstein, Joseph, et. al. Scanning Electron Microscopy and X-Ray Microanalysis 2nd Edition, Plenum Press, NY, 1992.

⁴⁴<http://www-rim.sci.kun.nl/lcl/research/dls/dls.htm>; 19 August 2002.

⁴⁵Kaszuba, Mike. Photon Correlation Spectroscopy Training Manual, February 1, 1998.

⁴⁶Grosberg, A. and R. Khoklov. Statistical Physics of Macromolecules. AIP Press, NY, 1994.

APPENDICES

Appendix A: Additional studies

- A.1. High performance liquid chromatography
- A.2. Scanning electron microscopy

A.1. HPLC

The following includes a paper entitled “Calcium Polyaspartate Separation” written by undergraduate researcher Lucas Revellon as a requirement for independent research course CHE 497 at NCSU for the Fall semester, 2001.

Objective:

The primary purpose of this research was to study the separation of Calcium-Polyaspartate complexes (see Figure A.1.1) such as Ca-PASP1 and Ca-PASP2 using high-pressure liquid chromatography (HPLC) and UV/VIS spectroscopy. In addition, the consistency and efficacy of the column for these experiments were determined. Prior to the separation studies, an efficiency evaluation was performed on the column used in this study. This test was done in order to ensure that the packing and elution times were properly calibrated.

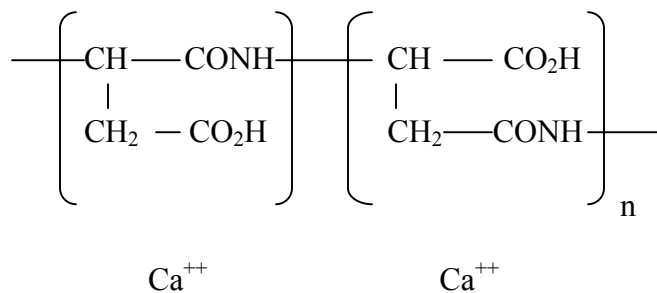


Figure A.1.1. General molecular structure of PASP [1].

Theory:

High-pressure liquid chromatography is unquestionably the most widely used of all analytical separation techniques [1]. The reasons for the popularity of the method are its sensitivity, its ready adaptability to accurate determinations, and its widespread

applicability to substances that are of prime interest to industry, to many fields of science, and to the public. In this study size-exclusion chromatography is used as a primary technique for separations. Size-exclusion is a powerful technique that is applicable to high-molecular weight species [2]. Packings for size exclusion chromatography consist of small ($\sim 10\mu\text{m}$) silica or polymer particles containing a network of uniform pores into which solute and solvent molecules are effectively trapped and removed from the mobile phase. The separation of different components of a sample is directly related to the sensitivity, or efficiency, of the column. Molecules that are larger than the average pore size of the packing are excluded and thus suffer essentially no retention; such species are the first to be eluted. Molecules having diameters that are significantly smaller than the pores can penetrate throughout the pore maze and are thus entrapped for the greatest time; these are last to be eluted.

Once these particles have traveled through the column, they can be detected using an ultra-violet (UV) detector. The eluting sample compound is subjected to the 300 nm wavelength beam of ultra-violet light and the UV detector records the quantity of light that is transmitted through the sample, which is a reflection of the amount of light that the compound absorbs. The UV detector sends its data to a computer, which subsequently signals a “peak” on a chromatogram, which is a record of the absorbance intensity of the eluted compounds. UV detection is positioned immediately after the stationary phase in order to detect the compounds as they elude from the column [2]. The bandwidth and height of the peaks may usually be adjusted (in order to create a more practical scale on the chromatogram) using the coarse and fine tuning controls, and the detection and sensitivity parameters may be controlled. The UV detector measures the ability of a

sample to absorb light. Typical ranges go from 190nm to 1100nm, in our studies PASP absorbs light better at 300nm, therefore the wavelength is set to this value.

Equipment and experimental procedures:

The following are the major instruments used throughout this research:

- Pump: Perkin Elmer series 2000 lc Pump.
- UV/VIS Detector: Spectroflow 783 programmable Absorbance detector, ABI Analytical Kratos Division.
- Column: PL aquagel-OH 30 80 μ m Polymer Laboratories. Use water as the solvent carrier.
- Software: Dynamax for HPLC systems, Macintosh.
- Polyaspartate acid stock solution: 0.1M solution of PASP is made by diluting 3.425 g of PASP to 100 mL with DI water.
- 0.05M mixture of 3,000 Mw and 10,000 Mw PASP and 8 ppm calcium (as used in the rotating disk experiments). This solution was provided by Kathie Burns.

Block flow diagram:

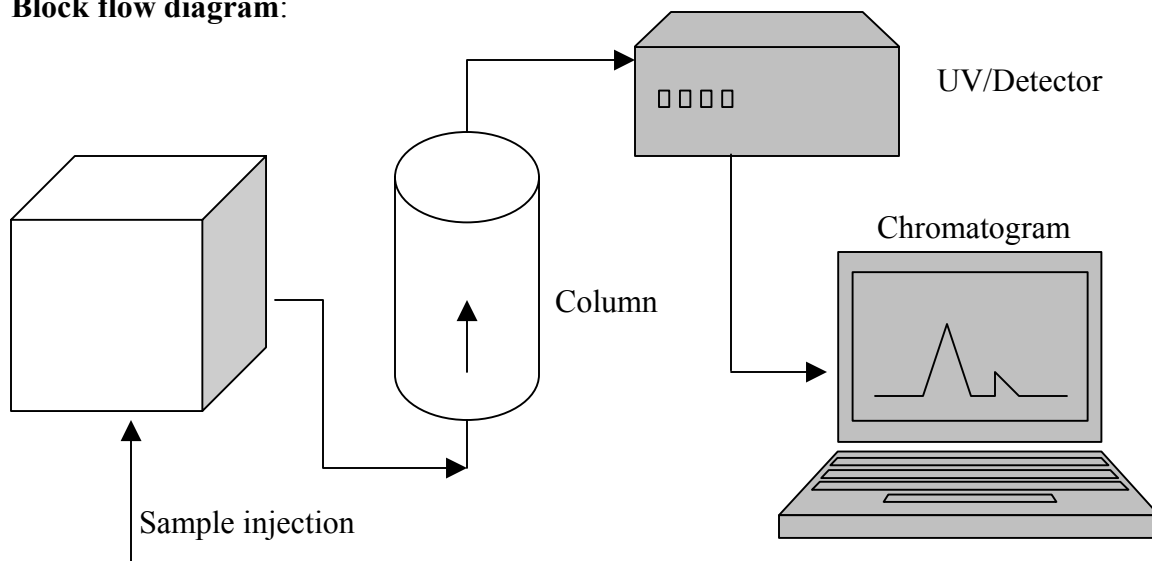


Figure A.1.2 Block flow diagram of HPLC experimental setup.

Procedure:

The column must first be prepared for the injection. This preparation involves rinsing the column with water to remove particles from previous column use, debris, or PASP from previous trials of this experiment. The amount of rinsing that is needed is dependent on the column flow rate, the amount of unwanted material in the column, and the particle size of the material to be rinsed. Adequate rinsing is achieved once the chromatogram no longer reflects any peaks, indicating the column is free of any chemical substances or debris. Rinsing the column in this particular experiment requires approximately two hours using a flow rate of 1mL/min. Once the column is sufficiently rinsed, the pressure in the pump is adjusted so that it will not exceed the operational limit

of the column, which is 2000 psi and 2 mL/min. The flow rate is set to 1 mL/min, which was designated by the column manufacturer as the optimum flow rate.

The UV detector is set to a wavelength of 300nm, which is the optimum absorbance range for the PASP molecule. This value was obtained through previous studies at NIST. In these studies, a sample of PASP was placed in the UV detector cuvette and the sample was exposed to a range of light from 100 nm to 1100 nm.

The software used in this project is called Dynamax; the following are the instructions for the proper operation conditions of the program. Select the icon DA1 (Dynamax), and then select data trace on the toolbar. Under the topic control trace, the chromatogram window will appear. Once manual control is selected from the toolbar, the desired acquisition time can be entered. Subsequently, "Start Acqu" can be selected with simultaneous injection of the solution into the injection port. Before an injection takes place in the system, the injection port must be in the "load" position. The sample is then loaded, and the knob is positioned to the right, or to the "inject" position. Once the sample is in the column, data is collected as the eluate begins to flow. Data reflecting the position of the peaks as a function of time are sent to a computer, which prints the data on a chromatogram.

The peaks produced on the chromatogram can be used to analyze the separation profile of the different molecular weights of PASP (3000 Mw and 10000 Mw) and the column efficiency, since similar molecules require efficient separation by a very sensitive column to make distinctive peaks. The potential effect of calcium ion interaction with the polymer molecules in producing greater separation can also be observed by noting differences in the peak position on the chromatogram following calcium addition.

Results and discussion:

One of the achievements of this project was the determination that consistent results could be obtained using this column. The peak profiles and elution times obtained during research at NIST were consistent with those obtained at NC State. Once it was known that the column was working consistently and the separation profiles were the same, other experiments were performed. Subsequently, several trials were completed in order to determine the interaction of Ca with PASP in solution. The solutions used for this study contain 0.05M of PASP 3000 molecular weight as well as 0.05M PASP 10000 molecular weight. The solutions also contained 8 ppm of free calcium ion, similar to conditions of the rotating disk experiments.

The elution time of the 3000 Mw PASP sample at concentrations of 0.1M, 0.01M, and 0.05M was determined to be approximately 5 minutes after injection in each test. This time was consistent with elution times observed at NIST. Once it was determined that the column was operating consistently, the separation experiments were performed at a flow rate of 1 mL/min. In the separation experiments, elution times for a 1:1 mixture of 0.05M each 3000 and 10000 Mw PASP was measured as approximately 5 minutes as before.

The full separation of the two peaks (3000 and 10000 Mw) was not achieved. This indicates that there is no “lag time” between each peak that is observable using the described experimental design, and as a result, both peaks are integrated into one single curve. Different options (flow rate and pressure change in the system) were implemented in order to prevent such phenomena. However, increasing the flow rate to 2.5 mL/min

and reducing the flow rate to below 1 mL/min failed to produce proper peak separation. None of the changes in the experimental options appeared to affect the amount of peak separation.

Conclusions:

The objective of these experiments was to study the separation of calcium-PASP complexes. In addition, the studies sought to evaluate the effectiveness of the HPLC and UV spectrometry experimental design in order to improve the process for future experiments. Our results were not entirely as expected, but several important conclusions resulted from this research.

First, the experimental trials failed to produce adequate separation of the peaks on a chromatogram to accurately depict the different molecular weight species of PASP present in the mixture. It was hypothesized that the difference in Mw between the 3000 and 10000 Mw PASP species would produce distinct peaks on the chromatogram. Instead of two well-defined peaks, however, the peaks appeared to overlap. The reason for this overlap is unknown, but it may be due to interactions between the two Mw species to produce complexes with an intermediate appearance.

Second, the addition of calcium to the mixture did not appear to mitigate this overlapping effect. It was hypothesized that the addition of calcium would interact with the different Mw species of PASP and affect the separation profile; however, this effect was not observed. Peak profile outcome might be influenced by unexpected interactions of the calcium with the PASP, or less than ideal incorporation of calcium ions with PASP molecules, leaving residual calcium and free PASP. The similarity in Mw of free PASP and Ca-PASP increases the difficulty in separating these molecules. The possibility

remains that a different experimental design may reveal an interaction with calcium that allows separation of the PASP complexes.

In conclusion, further research is needed to fully understand the interaction and separation of Ca-PASP complexes. These studies might be accomplished by changing the parameters of the experimental design. A combination of columns in series, very slow flow rate (perhaps overnight), and a more sensitive packing material may yield adequate column efficiency to produce peak separation. In addition, mass spectrometry studies may be useful in elucidating the relationship of the calcium and PASP molecules. Further research may yield information or increased efficiency of the design so that the resolution and correct separation profile are achieved.

Acknowledgements:

I would like to express my thanks to Dr. Carbonell's Group for allowing me to use their lab and all of their instruments. I would like also to thank Dr. Lee Yu from NIST, who kept in contact with me throughout this research (see correspondence). In addition, I would like to thank Dr. You-Ting Wu and Kathie Burns for their patience and willingness to answer my questions. Finally, I would like to express my most sincere gratitude to Dr. Christine Grant for allowing me to work in her group and for providing me with all the tools and guidance that was needed for this project.

References:

- ¹Stinson, Stephen. "Polyaspartic acid process developed.", *Chemical and Engineering News*, Vol. **70**, No. 29, July 20, 1992.
- ²Skoog, Douglas, and James Lerry. Principles of Instrumental Analysis. 4th edition, Sanders College Publishers, 1992.

A.2. SEM

Figures A.2.1-A.2.20 are scanning electron images of calcite surfaces before and after dissolution with and without polyaspartic acid (PASP). Figures A.2.3 and A.2.4 were obtained in secondary electron (SE) mode at beam voltages of 2-5 kV and the remaining images were obtained in backscattered electron (BSE) mode at voltages of 4-15 kV. Figure A.2.1. shows a polished calcite disk prior to dissolution. Figures A.2.2-A.2.20 are images taken after calcite dissolution at the listed conditions. Several images are shown for the same conditions at different magnifications.

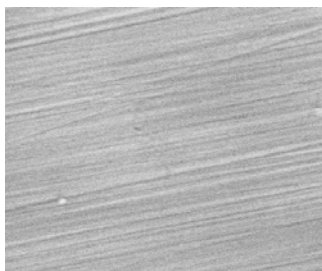


Figure A.2.1. Polished calcite surface before dissolution (x2000).

pH 10

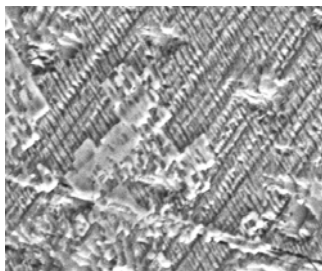


Figure A.2.2.
0 M PASP pH 10, 1200 rpm,
1 hr (x2000)

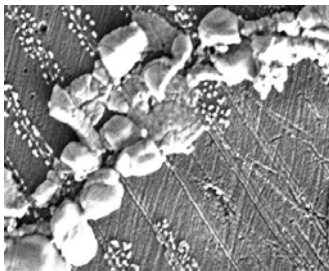


Figure A.2.3.
0.1M 10,000 Mw PASP pH
10, 150 rpm, 0.5 hr (x1000)

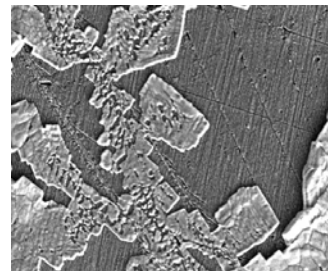


Figure A.2.4.
0.1M 10,000 Mw PASP pH
10, 150 rpm, 0.5 hr (x1000)

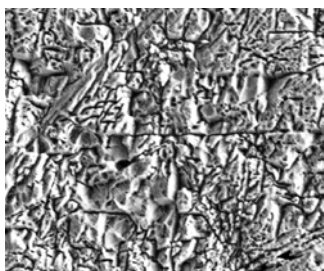


Figure A.2.5.
0.1 M 10,000 Mw PASP pH
10, 1500 rpm, 3.5 hr (x1000)

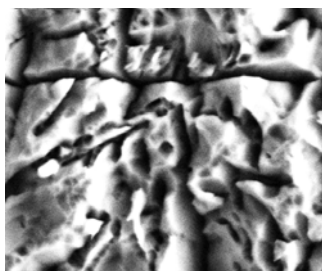


Figure A.2.6.
0.1 M 10,000 Mw PASP pH
10, 1500 rpm, 3.5 hr (x4000)

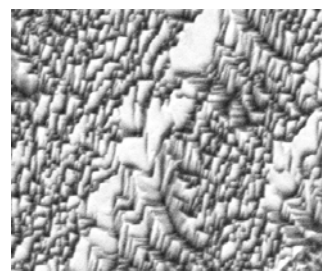


Figure A.2.7.
0.1 M EDTA, pH 10, 1200
rpm, 1 hr (x2000)

Comparing Figure A.2.2 to Figures A.2.5 and A.2.6 for dissolution at high rotating speed, we observe the effect of PASP on the surface morphology of calcite at pH 10. The surfaces in Figures A.2.5 and A.2.6 are considerably rougher, with extensive carvings and grooves due to ligand complexation during dissolution. To evaluate the influence of rotating speed for dissolution at high PASP concentration (0.1M) at pH 10, Figures A.2.5 and A.2.6 (1500 rpm) may be compared to Figures A.2.3 and A.2.4 (150 rpm). At the lower rotating speed, the surface is still somewhat uniform, with undissolved calcite crystals remaining on the surface. Figure A.2.7 is an image of the calcite surface upon dissolution in 0.1M EDTA. This surface is significantly etched by the EDTA, and the pattern contains many step retreats in the shape of rhomboids, the crystalline structure of calcite. This is quite different from the erratic pattern visible on the surface of calcite dissolved in PASP (Figure A.2.5). The non-uniform etching in the presence of PASP may be due to the adsorption of long polymer chains onto calcite, as opposed to smaller monomeric EDTA molecules.

pH 5

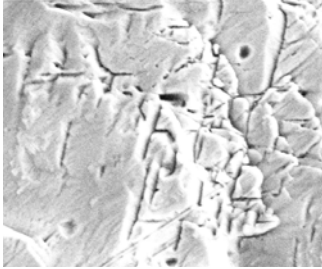


Figure A.2.8.
0.01M 10,000 Mw PASP pH 5, 1200 rpm, 1 hr (x2000)

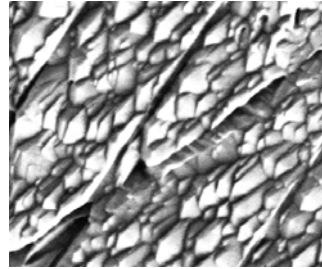


Figure A.2.9.
0.1 M 10,000 Mw PASP pH 5, 1200 rpm, 0.5 hr (2000)

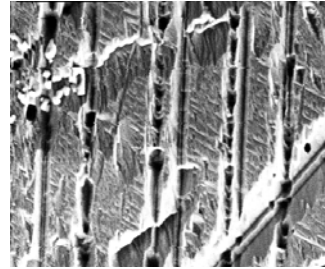


Figure A.2.10.
0.1M 10,000 Mw PASP pH 5, 1200 rpm, 0.5 hr (x500)

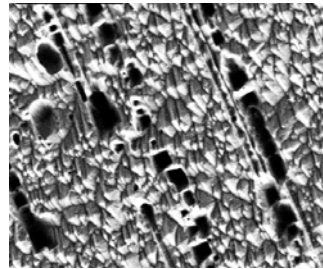


Figure A.2.11.
0.1M 3,000 Mw PASP pH 5, 1200 rpm, 1 hr (x1000)

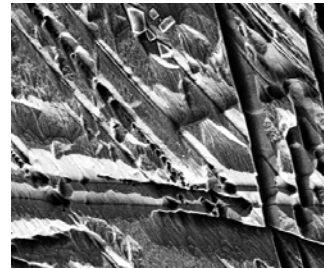


Figure A.2.12.
0.1M 3,000 Mw PASP pH 5, 1200 rpm, 1 hr (x500)

Figures A.2.8-A.2.10 illustrate the effect of PASP concentration on dissolution at pH 5. For the same rotating speed, the calcite surface is significantly more etched in 0.1M PASP (Figures A.2.9 and A.2.10) after 30 minutes than in 0.01M PASP (Figure A.2.8) after 60 minutes. In addition, the etch pattern begins to resemble that of calcite dissolved in EDTA, with repeated rhombic shapes observed along the surface. The influence of molecular weight at pH 5 and constant rotating speed (1200 rpm) is shown in Figures A.2.9 and A.2.10 for dissolution in 10,000 Mw PASP and Figures A.2.11 and

A.2.12 for dissolution in the same concentration of 3,000 Mw PASP. The same rhombic contours are identified in Figure A.2.11 (3,000 Mw) as in Figure A.2.9 (10,000 Mw), but large, deep holes are also visible in Figure A.2.11. This is related to the increased rate of dissolution in 3,000 Mw PASP at low pH.

pH 3.5

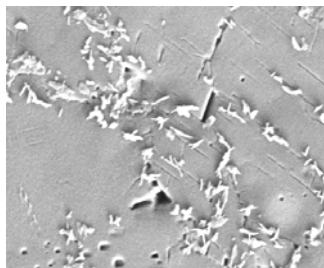


Figure A.2.13.
0 M PASP pH 3.5, 1200 rpm,
0.5 hr (x1000)

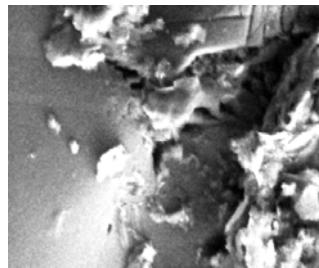


Figure A.2.14.
0 M PASP pH 3.5, 1200 rpm,
1 hr (x2000)

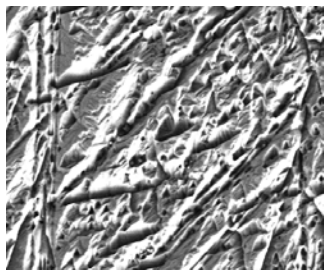


Figure A.2.15.
0.01M 10,000 Mw PASP pH 3.5,
300 rpm, 0.5 hr (x1000)

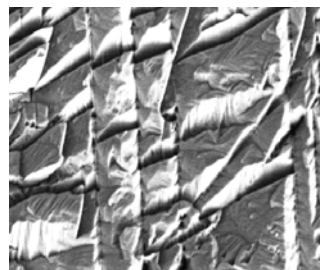


Figure A.2.16.
0.01 M 10,000 Mw PASP pH
3.5, 600 rpm, 0.5 hr (x2000)

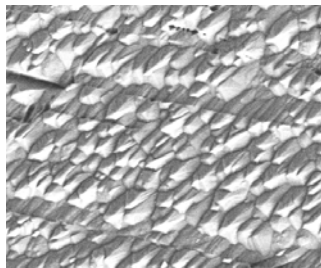


Figure A.2.17.
0.01M 10,000 Mw PASP pH
3.5, 1200 rpm, 0.5 hr (x1000)

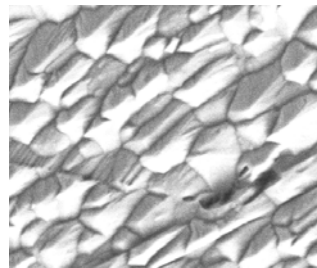


Figure A.2.18.
0.01M 10,000 Mw PASP pH
3.5, 1200 rpm, 0.5 hr (x2000)

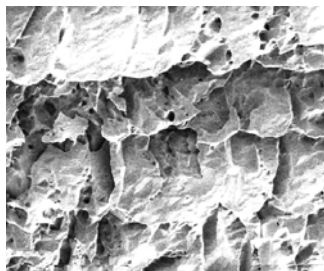


Figure A.2.19.
0.1 M 3,000 Mw PASP pH
3.5, 1500 rpm, 1 hr (x350)

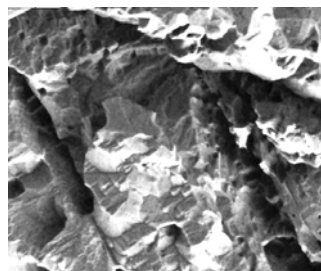


Figure A.2.20.
0.1 M 3,000 Mw PASP pH
3.5, 1500 rpm, 1 hr (x1000)

Figures A.2.13 and A.2.14 show the surface morphology of calcite after dissolution in water at pH 3.5. The surface is relatively smooth and uniform, with clusters of residual calcite crystals left on the surface. In the presence of PASP, the surface becomes extremely rough and pitted, as in Figures A.2.15-A.2.20. The effect of rotating speed at pH 3.5 is illustrated in Figures A.2.15-A.2.18 for dissolution in 0.01M PASP (10,000 Mw) at 300, 600 and 1200 rpm. As ω increases, the surface morphology gradually transitions from random etching to a repetitive rhombic pattern, with a larger number of pits and steps as a result of increasing dissolution rates. Figures A.2.19 and A.2.20 show the calcite surface after dissolution in the highest concentration (0.1M) and lowest molecular weight (3,000 Mw) of PASP studied, and at the highest rotating speed (1500 rpm) studied in the thesis. These conditions correspond to the highest rates of dissolution measured. The calcite surface is characterized by extreme non-uniformity, with a considerable number of steps, pits and deep holes marking the surface.

Appendix B: Details of experimental method

B.1. Material preparation

Calcite marble disks

Calcium standards for atomic absorption calibration

Calcium standards for Ca²⁺ ISE calibration

Polymer solution for dissolution experiment

Polymer stock solution

B.2. Instrument calibration

pH and ISE electrodes

AA

B.3. Instrument operation

Winwedge software (for electrode data acquisition)

AA

Electrode storage

B.1. Material preparation

Calcite marble disks

1. Cut marble disk from core to diameter of ~ 3.2 cm and thickness of 1.5 cm.
2. Polish disk to surface smoothness of 3,000 mesh using 150, 300, 600, 1,000 and 3,000 mesh diamond polishing disks successively.
3. Coat sides of disk using polystyrene/carbon tetrachloride solution to isolate top surface for dissolution.
4. Attach round magnet piece to bottom surface of disk using epoxy resin.
5. Rinse disk with DI water to wash off excess dirt and marble residue from polishing.
6. Attach disk to rotor (the magnet attaches to a connector piece at the end of the rotor shaft)
7. Spin the disk to knock off excess water before dissolution experiments.

Ca²⁺ standards for calibration of calcium ISE electrode (0.01, 0.1, 1, 10 ppm)

1. Micropipette appropriate volume of 100 ppm Ca⁺⁺ standard (made from 0.1M standard from Fisher) into 100 mL flask. (Example: to make a 1 ppm Ca²⁺ standard, transfer 1 mL of 100 ppm Ca²⁺ standard into 100 mL flask.)
2. Add 4 mL of Orion Ion Strength Adjustor solution to prevent problems due to ion strength fluctuations.

Ca²⁺ standards for calibration of atomic absorption spectrometer (0, 1, 2, 4, 8 ppm)

1. Micropipette appropriate volume of 100 ppm Ca⁺⁺ standard (made from 0.1M standard from Fisher) into 100 mL flask. (Example: to make an 8 ppm Ca²⁺ standard, transfer 8 mL of 100 ppm Ca²⁺ standard into 100 mL flask.)
2. Add 5 mL of 4.0 M KCl standard (previously prepared by diluting 29.82 grams analytical grade KCl crystals to 100 mL using DI water) to yield 0.2M ion strength for standards.
3. Dilute to 100 mL with DI water.

*For dissolution experiments with medium and high concentrations of polyaspartic acid, it is important to add the corresponding concentration of PASP into the standard to correct for matrix effects. Particularly with 0.1M polymer concentration, PASP in solution interferes with calcium measurements and results in [Ca] readings that are lower than the true value. Thus, standards must account for this interference. (For 0.1M PASP standards, add 3.425g of PASP to flask before dilution, and for 0.01M PASP standards, add 10 mL of 0.1M PASP solution as previously prepared to flask before dilution).

Polyaspartic acid solution (800 mL)

1. Weigh out an amount of undiluted (40 wt %) polymer stock solution corresponding to the desired concentration (137 equivalent g/mol). For 0.1M PASP, weigh out 27.4 g stock solution (3,000 Mw or 10,000 Mw); for 0.01M

PASP, use 2.74 g of stock solution; for 0.001M PASP, use 8 mL of 0.1M PASP solution prepared as below.

2. Add KCl to obtain total ion strength of 0.2M for the polymer solution. For a 0.1M PASP solution, the polymer contributes 0.05M ion strength to the solution, so we add 0.15M KCl, which is 8.93 g for 800 mL solution.
3. Dilute to 800 mL solution in a 1 L beaker using DI water.
4. Place in water bath to warm up to 25°C.
5. Mix solution well using magnetic stirring plate.
6. Adjust solution pH. Add HCl to lower pH and NaOH to increase pH. Low concentrations of acid and base (0.01M or 0.1M) are used for solutions with water or small amounts of PASP, while higher HCl and NaOH concentrations (1M) will be needed for solutions with high PASP concentration, since PASP acts as a buffer.

0.1M (Diluted) stock solution of PASP

Dilute 3.425g of PASP stock (40% wt solids and 137 equivalent molecular weight) to 100 mL using DI water. Do this for each molecular weight (3,000 and 10,000).

B.2 Instrument calibration

pH electrode

Calibrate pH electrode using buffer solutions of pH 4.00, 7.00 and 10.00 supplied by Fisher Scientific. Use automatic calibration mode to account for fluctuations in solution temperature. Rinse electrode with DI water between buffers.

Calcium ion selective electrode

Calibrate calcium ISE using Ca^{2+} standards prepared in Appendix B-1. Choose standard concentrations to cover the range of calcium concentrations that will be measured during the experiment. (For example, if the dissolution experiment is conducted at low pH and low PASP concentration, Ca^{2+} concentrations are expected to be large, so standards of 0.1, 1 and 10 ppm should be used for electrode calibration. On the other hand, if the experiment is done at high pH and high PASP concentration, the free calcium concentration will be very small. In this case, 0.01, 0.1 and 1 ppm Ca^{2+} standards are to be used for calibration). Use at least three standards for each calibration and move from the lowest to highest concentration. Avoid using a calibration standard of zero concentration, as this drastically increases the time necessary for electrode measurements.

Atomic absorption spectrometer

Check that the calibration standards are set to the appropriate concentrations. To do this, click on the tab at the bottom of the Method Editor window that says 'Calib.' Then click on the tab labeled 'Standard Concs' and scroll through the list of standards to make sure the standards are set to cover the range of concentrations that are expected to

be analyzed. For example, if an experiment is performed at low pH (<5), the highest standard concentration should be at least 8 or 12 ppm Ca⁺⁺, and for high pH (>8), the standards should cover a lower range of concentrations. Modify the values as necessary, and close the window when finished.

To begin calibration, place aspiration tube in DI water and click 'Analyze Blank'. This established the base concentration of zero. Then place tube in the lowest concentration standard solution (1 ppm Ca) and click 'Analyze Standard'. The computer displays an average reading from three absorbance measurements and equates this to the assigned concentration. Insert tube into the next standard, moving from lowest to highest concentration, and repeat for each standard until a calibration curve is obtained.

B.3. Instrument operation

Winwedge software

1. Open WinwedgePro from the Startup menu on the computer.
2. From the menu bar, select File > Open, and open the file 'pHmeter.sw3'. From the menu bar, select Activate > Normal Mode. Readings will automatically appear in a notepad file as they are read from the pH/ISE meter. The interval time between readings is set to 15 seconds. This interval can be changed in the menu of the pH meter instrument.
3. To exit the Winwedge program, close the 'Software Wedge – COM1' window.

AA

1. Flip On/Off switch to AA machine.
2. Double click AAWinLab Analyst software icon on connected computer. The software will check connections between the computer and the equipment. Once this is complete, click the green beaker icon for manual sampling.
3. A list of Methods will appear. Each of the methods uses different standard concentrations for AA calibration to cover high and low calcium concentration ranges. Choose the desired Method from the list.
4. Once the software is open, from the menu, go to File > Open > Workspace. Select 'setup.flm'. This opens all the windows needed for analysis.
5. To select or modify the method, Click on the Method Editor icon from the menubar. Check that the following settings are correct: Wavelength = 422.7 nm, slit width = 0.7 nm, Flame type = Air/C₂H₂, Oxid. Flow = 6 and Fuel Flow = 2.

6. Open gas valves: Open acetylene tank to a minimum of 12 psi line pressure (make sure that the bottle pressure is no less than 100 psi), and air pressure to 60 psi.
7. Place the AA sample respirator tubing in a 250 mL beaker of DI water.
8. Turn on the flame. Click the ON button in the Flame Control window. Check that the flame is blue and uniform across the slit of the source.
9. Let flame stabilize for at least 15-20 minutes. Once stabilized, click 'Analyze Blank'. There will be an automated correction for the blank, and the absorbance will be set to zero for this concentration. Make sure that the lamp energy reading is at least 67. If it is less than 67, let the flame run an additional 10 minutes.
10. To shut down the equipment:
 - a. Turn the flame position to OFF in the Flame window on the computer.
 - b. Manually close the acetylene tank and air valves.
 - c. Bleed the gas lines by clicking the 'Bleed' icon in the Flame window.
Repeat this 3 times to ensure that there is no gas remaining in the lines.
 - d. Switch the AA machine off. This is important to conserve the lamp energy for a longer lamp life.

Electrode storage

Store the pH electrode overnight in reference electrode solution, and cover the opening at the top of the electrode. Store the Ca⁺⁺ electrode overnight in a 10 ppm Ca⁺⁺ solution, covering both the opening at the top of the electrode and the solution beaker (50 mL).

Appendix C: Data Analysis

- C.1. Rotating disk raw data and dissolution rate calculations
- C.2. Reproducibility of dissolution experiments
- C.3. Alternative method of dissolution analysis
- C.4. Summary of dissolution experiments
- C.5. Dynamic light scattering analysis

C.1. Rotating disk raw data and dissolution rate calculations

Raw data for dissolution using an intermediate concentration (0.01M) of 3,000 Mw PASP at 300 rpm are shown in Figures C.1-C.3 for pH 3.5, 5, and 10. These data are representative of the trends observed at other conditions of PASP concentration, molecular weight, and rotating speed. As shown in the graphs, calcium concentration $[Ca]_T$ vs. time data for pH 3.5 and 5 yield very straight lines, but at pH 10, calcium concentrations level off over time, producing a polynomial curve of second order. This is believed to be due to changes in surface morphology from etching and pitting during chelation. Therefore, to eliminate the effects of surface changes, the data from only the first 10-12 minutes was used to calculate the linear slope, $d[Ca]_T/dt$ at pH 10 (Figure C.3). From the slopes of these curves, the dissolution rates were calculated by multiplying by the volume of the reaction vessel (800 mL) and dividing by the surface area of the calcite disk (πr^2 ; where $r = 1.59$ cm):

$$\text{Rate (mol/m}^2\text{-s)} = \frac{[(d[Ca]_T/dt) \text{ ppm/min} * 0.000025 \text{ mol L}^{-1}/\text{ppm Ca} * 0.8 \text{ L}]}{[\pi * (1.59 \text{ cm})^2 * 1E^{-4} \text{ m}^2/\text{cm}^2 * 60 \text{ sec/min}]} \quad (\text{C.1})$$

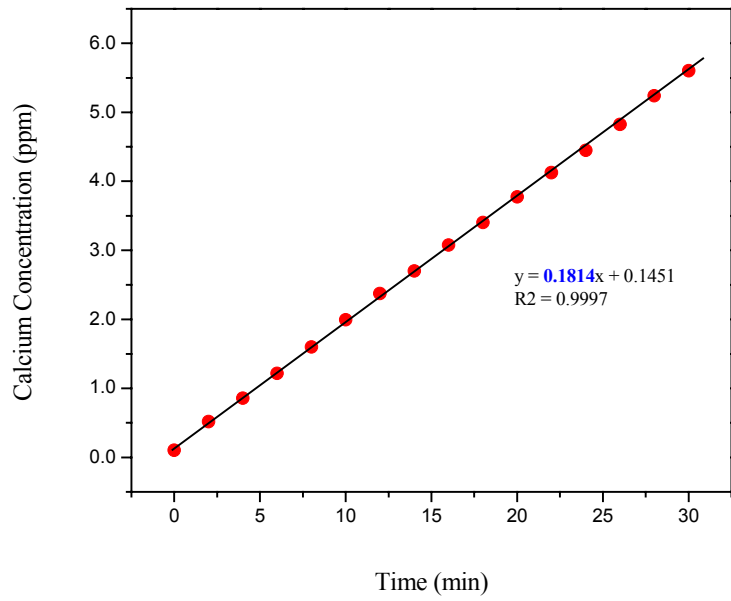


Figure C.1. Calcium concentration versus time for dissolution in 0.01M 3,000 Mw PASP, 300 rpm, at pH=3.5.

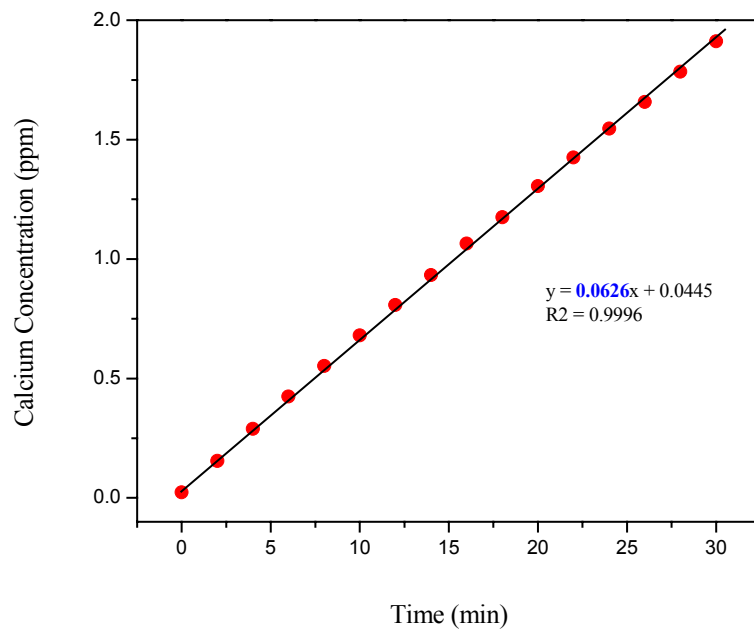


Figure C.2. Calcium concentration versus time for dissolution in 0.01M 3,000 Mw PASP, 300 rpm, at pH=5.

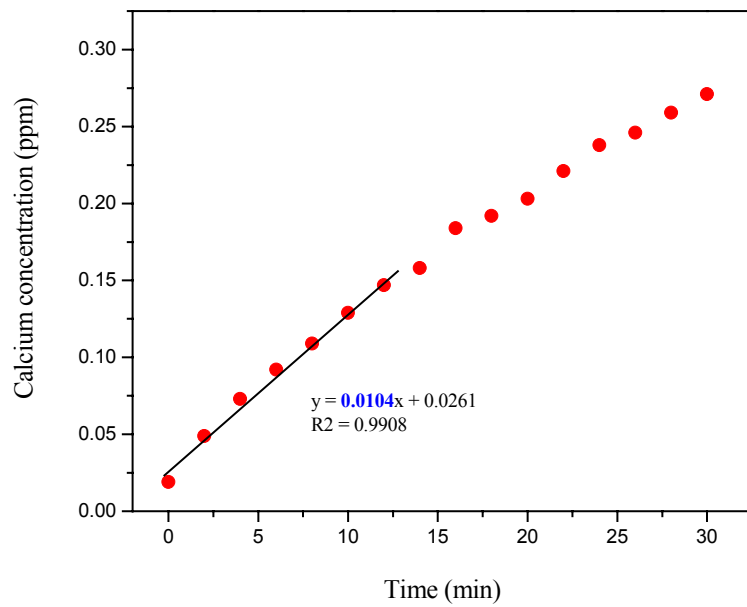


Figure C.3. Calcium concentration versus time for dissolution in 0.01M 3,000 Mw PASP, 300 rpm, at pH=10.

C.2. Reproducibility of dissolution experiments

In general, the rotating disk experiments exhibit good reproducibility. This is demonstrated by Figures C.4 and C.5, for repeated runs of dissolution in polyaspartic acid at pH 5 and 10, respectively. In addition, a series of experiments was repeated at pH 5 for 0.01M PASP (3,000 Mw) over the range of rotating speed (Figure C.6). Results are highly reproducible at low pHs (<6), where calcium versus time plots yield straight lines with high R^2 correlation. Results are less reproducible at higher pHs (>6), due to the curved nature of the plots. Nevertheless, results are considerably reproducible over the entire range of conditions studied.

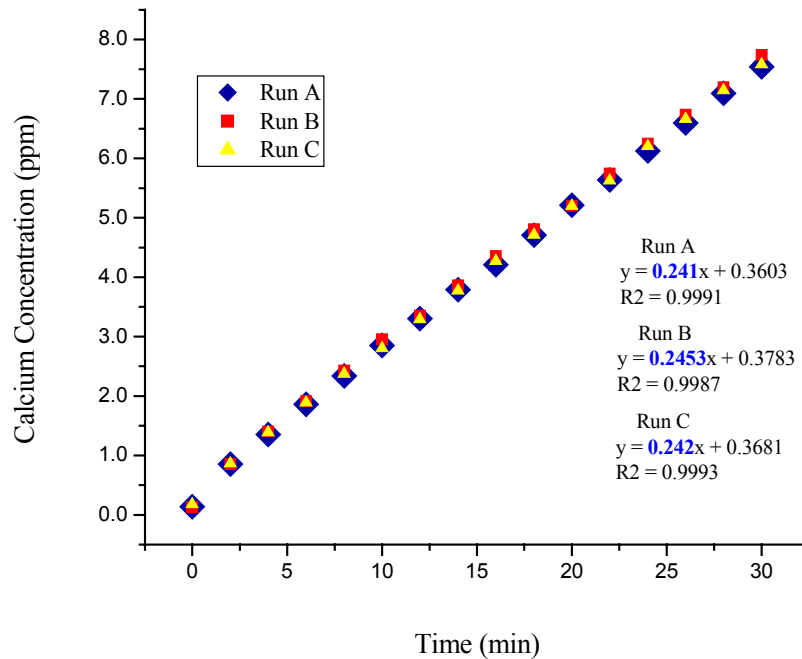


Figure C.4. Reproducibility of dissolution experiment at pH=5, in 0.1M 3,000 Mw PASP at 1200 rpm.

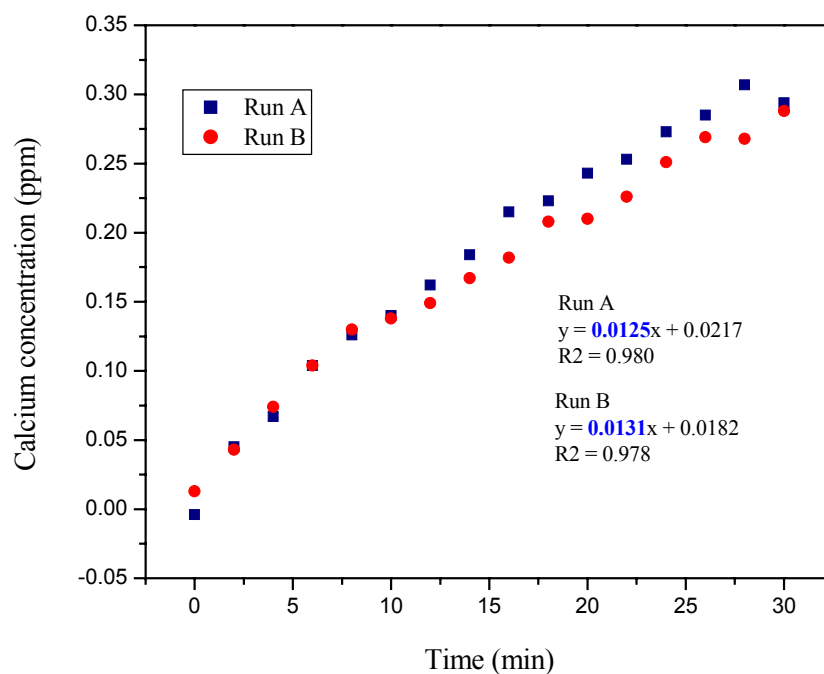


Figure C.5. Reproducibility of dissolution experiment at pH=10, in 0.1M 10,000 Mw PASP at 1200 rpm.

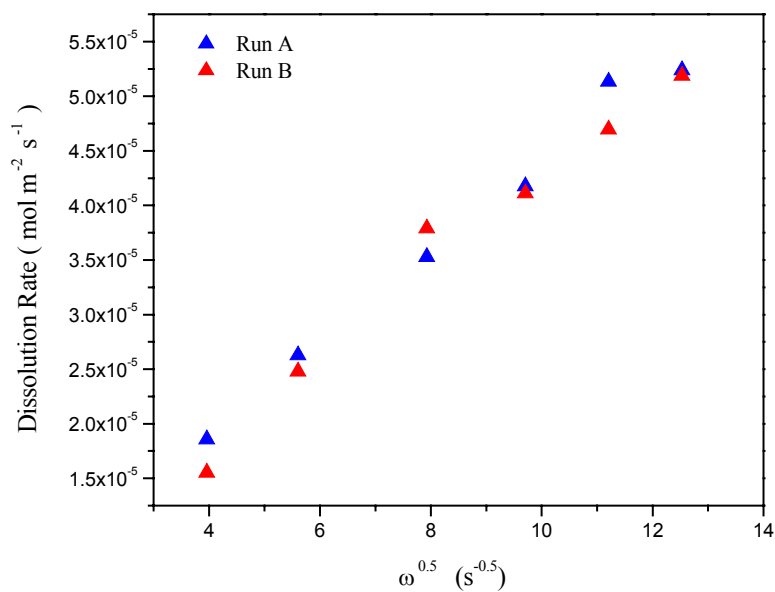


Figure C.6. Reproducibility of dissolution experiment at pH=5, in 0.01M 3,000 Mw PASP over full range of rotating speeds.

Though reproducibility is high for the rotating disk experiments, some of the challenges in experimental precision include:

- Disk polishing. Since the same disks are used and repolished for all experiments, if the disk is not well-polished, there may be inclusions or rough patches remaining on the surface, which leads to non-uniform dissolution.
- Instability of AA. If the atomic absorption spectrometer is not allowed to warm up for at least 20-30 minutes, the flame may be unstable, and concentration readings will fluctuate. Additionally, if the lamp energy is below ~67-69 mA at the start of a sample analysis, a jump in the energy level during the analysis will shift concentration readings down, causing a discontinuity in the data (Figure C.7)
- Sensitivity of AA. At extremely low concentrations of calcium (below ~0.1 ppm Ca), the limited sensitivity of the spectrometer leads to fluctuations in concentration measurements. This is normally only a problem for experiments carried out at high pH (10), low rotating speed (150 rpm), and the lowest concentration of PASP (0.001M).
- Low flow rate through AA. As a sample is aspirated through the plastic tubing during AA analysis, if the fluid flow is blocked, the reduced flow rate causes a decrease in the concentration reading.

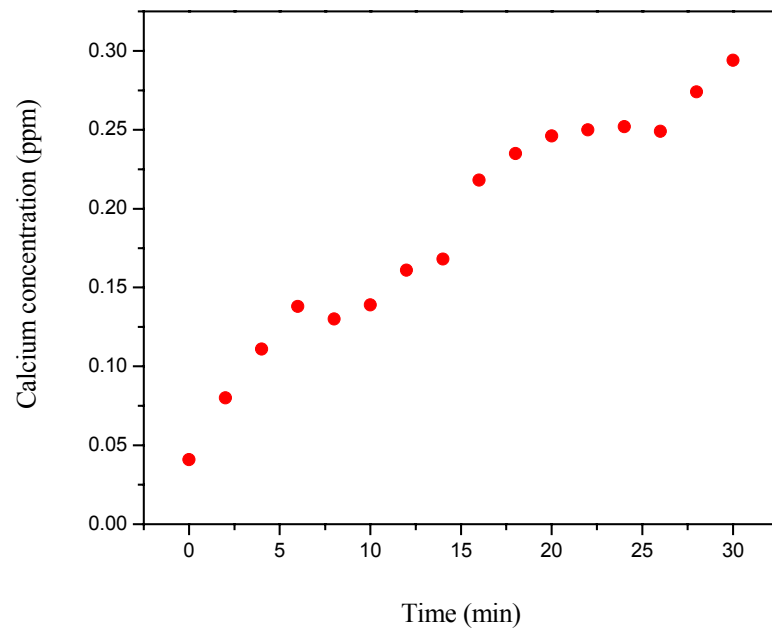


Figure C.7. Effect of shifts in AA lamp energy on calcium concentration measurement (Dissolution at pH=10, 900 rpm, in 0.1M PASP).

C.3. Alternative method of dissolution analysis

While theory predicts that at $\omega=0$ the rate of dissolution is zero, it should be noted that the fitted curves were constrained to go through the origin, following the methods of Fredd and Fogler [1,11] and Lund [2]. In some cases, it is arguable that some of the data for experimental rate or flux, J_{exp} vs. $\omega^{0.5}$ might be more accurately fitted to a straight line with a non-zero intercept. In this situation, the data would be consistent with the form:

$$\text{Rate} = k_1 [\text{reactant}] + k_2 \quad (\text{C.2})$$

which is analogous to equation 2.4 in the text. In equation (C.3.1), $k_1 [\text{reactant}]$ is the contribution of mass transport to overall dissolution, and k_2 describes the rate of reaction of either water or PASP with the calcite surface. This is similar to expressions derived by other investigators to describe rates of calcite dissolution in water [27-29].

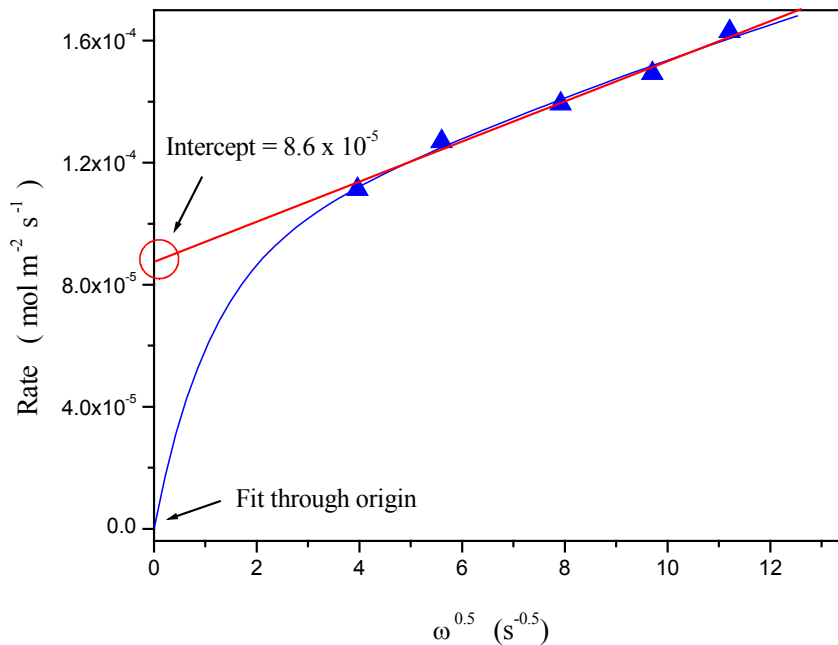


Figure C.8. Comparison of data analysis for dissolution at pH 3.5, for 0.1 M PASP (3,000 Mw).

Using this method of analysis, the data from the experiments performed in this work were fit to lines with non-zero intercepts when possible. For pH 10, linear regression did not yield the best fit for the data, however values for a hypothetical k_2 from this analysis are listed in Table C.1. Moving from 0 to 0.001M PASP, k_2 is decreased by a factor of 2 and slowly increases with polymer concentration until it nearly reaches the initial value in water. According to this trend, the contribution of the surface reaction initially decreases in the presence of small amounts of PASP and then increases at large concentrations of PASP. Therefore, the end result from this analysis is still the same as before. We still resolve that interfacial reaction is a limiting step during dissolution. We also determine that the rate of the surface reaction is diminished at low PASP concentration but heightened at high PASP concentration.

Repeating this procedure for data at pH 5 and 3.5, we find that using linear regression yields an excellent fit through the origin for data at 0 and 0.001M PASP, while lines with non-zero intercepts were generated at 0.01 and 0.1M. Values for k_2 at these conditions are also presented in Table C.1. As before, the magnitude of k_2 increases with increasing PASP concentration, and k_2 values are also higher for 3,000 Mw PASP. The conclusions again agree with those obtained by forcing the data through the origin.

Table C.1. Intercept of dissolution rate vs. square root rotating speed from linear regression.

| pH | PASP Mw | PASP Conc (M) | Intercept (k_2) (mol/m ² -s) |
|-----|---------|------------------|--|
| 10 | 0 | 0 | 2.22E-06 |
| 10 | 10,000 | 0.001 | 1.16E-06 |
| 10 | 10,000 | 0.01 | 1.68E-06 |
| 10 | 10,000 | 0.1 | 1.93E-06 |
| 5 | 0 | 0 | 0 |
| 5 | 10,000 | 0.001 | 0 |
| 5 | 10,000 | 0.01 | 0 |
| 5 | 3,000 | 0.01 | 2.90E-06 |
| 5 | 10,000 | 0.1 | 3.08E-05 |
| 5 | 3,000 | 0.1 | 4.33E-05 |
| 3.5 | 0 | 0 | 0 |
| 3.5 | 3,000 | 0.001 | 0 |
| 3.5 | 10,000 | 0.01 | 1.54E-05 |
| 3.5 | 3,000 | 0.01 | 3.57E-05 |
| 3.5 | 3,000 | 0.1 | 8.63E-05 |

One dissolution experiment was performed at $\omega=0$, for 0.1M 3,000 Mw PASP at pH 3.5. These conditions were chosen because the rate vs. $\omega^{0.5}$ curve for these conditions appeared to be highly linear with the largest intercept (which should be the easiest to measure). The experiment was done by inserting a polished disk into the solution for 30 seconds, removing the disk and stirring with a stirbar before taking a bulk sample for concentration measurement. The sample was stirred to ensure uniform bulk concentrations of calcium, and the disk was removed before stirring to prevent effects of mass transfer. This procedure was repeated for 10 minutes.

From this experiment, the value for k_2 at these conditions was calculated as 1.19×10^{-4} mol/m²-s. This is slightly higher than the theoretical value of 8.63×10^{-5}

mol/m²-s calculated from linear regression. This value is likely high due to stirring, as it was impossible to entirely eliminate mass transfer effects in the experiment.

C.4. Summary of dissolution experiments

Table C.2. Summary of dissolution experiments

| RUN | DATE | PH | ROTATING SPEED (rpm) | PASP CONCENTRATION (M) | MOLECULAR WEIGHT | SEM FIGURE NUMBER | COMMENTS |
|-------------------------|-----------|----|----------------------------|------------------------------|---------------------|----------------------|----------------------------------|
| Studies at pH 10 | | | | | | | |
| 1 | 7/17/2001 | 10 | 1500 | 0 | ---- | | |
| 2 | 8/9/2001 | 10 | 1500 | 0.001 | 10,000 | | |
| 3 | 8/3/2001 | 10 | 1500 | 0.01 | 10,000 | | |
| 4 | 6/13/2001 | 10 | 1500 | 0.1 | 10,000 | A.2.5, A.2.6 | |
| 5 | 8/8/2001 | 10 | 1500 | 0.01 | 3,000 | | |
| 6 | 7/23/2001 | 10 | 1200 | 0 | ---- | A.2.2 | |
| 7 | 8/21/2001 | 10 | 1200 | 0.001 | 10,000 | | |
| 8 | 1/23/2002 | 10 | 1200 | 0.005 | 10,000 | | Test intermediate concentrations |
| 9 | 8/7/2001 | 10 | 1200 | 0.01 | 10,000 | | |
| 10 | 6/17/2002 | 10 | 1200 | 0.05 | 10,000 | | Test intermediate concentrations |
| 11 | 8/27/2001 | 10 | 1200 | 0.1 | 10,000 | | |
| 12 | 6/27/2001 | 10 | 1200 | 0.01 | 3,000 | | |
| 13 | 2/26/2002 | 10 | 1200 | 0.1 | 3,000 | | |
| 14 | 7/18/2001 | 10 | 1200 | 0.1 M EDTA | ---- | A.2.7 | Compare PASP to EDTA at pH 10 |
| 15 | 7/17/2001 | 10 | 900 | 0 | ---- | | |
| 16 | 8/20/2001 | 10 | 900 | 0.001 | 10,000 | | |
| 17 | 8/6/2001 | 10 | 900 | 0.01 | 10,000 | | |
| 18 | 4/23/2002 | 10 | 900 | 0.1 | 10,000 | | |
| 19 | 7/16/2001 | 10 | 600 | 0 | ---- | | |
| 20 | 8/8/2001 | 10 | 600 | 0.001 | 10,000 | | |
| 21 | 8/3/2001 | 10 | 600 | 0.01 | 10,000 | | |
| 22 | 8/22/2001 | 10 | 600 | 0.1 | 10,000 | | |

Table C.2 cont'd

| | | | | | | |
|------------------------|------------|----|------|-----------------------------------|--------|--------------------------------------|
| 23 | 8/8/2001 | 10 | 600 | 0.01 | 3,000 | |
| 24 | 7/16/2001 | 10 | 300 | 0 | ---- | |
| 25 | 8/20/2001 | 10 | 300 | 0.001 | 10,000 | |
| 26 | 8/6/2001 | 10 | 300 | 0.01 | 10,000 | |
| 27 | 9/20/2001 | 10 | 300 | 0.1 | 10,000 | |
| 28 | 4/25/2002 | 10 | 300 | 0.01 | 3,000 | |
| 29 | 7/23/2001 | 10 | 150 | 0 | ---- | |
| 30 | 8/21/2001 | 10 | 150 | 0.001 | 10,000 | |
| 31 | 7/25/2001 | 10 | 150 | 0.01 | 10,000 | |
| 32 | 9/5/2001 | 10 | 150 | 0.1 | 10,000 | A.2.3, A.2.4 |
| 33 | 8/21/2001 | 10 | 150 | 0.01 | 3,000 | |
| Studies at pH 5 | | | | | | |
| 34 | 8/31/2001 | 5 | 1500 | 0 | ---- | |
| 35 | 9/17/2001 | 5 | 1500 | 0.01 | 10,000 | |
| 36 | 10/10/2001 | 5 | 1500 | 0.1 | 10,000 | |
| 37 | 10/4/2001 | 5 | 1500 | 0.01 | 3,000 | |
| 38 | 10/11/2001 | 5 | 1500 | 0.1 | 3,000 | |
| 39 | 8/30/2001 | 5 | 1200 | 0 | ---- | |
| 40 | 1/23/2002 | 5 | 1200 | 0.001 | 3,000 | |
| 41 | 10/1/2001 | 5 | 1200 | 0.01 | 3,000 | |
| 42 | 2/28/2002 | 5 | 1200 | 0.1 | 3,000 | A.2.11, A.2.12 |
| 43 | 6/18/2001 | 5 | 1200 | 0.001 | 10,000 | |
| 44 | 6/15/2001 | 5 | 1200 | 0.01 | 10,000 | A.2.8 |
| 45 | 10/9/2001 | 5 | 1200 | 0.1 | 10,000 | A.2.9, A.2.10 |
| 46 | 10/2/2001 | 5 | 1200 | 0.05M (3,000) + 0.05M (10,000) | | To test mixtures of two mol. weights |
| 47 | 7/18/2001 | 5 | 1200 | 0.01 M EDTA | ---- | Compare PASP to EDTA at pH 5 |
| 48 | 8/30/2001 | 5 | 900 | 0 | ---- | |
| 49 | 10/3/2001 | 5 | 900 | 0.01 | 3,000 | |
| 50 | 10/11/2001 | 5 | 900 | 0.1 | 3,000 | |
| 51 | 9/27/2001 | 5 | 900 | 0.001 | 10,000 | |
| 52 | 9/17/2001 | 5 | 900 | 0.01 | 10,000 | |

Table C.2 cont'd

| | | | | | | |
|--------------------------|------------|-----|------|------------------------------------|--------|----------------------------------|
| 53 | 10/9/2001 | 5 | 900 | 0.1 | 10,000 | |
| 54 | 8/24/2001 | 5 | 600 | 0 | ---- | |
| 55 | 10/1/2001 | 5 | 600 | 0.01 | 3,000 | |
| 56 | 10/8/2001 | 5 | 600 | 0.1 | 3,000 | |
| 57 | 9/27/2001 | 5 | 600 | 0.001 | 10,000 | |
| 58 | 9/17/2001 | 5 | 600 | 0.01 | 10,000 | |
| 59 | 9/19/2001 | 5 | 600 | 0.1 | 10,000 | |
| 60 | 10/5/2001 | 5 | 600 | 0.05M (3,000) + 0.05M (10,000)) | | |
| 61 | 7/11/2002 | 5 | 600 | 0.1 | 50,000 | |
| 62 | 8/28/2001 | 5 | 300 | 0 | ---- | |
| 63 | 1/24/2002 | 5 | 300 | 0.001 | 3,000 | |
| 64 | 10/3/2001 | 5 | 300 | 0.01 | 3,000 | |
| 65 | 10/11/2001 | 5 | 300 | 0.1 | 3,000 | |
| 66 | 9/28/2001 | 5 | 300 | 0.001 | 10,000 | |
| 67 | 9/17/2001 | 5 | 300 | 0.01 | 10,000 | |
| 68 | 10/10/2001 | 5 | 300 | 0.1 | 10,000 | |
| 69 | 8/28/2001 | 5 | 150 | 0 | ---- | |
| 70 | 10/2/2001 | 5 | 150 | 0.01 | 3,000 | |
| 71 | 10/10/2001 | 5 | 150 | 0.1 | 3,000 | |
| 72 | 9/17/2001 | 5 | 150 | 0.01 | 10,000 | |
| 73 | 9/20/2001 | 5 | 150 | 0.1 | 10,000 | |
| Studies at pH 3.5 | | | | | | |
| 74 | 10/16/2001 | 3.5 | 1500 | 0 | ---- | |
| 75 | 11/8/2001 | 3.5 | 1500 | 0.001 | 3,000 | |
| 76 | 10/25/2001 | 3.5 | 1500 | 0.01 | 3,000 | |
| 77 | 10/16/2001 | 3.5 | 1500 | 0.1 | 3,000 | A.2.19, A.2.20 |
| 78 | 11/21/2001 | 3.5 | 1500 | 0.01 | 10,000 | |
| 79 | 10/17/2001 | 3.5 | 1200 | 0 | ---- | A.2.13, A.2.14 |
| 80 | 11/7/2001 | 3.5 | 1200 | 0.001 | 3,000 | |
| 81 | 6/19/2002 | 3.5 | 1200 | 0.005 | 3,000 | Test intermediate concentrations |
| 82 | 10/24/2001 | 3.5 | 1200 | 0.01 | 3,000 | |

Table C.2 cont'd

| | | | | | | |
|-------------------------------------|------------|-----|------|-------|--------|----------------------------------|
| 83 | 6/20/2002 | 3.5 | 1200 | 0.05 | 3,000 | Test intermediate concentrations |
| 84 | 3/21/2002 | 3.5 | 1200 | 0.1 | 3,000 | |
| 85 | 9/14/2001 | 3.5 | 1200 | 0.001 | 10,000 | |
| 86 | 11/20/2001 | 3.5 | 1200 | 0.01 | 10,000 | A.2.17, A.2.18 |
| 87 | 3/21/2002 | 3.5 | 1200 | 0.1 | 10,000 | |
| 88 | 11/12/2001 | 3.5 | 900 | 0 | ---- | |
| 89 | 11/8/2001 | 3.5 | 900 | 0.001 | 3,000 | |
| 90 | 10/24/2001 | 3.5 | 900 | 0.01 | 3,000 | |
| 91 | 12/6/2001 | 3.5 | 900 | 0.1 | 3,000 | |
| 92 | 11/20/2001 | 3.5 | 900 | 0.01 | 10,000 | |
| 93 | 4/16/2002 | 3.5 | 900 | 0.1 | 10,000 | |
| 94 | 10/16/2001 | 3.5 | 600 | 0 | ---- | |
| 95 | 11/7/2001 | 3.5 | 600 | 0.001 | 3,000 | |
| 96 | 10/22/2001 | 3.5 | 600 | 0.01 | 3,000 | |
| 97 | 11/29/2001 | 3.5 | 600 | 0.1 | 3,000 | |
| 98 | 11/14/2001 | 3.5 | 600 | 0.01 | 10,000 | A.2.16 |
| 99 | 10/12/2001 | 3.5 | 300 | 0 | ---- | |
| 100 | 11/8/2001 | 3.5 | 300 | 0.001 | 3,000 | |
| 101 | 6/14/2002 | 3.5 | 300 | 0.005 | 3,000 | Test intermediate concentrations |
| 102 | 10/24/2001 | 3.5 | 300 | 0.01 | 3,000 | |
| 103 | 6/14/2002 | 3.5 | 300 | 0.05 | 3,000 | Test intermediate concentrations |
| 104 | 12/4/2001 | 3.5 | 300 | 0.1 | 3,000 | |
| 105 | 11/20/2001 | 3.5 | 300 | 0.01 | 10,000 | A.2.15 |
| 106 | 4/16/2002 | 3.5 | 300 | 0.1 | 10,000 | |
| 107 | 10/12/2001 | 3.5 | 150 | 0 | ---- | |
| 108 | 11/8/2001 | 3.5 | 150 | 0.001 | 3,000 | |
| 109 | 10/22/2001 | 3.5 | 150 | 0.01 | 3,000 | |
| 110 | 12/3/2001 | 3.5 | 150 | 0.1 | 3,000 | |
| 111 | 11/19/2001 | 3.5 | 150 | 0.01 | 10,000 | |
| 112 | 8/6/2002 | 3.5 | 0 | 0.1 | 3,000 | |
| Studies at intermediate pH's | | | | | | |

Table C.2 cont'd

| | | | | | |
|-----|-----------|-----|------|-------|--------|
| 113 | 1/25/2002 | 4 | 1200 | 0 | ---- |
| 114 | 2/26/2002 | 4 | 1200 | 0.001 | 3,000 |
| 115 | 1/29/2002 | 4 | 1200 | 0.01 | 3,000 |
| 116 | 2/5/2002 | 4 | 1200 | 0.1 | 3,000 |
| 117 | 1/29/2002 | 4 | 1200 | 0.01 | 10,000 |
| 118 | 4/2/2002 | 4 | 1200 | 0.1 | 10,000 |
| 119 | 4/23/2002 | 4 | 300 | 0 | ---- |
| 120 | 3/7/2002 | 4 | 300 | 0.01 | 3,000 |
| 121 | 3/5/2005 | 4 | 300 | 0.1 | 3,000 |
| 122 | 4/4/2002 | 4.2 | 1200 | 0.1 | 10,000 |
| 123 | 3/25/2002 | 4.2 | 1200 | 0.1 | 3,000 |
| 124 | 6/19/2002 | 4.7 | 1200 | 0 | ---- |
| 125 | 5/2/2002 | 4.7 | 1200 | 0.01 | 3,000 |
| 126 | 4/16/2002 | 4.7 | 1200 | 0.1 | 3,000 |
| 127 | 6/5/2002 | 4.7 | 1200 | 0.01 | 10,000 |
| 128 | 5/9/2002 | 4.7 | 1200 | 0.1 | 10,000 |
| 129 | 5/2/2002 | 4.7 | 300 | 0.1 | 3,000 |
| 130 | 6/20/2002 | 5.2 | 1200 | 0 | ---- |
| 131 | 6/18/2002 | 5.2 | 1200 | 0.01 | 3,000 |
| 132 | 3/25/2002 | 5.2 | 1200 | 0.1 | 3,000 |
| 133 | 6/18/2002 | 5.2 | 1200 | 0.01 | 10,000 |
| 134 | 4/4/2002 | 5.2 | 1200 | 0.1 | 10,000 |
| 135 | 1/29/2002 | 6 | 1200 | 0 | ---- |
| 136 | 1/31/2002 | 6 | 1200 | 0.01 | 3,000 |
| 137 | 2/12/2002 | 6 | 1200 | 0.1 | 3,000 |
| 138 | 1/29/2002 | 6 | 1200 | 0.01 | 10,000 |
| 139 | 3/21/2002 | 6 | 1200 | 0.1 | 10,000 |
| 140 | 4/25/2002 | 6 | 300 | 0 | ---- |
| 141 | 4/25/2002 | 6 | 300 | 0.01 | 3,000 |
| 142 | 2/21/2002 | 6 | 300 | 0.1 | 3,000 |
| 143 | 2/5/2002 | 7 | 1200 | 0 | ---- |
| 144 | 4/2/2002 | 7 | 1200 | 0.01 | 3,000 |

At pH 4.2, nearly equal amounts of H₂L and HL (40% total PASP each)

At pH 4.7, maximum concentration of HL (60% total PASP)

At pH 5.2, HL still dominant (52% total PASP), but L concentration large (41%)

Table C.2 cont'd

| | | | | | | |
|--------------------------------|-----------|----|------|------|--------|---|
| 145 | 2/12/2002 | 7 | 1200 | 0.1 | 3,000 | |
| 146 | 1/31/2002 | 7 | 1200 | 0.01 | 10,000 | |
| 147 | 3/22/2002 | 7 | 1200 | 0.1 | 10,000 | |
| 148 | 4/30/2002 | 7 | 300 | 0 | ---- | |
| 149 | 4/30/2002 | 7 | 300 | 0.1 | 3,000 | |
| 150 | 9/11/2001 | 8 | 1200 | 0 | ---- | |
| 151 | 9/10/2001 | 8 | 1200 | 0.01 | 10,000 | |
| 152 | 9/11/2001 | 8 | 1200 | 0.1 | 10,000 | |
| Reproducibility Studies | | | | | | |
| 153 | 6/21/2002 | 10 | 600 | 0.01 | 10,000 | To replicate experiments at high pH; chose intermediate speed and PASP concentration as representative of range of conditions |
| 154 | 6/21/2002 | 10 | 600 | 0.01 | 10,000 | |
| 155 | 7/8/2002 | 10 | 600 | 0.01 | 10,000 | |
| 156 | 7/2/2002 | 5 | 150 | 0.01 | 3,000 | Done at intermediate PASP concentration and intermediate pH to represent entire range of experiments (both high/low pH and high/low PASP concentration); 0.01M also requires less sample than 0.1M. |
| 157 | 7/2/2002 | 5 | 300 | 0.01 | 3,000 | |
| 158 | 7/3/2002 | 5 | 600 | 0.01 | 3,000 | |
| 159 | 7/3/2002 | 5 | 900 | 0.01 | 3,000 | |
| 160 | 7/8/2002 | 5 | 1200 | 0.01 | 3,000 | |
| 161 | 7/8/2002 | 5 | 1500 | 0.01 | 3,000 | |
| 162 | 7/10/2002 | 5 | 150 | 0 | ---- | To replicate experiments in water at same conditions as above |
| 163 | 7/10/2002 | 5 | 600 | 0 | ---- | |
| 164 | 7/10/2002 | 5 | 1200 | 0 | ---- | |

C.5. Dynamic light scattering analysis

An example of raw data from dynamic light scattering experiments is shown in Figure C.9, which plots the scattering intensity correlation function, $G(t)$, versus time on a log-log scale.

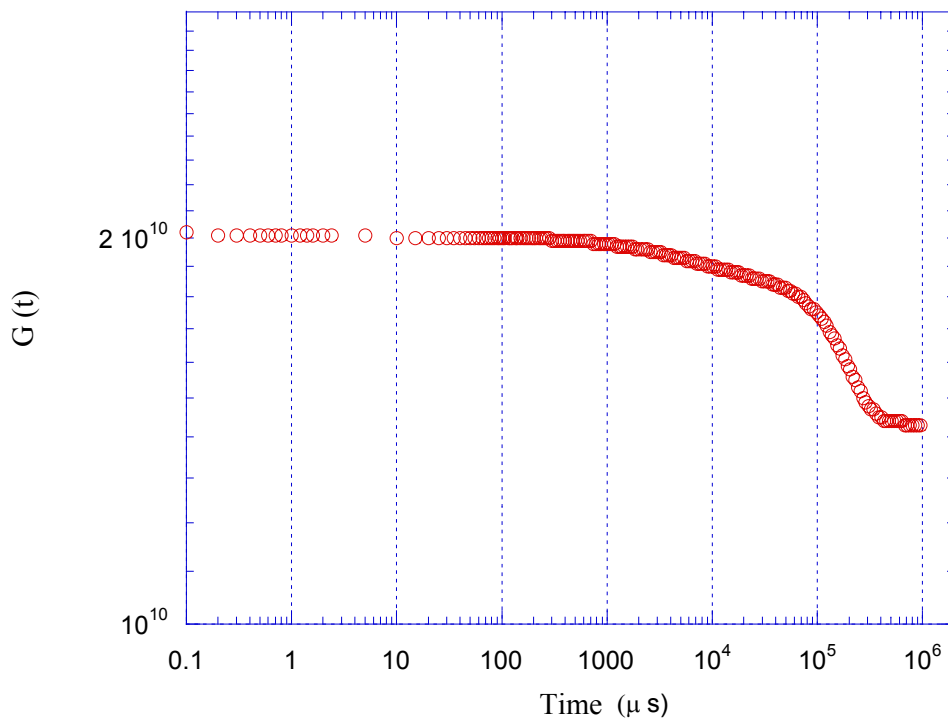


Figure C.9. Scattering data for 0.001M PASP (3,000 Mw) in 0.2M KCl aqueous solution at pH 10 (log-log plot).

From the log-log plot, we see that the decay of the correlation function occurs over approximately one decade of the time scale (10^5 - $10^6 \mu s$). Thus, data from this decay

portion were plotted on a linear-linear scale (Figure C.10) and were fit to an exponential curve of the form:

$$y = A + B \cdot \exp(-\Gamma t) \quad (\text{C.3})$$

where $\Gamma = 2\mathcal{D}q^2$; q is the scattering vector and \mathcal{D} is the diffusion coefficient of polymer molecules. Equation (C.3) is analogous to equation 3.1 in Chapter 3.

Obtaining the value of Γ from the exponential fit, and calculating q according to equation 3.2 in Chapter 3 (using $n=1.337$, $\lambda = 514 \text{ nm}$, and $\theta = 90^\circ$), the diffusion coefficient, \mathcal{D} , was determined for the polymer molecules in solution. Then, using this value, the hydrodynamic radius, R_H , was calculated using equation 2.48 for $\eta \approx 1 \text{ cp}$, $k_B = 1.38 \times 10^{-23} \text{ J/K}$ and $T = 298 \text{ K}$.

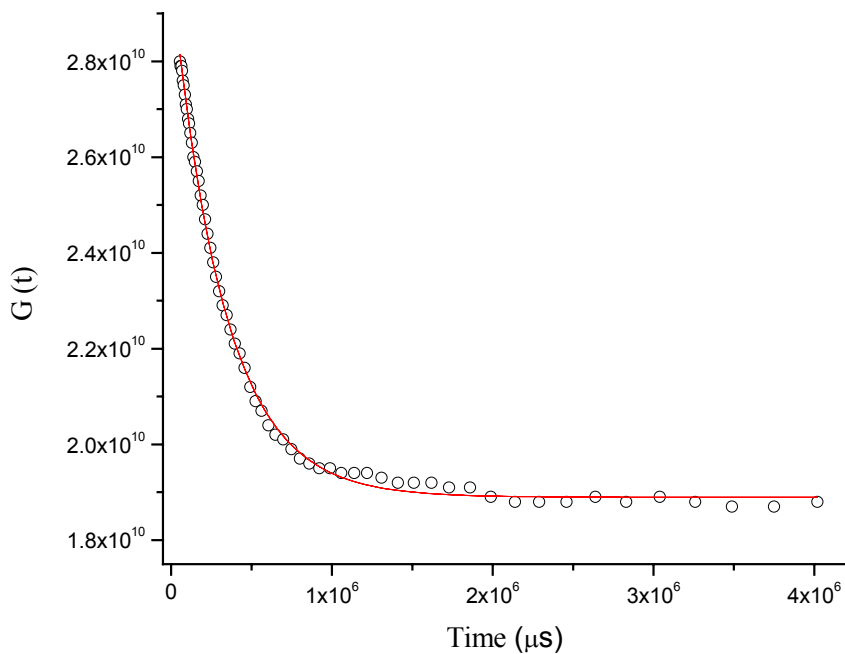


Figure C.10. Exponential fit of decay portion of correlation function.